Annual and Seasonal variability of Chlorophyll-*a* and Sea Surface Temperature in the Equatorial Indian Ocean

A thesis submitted to the University of Hyderabad in partial fulfillment of the award of a **Ph.D degree** in Earth and Space Sciences

by

SHIVA KUMAR GATLA

University Centre for Earth and Space Sciences
(School of Physics)

University of Hyderabad
(P.O) Central University, Gachibowli
Hyderabad – 500046
India

June 2016

DECLARATION

I, Shiva Kumar Gatla, hereby declare that this thesis entitled **"Annual and Seasonal variability of Chlorophyll-*a* and Sea Surface Temperature in the Equatorial Indian Ocean"** is a record of bonafide research work, free from plagiarism, carried out by me under the guidance of Prof. A.C. Narayana. I also declare that it has not been submitted previously in part or in full to this University or any other University or Institution for the award of any degree. I hereby agree that my thesis can be deposited in Shodganga/INFLIBNET.

Date: **Name: Shiva Kumar Gatla**

Signature of the student

Regd. No. 12ESPE05

CERTIFICATE

This is to certify that the thesis entitled **"Annual and Seasonal variability of Chlorophyll-*a* and Sea Surface Temperature in the Equatorial Indian Ocean"** submitted by Shiva Kumar Gatla, bearing Reg. No. 12ESPE05, in partial fulfillment of the requirements for the award of Doctor of Philosophy in Earth and Space Sciences is a bonafide work carried out by him under my supervision and guidance which is a plagiarism free thesis.

The thesis has not been submitted previously in part or in full to this or any other university or institution for the award of any degree or diploma.

Date: **(A.C. Narayana)**

Research Supervisor

ACKOWLEDGEMENTS

It is with all sincerity and high regards that I express my deep sense of gratitude to Prof. A.C. Narayana for his guidance, encouragement, support and valuable suggestions throughout this research work. I will ever remain grateful to him for his unfailing attention, for suggesting an interesting research topic and guiding throughout its solutions. I express my sincere gratitude for his valuable advices and motivation.

I record my respectful thanks to Doctoral Committee members - Dr. M. Ravichandran and Dr. Satya Prakash, Indian National Centre for Ocean Information Services (INCOIS), and Dr. V. Chakravarti, UCESS - for their valuable suggestions during the course of this study.

I express my sincere thanks to Dr. S. Srilakshmi, UCESS, for her help and guidance in the Spectral Analysis and MATLAB methods.

I place on record my grateful thanks to Prof. R. Ramesh, PRL, Ahmedabad, for his valuable suggestions and thoughtful discussions on the research topic and during the finalization of the thesis.

I sincerely thank Dr. A. Suryachandra Rao, IITM, Pune and Dr. K. Ashok, UCESS, for their valuable suggestions. I am very thankful to Sri. T. Suryanarayana, former DGM, NMDC, for his help and guidance in statistical applications. I am also thankful to JVS Raju, INCOIS, for his help.

I am extremely thankful to the Head, University Centre for Earth and Space Sciences, University of Hyderabad, for the facilities made available for the research work.

I gratefully acknowledge the help received from Dr. N. Sravanthi, Pawan Kumar Gautam, B. Sarang, P. Bhavani, Debasri Garai, B. Anjaiah, and also thankful to all the research scholars of the Centre for their friendly support. I also place on record my thanks to the non-teaching staff of the UCESS.

I express my sincere thanks to Dr. S. Siva Reddy and Dr. N. Srinivasa Rao for their encouragement in my research. I also thank my friends K. Shravan and M. Narsimhappa, CASEST, for their support and encouragement.

I am deeply indebted to my parents, uncles, brother and sister, who have always been a source of inspiration. They gave me unconditional love and support throughout my life and have enabled me to achieve this goal. Last but not the least, I thank each and every person who had directly or indirectly helped me to complete this thesis.

Shiva Kumar Gatla

CONTENTS

List of Tables

List of Figures

Chapter 1
Introduction

1.1 General Introduction

Earth is a unique planet in our solar system that has a large ocean (70% of the surface area, with an average depth of ~4 km) and, more importantly, hosts life. Probably life originated only in the Earth, and not in other planets, because water exists on it in the three states- vapour, liquid and ice. Ocean helps the life on Earth by regulating its surface temperature, acting as a thermostat due to the high specific heat of water. It also helps regulating the Earth's atmospheric composition, as different gases dissolve in the ocean to varying extents. In fact oceans play a major role in regulating the current Global Warming by removing the anthropogenic excess CO_2. This is achieved through photosynthetic algae that live in the sunlit surface layers of the ocean. The present thesis is an aspect of the study of the interaction between climate, oceans and marine algae, and is a modest effort to unravel some aspects of the complex interactions between physics, chemistry and biology of a small but significant part of the Oceans, *viz*., the Equatorial Indian Ocean.

1.2 Proxies for productivity studies

Productivity, also known as primary productivity refers to the rate at which carbon is fixed in the sea by photosynthetic organisms that contain chlorophyll. The unit of measurement is milligrams carbon/m^2/day (mg C/d). This refers to the column production, i.e. by the column of water that extends from the surface to the depth at which sunlight can penetrate (typically ~100 m). *In situ* measurements, however, use limited volume of water (e.g., Battathiri et al., 1980) and the corresponding units are mg C/m^3/d. Such *in-situ* measurements are quite sparse. Therefore one uses proxies such as Sea Surface Temperature (SST), Wind Speed (WS), Sea Surface Height (SSH) and chlorophyll-*a* (chl-*a*) concentrations. The reason why these serve as proxies for productivity is discussed below.

Coastal regions in the world oceans seasonally experience upwelling, driven by strong surface winds (Shetye et al., 1991) which move the surface waters away from the coast (e.g. Somali and Peruvian coasts). When upwelling takes place, cooler waters from depths of a few hundred metres come to the surface. This causes a reduction in SST by up to 4°C, as deeper waters are cooler relative to the surface. In addition, the deeper waters are rich in nutrients

such as nitrate, phosphate and silicate. This injection of new nutrients to the surface causes seasonal (usually spring) plankton blooms, increasing the chlorophyll concentration and productivity in the sunlit surface layer known as the photic zone. While *in-situ* productivity measurements are difficult to make (they depend on the availability of ship time, and suitable non-stormy weather), parameters such as SST, WS and chl-*a* can be remotely sensed using satellites. Large scale data on spatial and temporal variations of productivity can be easily obtained. Another aspect of ocean warming is the thermal expansion of the ocean and the consequent increase in the sea level, in addition to that due to melting of polar ice sheets and glaciers. The measure of sea level is SSH. It can also be measured through satellite altimetry. There are cold core and warm core eddies in the ocean that can be detected using SSH. Cold core eddies cause some vertical mixing and cause an increase in the productivity, to a lesser degree than upwelling. As eddies persist for more time (conservation of angular momentum), they can contribute to higher productivity. SSH measurements have been used to identify mesoscale eddies with diameters between 250 to 1000 km and maximum amplitudes up to 45 cm in the northern Indian Ocean during monsoons (Jensen et al., 2014). Han et al. (2010) reported that sea level had decreased substantially in the south tropical Indian Ocean since the 1960s, driven by changing surface winds with a combined invigoration of Hadley and Walker cells of the Indian Ocean. Thus all these parameters, *viz*., SST, WS, SSH and chl-*a* can act as effective proxies for marine productivity.

Anthropogenic carbon input to the atmosphere is counter-balanced by photosynthesis of land and marine plants. It is estimated that ~50% of the annual carbon injected is retained in the atmosphere and the remaining is taken up by land and marine plants roughly in equal proportion (Falkowski et al., 1998). It is especially important to measure the carbon uptake rate by ocean biota, as there is a large spatial and temporal variability. Satellites are useful in providing a large and temporal coverage of marine productivity by monitoring the ocean colour (pigments such as chl-*a*).

Due to their broad and synoptic coverage remotely sensed images of ocean colour are considered important for spatial extrapolation of local data collected from ships in ocean biogeochemical studies (Platt and Sathyendranath, 1993). These are also the only practical ways of monitoring the spatial and temporal variation of phytoplankton and for studying ocean primary productivity, global carbon and biogeochemical cycles.

The aim of the ocean colour remote sensing is to estimate the ocean constituents (such as chlorophyll, suspended particulate matter, yellow substances etc.) from the spectral nature of the backscattered solar radiation from the ocean waters. The visible portion (wavelength ~ 400-670nm) of the solar spectrum only penetrates into the water and undergoes absorption and multiple scattering due to a series of interactions with suspended (phytoplankton, sediment etc.) and dissolved organic matter (DOM) present. A small portion of this visible radiation is scattered out of the water and is captured by ocean colour sensor. These radiances are detected in a set of selected wavelengths and the concentrations of ocean constituents are estimated using a variety of empirical, semi-empirical and analytical algorithms (e.g., Vinayachandran and Mathew, 2003).

Some scientists use modeling for the estimation of productivity. Modelling the vertical insertion of photosynthetically active radiation (PAR) and its usage by phytoplankton is basic for the simulation of ocean primary composition. The variation in attenuation and absorption of high wavelength suggests that the photosynthesis be shaped at high spectral resolution, but computating this one is costly. Kettle and Merchant (2008) investigated the effects of variation of the spectral resolution of the underwater light field on the primary production of phytoplankton (a*) and its photosynthetic efficiency were examined by Kettle and Merchant (2008) by utilizing a 1-d coupled ocean turbulence model. The model was applied at three sites in the Atlantic Ocean PAP (~50°N), ESTOC (~30°N) and CIS (~60°N) to study the effects of various meteorological forcings. They have also studied three distinct methods for shaping a* – (i) using a fixed constant, (ii) altering both wavelength and chlorophyll concentrations (Bricaud et al., 1998), and (iii) a non-spectral parameterization (Anderson, 1993). After choosing the suitable ecosystem parameters for all of the three sites they changed the spectral resolution of light and a* from 1 to 61 wavelength bands and studied the effects with three distinct a* methods of estimation. The results suggest that modeled results of marine primary productivity are extremely sensitive to the spectral resolution and a*. They further suggest that a spectral resolution of minimum six wavelength bands are necessary, if a* is a function of wavelength and chlorophyll, and three wavebands if a* is a constant value, for accurate simulations of primary production and chlorophyll concentration.

1.3 Study Area- Equatorial India Ocean

The equatorial regions of the world are areas of special interest. They receive solar radiation throughout the year. Equatorial oceans contribute the maximum to the Earth' hydrological cycle, as both evaporation and precipitation are high in these regions. Equatorial oceans are sites of intense air-sea interactions and are strongly influenced by several mutually interacting physical processes at intra-seasonal and inter-annual scales. The strong coupling between the atmosphere and the ocean makes the equatorial regions sensitive, and hence important for climate (Murtugudde et al., 2000).

The Equatorial Indian Ocean has been chosen for this study based on the following motivation. First, it still remains the least sampled and studied region of the Indian Ocean. Secondly, it is different from Equatorial Atlantic and Pacific Oceans, as the semi-annual reversal of winds (monsoons) causes reversal of surface currents. Further, Wyrtki jets (strong eastward currents in the Equatorial Indian Ocean, Joesph et al., 2012) occur semi-annually during the inter-monsoon periods (Wyrtki, 1973; Hat et al., 1999). Thirdly, there is no upwelling, unlike the equatorial Atlantic and Pacific, resulting in a relatively lower primary productivity. Relative to any other location in the Northern Indian Ocean, chlorophyll concentrations in the photic zone of the Equatorial Indian Ocean are quite low, and therefore it is often referred to as a 'biological desert' (Narvekar and Prasanna Kumar, 2010). Fourth, there is a unique phenomenon of the Indian Ocean Dipole (IOD) (Saji et al., 1999; Webster et al., 1999). It is a coupled ocean-atmosphere phenomenon, characterized by anomalous surface cooling in the Eastern Equatorial Indian Ocean (EEIO) and anomalous surface warming in the Western Equatorial Indian Ocean (WEIO). It is caused by changes in the normal convection situated over the EEIO (JAMSTEC, 2009). It happens during September-October, when the EEIO becomes unusually cold and the WEIO unusually warm. There seems to be some evidence for linking IOD with the El Nino Southern Oscillation (ENSO) that takes place in the Pacific (Annamalai et al., 2003), as in 1997 both co-occurred. SST anomalies in the Pacific that occur due to ENSO are disturbed because of IOD (Vinayachandran et al., 2009). Finally, Equatorial Indian Ocean is the seat of Madden-Julian Oscillations, which have a quasi-periodicity of 30 to 60 days and cause eastward moving precipitating cloud systems in the Equatorial Indian Ocean (Madden and Julian, 1971; Hendon and Salby, 1994). Along the Equator near 80°E, while the monsoon periods are

characterized by very weak winds, the inter-monsoon periods are characterized by strong westerlies (Risien and Chelton, 2008; Strutton et al., 2014).

Thus it would be interesting to know the effect of this complex system with interactions on different spatial and time scales on the primary production in the Equatorial Indian Ocean (figure 1).

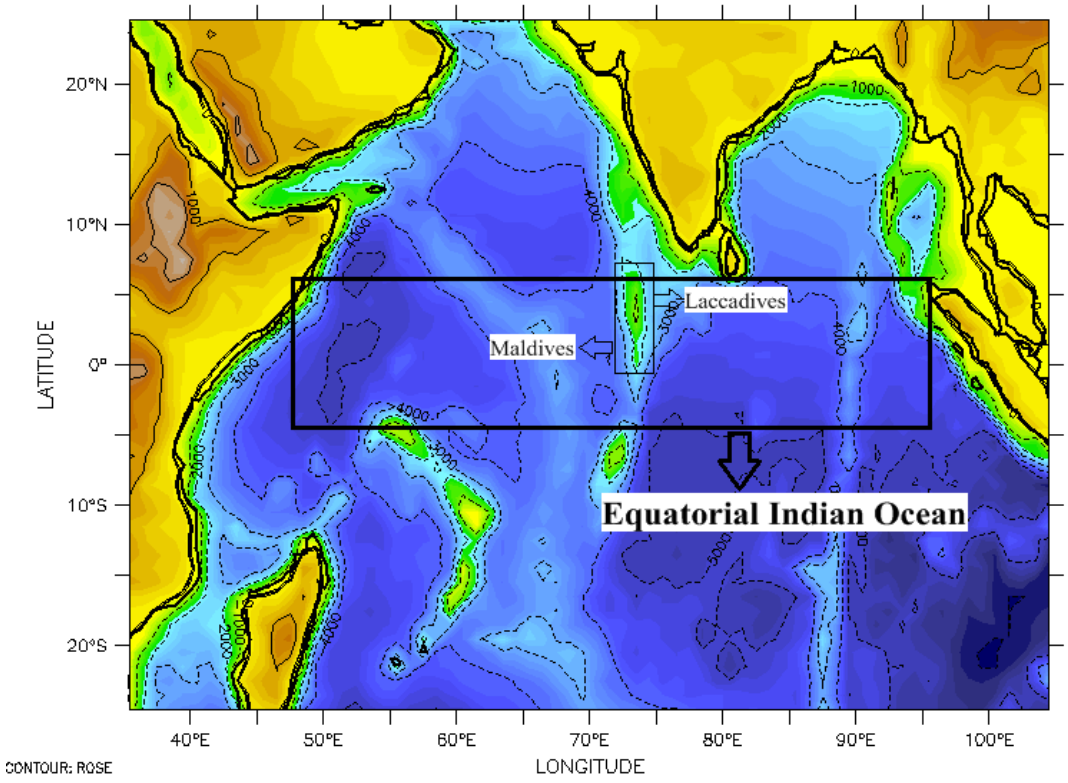

Figure 1 Map showing the Indian Ocean region. Study area i.e., Equatorial Indian Ocean (Latitude 5^{o}N – 5^{o}S, Longitude 45^{o}E-95^{o}E) is showing as a box.

1.4 Objectives and scope of the present work

As mentioned earlier, this thesis is a modest effort to understand the spatial and temporal variations in satellite derived chl-*a*, SST, SSH, and WS and the inter relationships, if any. In the context of Global Warming and Ocean Acidification (IPCC, 2013) one of the global concerns is their effect on the primary productivity in the oceans. It is well known that this primary productivity is at the base of the marine food chain and any adverse effect on it will eventually translate in reduced fish landings. About 35% of the world population lives on

the coastal regions and depends on sea food to a great extent. Therefore, the adverse effects on marine primary production have a direct effect on human food security in the near future.

From basic science ideas, it is known that winds induce coastal upwelling and cause increased primary productivity in the sunlit surface layers of the ocean. Simultaneously, there is also a reduction in SST due to upwelling, as the deeper layers of the ocean are relatively cooler. Supply of nutrients to the surface increases with higher rates of upwelling and causes more plankton to grow, thus increasing chl-*a* concentration in the photic zone. If any changes to these normal expectations has occurred due to the recent Global Warming and Ocean acidification, it is important to know how these quantities have changed. For example, warming may lead to higher stratification, prevent vertical mixing that bring nutrients to the surface and reduce surface productivity (Beherenfeld et al., 2006). Furthermore, it is also known that during IOD events, the weakening and reversal of wind in the Central Equatorial Indian Ocean (CEIO) leads to unusually warm SSTs in the WEIO. In the backdrop of these observations, the following science questions have been asked.

The main objectives of the present work are: (i) To understand the possible causes of the variability of SST, SSH and chl-*a* in the Equatorial Indian Ocean (ii) To assess the variation in the primary productivity in the Equatorial Indian Ocean using chl-*a* time series data from MODIS Aqua satellite. (iii) To assess the inter-dependence of chl-*a* and SST in the Eastern, Central and Western Equatorial Indian Oceans, which exhibit different oceanographic conditions at different times of the year and (iv) To examine the relationship between the wind speeds and chl-*a*.

1.5 Previous studies

Here, a brief discussion on the *in-situ* measurements of productivity found in the literature for the Northern Indian Ocean and their comparison with satellite derived data is presented first. This is followed by important earlier results from the Equatorial Indian Ocean.

A few papers comparing measured chl-*a* with that estimated from IRSP4 OCM data have been already published for the Arabian Sea (Sarangi et al., 2001, 2004; Chauhan et al., 2001; 2002; 2003). The Bay of Bengal lacks such studies, probably due to persistent cloud cover. Although Rao et al. (2006) reported increased productivity in the Bay of Bengal after a cyclone, their productivity model was not tested against *in situ* measurements. The recently

completed Bay of Bengal process studies (BOBPS) is an attempt to evaluate the biogeochemical characteristics of the Bay of Bengal (Prasanna Kumar et al., 2002). A few measurements exist on the primary productivity, which show a random distribution over space and time. Qasim (1977) observed that surface production in the Bay of Bengal is higher due to lower light intensities (persistent cloudiness) relative to the Arabian Sea, whereas photic column-integrated production is higher in the latter. Nair et al. (1973) have reported primary productivity values varying from 3.0 - 8.7 g C m^{-2} d^{-1} for nearshore waters of the east coast of India during the SW monsoon. Radhakrishna (1978) has reported the in the primary productivity (PP) values for the offshore regions varying from 129.99 to 329.45 mgC m^{-2} d^{-1} (av. 219 mg C m^{-2} d^{-1}) and 49.66 to 606.37 mg C m^{-2} d^{-1} (av. 315.43 mg C m^{-2} d^{-1}) for the slope region in the western margin of the Bay during August-September 1976. Bhattathiri et al. (1980) have reported 180-2200 mg C m^{-2} d^{-1} (av. 740mg C m^{-2} d^{-1}) for offshore and 120-3410 mg C m^{-2} d^{-1} (av. 1280 mg C m^{-2} d^{-1}) for slope region along Indian side for the same period for year 1978 and concluded that primary production of the Bay of Bengal (BoB) is not less than that reported for the Arabian Sea. Most recently Gomes et al. (2000) have studied the productivity and chl-*a* concentration for the three seasons in the BOB for both offshore and inshore regions. Average depth integrated chl-*a* values for inshore stations have been reported to be 30.4, 165 and 26.2 mg m^{-2} while for offshore stations it was found to be 18.8, 97.0, 27.6 mg m^{-2} for pre-southwest monsoon, southwest monsoon and northeast monsoon respectively. Whereas the average depth integrated PP for the above mentioned three seasons were 1.05, 0.55 and 0.44 g $Cm^{-2}d^{-1}$ for inshore waters, for the offshore waters these values were found to be less, averaging around 0.16, 0.30 and 0.30 g $Cm^{-2}d^{-1}$. Apart from the above mentioned average values Gomes et al. (2000) have also reported chl-*a* and production rates as high as 53 mg m^{-2} and 4.5 g C $m^{-2}d^{-1}$ for pre-southwest monsoon (March-April), which are attributed to nutrient deficient cooler waters brought to the surface by east India coastal current flowing poleward. The high chl-*a* but low productivity values reported for summer monsoon are attributed to light limitation due to intense cloud cover over BOB during this season. Madhupratap et al. (2003) have reported poor surface chl-*a* (0.06-0.28 mg m^{-3}) in open ocean and (0.06-0.16 mg m^{-3}) in the coastal region of BOB during the summer monsoon 2001. Column integrated PP has been reported between 90-220 mg C m^{-2} d^{-1} in the open ocean stations, which lie along 88^{o}E. Relatively higher values have been reported along coastal stations that fall in the range of 328-520 mgC m^{-2} d^{-1}. Although the fall (180 to 512 mgC m^{-2} d^{-1}, Gauns et al., 2005) and winter (149 mg C m^{-2} d^{-1}, Jyothibabu et al., 2004) primary productions in the BOB are low, high values have been reported off Chennai (up to

1229 mg C m^{-2} d^{-1}) immediately after a cyclone (Madhu et al., 2002). Sarma (2006) used SeaWiFS derived Chlorophyll, SSTs from AVHRR and SSHs from TOPEX/POSEIDON and found that in the Arabian Sea, chl-*a* was negatively correlated with anomalies in SST and SSH. He also found that during IOD events, column production decreased by ~30%. Currie et al. (2013) found that IOD and ENSO cause significant but predictable re-organization of chl-*a* because of their influence on near surface oceanography.

Coming to the Equatorial Oceans, Beherenfeld et al. (2006) reported a net reduction in productivity in the tropics. In the Western Indian Ocean, however, they reported an increase in productivity during 1998 to 2004, accompanying an increase in SSTs. This has been questioned recently by a preliminary study on the Western tropical Indian Ocean: Roxy et al. (2014) found that the Western Tropical Indian Ocean experienced an anomalous warming of summer SSTs by 1.2°C during 1901-2012. Further, Roxy et al. (2016) reported a decline of 20% in the phytoplankton population over the past 60 years, based on 16 years of satellite data and model simulations. It is unclear at present how much trust one can put on such models. Ma et al. (2015) studied the relationship between SST and chlorophyll-*a* (chl-*a*) concentrations for two IOD years (1997 and 2006) using a model. They found that during positive IOD years, when the chl-*a* concentration increases, SST too increased. They suggest that the inter-annual variability of chlorophyll concentrations in the Western Equatorial Indian Ocean could reduce the amplitude of IOD by ~6%. Sardesai et al. (2010) studied the nutrient characteristics of four water masses identified in the Equatorial Indian Ocean in winter, spring and summer monsoons along 77°E and 83°E transects (5°S to 5°N). The main component of the surface waters were the low salinity in the Bay of Bengal and the Indonesian Throughflow. Silicate was the nutrient with highest concentration in this water mass. Prasanna Kumar et al. (2001) had earlier reported high biological productivity (up to 1700 mg C m^{-2} d^{-1}) during the summer monsoon in the central Arabian Sea (11° to 19°N), believed to be induced by lateral advection and Ekman pumping. Jochum and Murtugudde (2005), analyzed a 40 year eddy-resolving model of SSTs of the tropical Indian Ocean and found that internal variability in the Western Indian Ocean contributed significantly to the inter-annual variability. Joseph et al. (2012) reported a weakening of the Wyrtki jets during 2006-2011. Strutton et al. (2015), and TMI (Tropical Microwave Imager) using mooring data found increased chl-*a* during development of fall Wyrtki jets. Sediment trap studies by Vidya et al. (2013) showed that elevated chl-*a* during the summer monsoon was caused by wind mixing.

Chapter 2

Oceanography and Productivity of Equatorial Indian Ocean

2.1 Introduction

In this chapter, the general oceanographic settings of the study region are described. Productivity is defined and various parameters controlling productivity are described. Their natural ranges of variations in different regions of the Oceans, are indicated with a special reference to the Equatorial Indian Ocean region.

2.2 Oceanography

It is well known that 70% of the world are covered by oceans. The Pacific Ocean occupies the largest area (almost 50% of the surface area of the Earth) and is the deepest. The Atlantic comes next, followed by the Indian Ocean. The Great 'Conveyer Belt' circulation (also called the Atlantic Meridional Overturning Circulation) starts with the Gulf Stream that originates in the Gulf of Mexico and travels all the way to the North Atlantic. This warm current carries heat to the North Polar Region. As discovered by Benjamin Franklin, England is warmer than Alaska present at the same latitude, because of the heat supplied by the Gluf Stream Current. The Gulf Stream loses heat to the atmosphere, cools, and therefore becomes dense and sinks. This is the way North Atlantic Deep Water (NADW) forms. This is the beginning of the Thermohaline circulation, and it travels south to the South Atlantic. Part of it comes to the southern Indian Ocean and a part goes to the North Pacific via the South Pacific, and upwells. This whole circulation has an approximate time scale of 1000 years, as determined by radiocarbon ages of the sea water samples at different points of the 'conveyor belt'.

There are other warm currents such as the Somali Current and the Agulhas Current in the Indian Ocean, Kuroshio Current in North West Pacific, Brazil current in the Atlantic and the Leeuwin Current in the South East Indian Ocean. All these, and the cold currents such as the California Current and the Peru Current in the East Pacific, Benguela Current in the South East Atlantic are driven by surface winds.

Coming to the Indian Ocean, the Arabian Sea is largely influenced by the Great Whirl (GW) (Schott and McCreary, 2001) during the southwest monsoon. The GW is a result of

strong northward flowing Somali Current (SC). But during the winter monsoon, the GW together with the connected upwelling wedges disappears due to the withdrawal of the SC. South Equatorial Current (SEC) provides the water from the Pacific Ocean to the Indian Ocean through the Indonesian through flow, which is relatively warm in contrast to the Indian Ocean. The SEC breaks into two parts at the point of Madagascar at 17°S, and the northward flowing branch Northeast Madagascar Current (NEMC) manages the northward moving East African Coast Current (EACC). During SWM the EACC feeds the northward flowing Somali Current that leads to the development of strong upwelling owing to the Ekman transport from the Somalian and Oman coast (Schott et al., 1990; Brock et al., 1991) and the upwelling velocities close to 3x10-3 cm/sec and an upwelling transport of 1.5 – 2 Sv occurs in the upper 50 m (Smith and Bottero, 1977; Shi et al., 2000) of the Western Arabian Sea. The typical temperature of the upwelled water is 19-23°C (Schott and McCreary, 2001). During the winter monsoon, the Somali Current converts its direction and flows southward and meets the EACC at 2-4°S that provides the eastward flowing South Equatorial Countercurrent (SECC) (Dueing and Schott, 1978; Swallow et al., 1991). The dry and cold Northeast monsoon wind accompanied by the Ekman pumping inhibits upwelling the northern Arabian Sea (Morrison, 1997; Schott and Fisher, 2000; Schott and McCreary, 2001). The cold wind induced convective overturning supports a reduced productivity in comparison to SWM (Banse and McClain, 1986; Madhupratap et al., 1996).

. 2.3 Productivity

Carbon dioxide dissolves in the ocean much more than oxygen and nitrogen as it is a reactive species. It makes, upon dissolution, carbonic acid, which decomposes to aqueous CO_2, bicarbonate and carbonate, the relative abundances of which depend on the p^H of seawater. In normal seawater of p^H 8.2, carbon stays mostly as bicarbonate. A major way by which man-made excess atmospheric carbon dioxide is removed by the ocean through marine productivity. This is called the biological pump. Productivity, also known as primary productivity refers to the rate at which carbon is fixed in the sea by photosynthetic organisms that contain Chlorophyll. The unit of measurement is milligrams carbon/m^2/day (mg C/d). This refers to the column production, i.e. by the column of water that extends from the surface to the depth at which sunlight can penetrate (typically ~100 m). *In situ* measurements however use limited volumes of water and the corresponding units are mg C/m^3/d. The net productivity is the gross productivity minus the respiration by primary producers. Secondary

producers such as zooplanktons eat primary producers and contribute to the biomass. The rate of carbon fixation primarily depends on sunlight availability and the SST, in addition to the supply of macronutrients such as nitrate, phosphate, silicate and micronutrients (iron). The availability of sunlight again depends on the nature of the sky (clear or overcast) and the clarity of the water (absence of suspended matter). Nutrients are supplied to the sunlit photic zone of primary production by upwelling, vertical mixing, lateral advection, aerosols or rivers (Singh and Ramesh, 2011). Various isotopic tracers (^{14}C, ^{15}N, ^{13}C, ^{18}O) have been used for on-deck measurements of productivity (Kumar et al., 2004a, 2004b; Kumar and Ramesh, 2005; Gandhi et al., 2010; 2011a,b).

The great gyres in the mid oceanic regions in the Northern and Southern hemispheres lack nutrients and the primary productivity is only of the order of a few hundred mg C/m^2/day. The downwelling and resultant deep nutricline characteristics of ocean gyres means that horizontal advection of nutrients from adjacent regions can play a greater role in chl-*a* responses there than the vertical changes in thermocline depth, according to Currie et al. (2013). It is only in the upwelling regions that the productivity seasonally reaches high values of a few grams C/m^2/day. These are the Somalia and Oman coasts in the Indian Ocean and the Peru and California coasts in the East Pacific. These regions, quite naturally, are known for intense denitrification (Howell et al., 1997) in the water column up to depths of ~1 km and are sources of nitrous oxide, another powerful greenhouse gas, to the atmosphere.

The Bay of Bengal (BOB) and Arabian Sea (AS), both are northern Indian Ocean (NIO) pans are significantly different in many aspects. During southwest monsoon, strong winds present intense upwelling over the northwestern Arabian Sea. Upwelling brings nutrients to enhances surface productivity. In the winter monsoon cooler winds, drive to convective mixing in the northeastern AS, and this brings nutrients from the deep to the surface enhancing the surface productivity. In extension, from the Sahara and Thar nutrients come to the AS in the form of dust. Because of this, AS is considered as the most productive regions in the world (Madhupratap et al., 1996; Smith, 2001; Prasanna Kumar et al., 2002; Prakash and Ramesh, 2007). another side, a huge influx of fresh water stratifies BOB surface, limiting surface productivity. The origin of atmospheric nitrogen at these two sites can be quite distinctive but supposed to be essentially from the industrial nations, China and India. Therefore, the two basins (BoB, AS) provide an ideal oceanic environment to study the impact of atmospheric deposition on the biogeochemistry of the surface ocean. Details

regarding the hydrography, circulation and winds of the northern Indian Ocean have been discussed by many authors including Thadathil et al. (2007) and Jyothibabu et al. (2010).

2.3.1 Chlorophyll-*a*

Compared to chl-*a* data from a single satellite sensor, merged products (such as from SeaWiFS and Modis-Aqua, as used in this thesis) have a wider mean global coverage and lower uncertainties. Though small systematic differences do exist among the products of individual sensors, the large scale chl-*a* distributions produced by these major ocean color missions are consistent over a wide range of conditions (Currie et al., 2013).

Area averaged monthly time-series of SeaWiFS derived chl-*a* in the Arabian Sea (45° to 80°E and 0° to 25°N) for the years 1997 to 2010 (Prakash et al., 2012) indicate that chl-*a* concentrations vary from 0.2 to 12. mg m^{-3} (roughly the same as μg/L). They also showed that in coastal upwelling regions off Somalia, Gulf of Aden and the Indian West coast, the chl-*a* could reach up to 4 to 8 mg m^{-3} in the plankton bloom periods. These observations were extension of earlier observations of Sarma (2006), who had reported values of similar order of magnitude. Currie et al. (2013) studied the IOD and ENSO impacts on regional chlorophyll anomalies in the Indian Ocean. They inferred that ENSO had a greater influence that IOD only in the Somalia upwelling region. They suggest that ENSO and IOD cause significant and predictable regional reorganization of chlorophyll via their influence on near surface oceanography. Strutton et al. (2015) reported chl-*a* values for the Central Equatorial Indian Ocean in the range of 0.1 to 0.2 mg m^{-3}.

2.3.2 Sea Surface Temperature

SST of the oceans is regulated by solar radiation, upwelling, evaporation, sensible heat loss and radiation to space. Eddies also play an important role in modulating SST (Prasanna Kumar et al., 2004; Nuncio and Prasann Kumar, 2012). Oceanic eddies are circulating water bodies which are either cyclonic (colder water and lower sea level at the center) or anticyclonic (warmer water and elevated sea level at the center) (Falkowski et al., 1991). Cold-core eddies cause an upward displacement of the nutricline along isopycnals and inject nutrients to the surface (Falkowski et al., 1991), enhancing biological productivity and carbon export downwards in the Bay of Bengal (Ramasastry and Balaramamurty 1957; Shetye et al. 1993; Prasanna Kumar et al. 2007). Gopalan et al. (2000) found spatially a strong inter-

annual variability and intensity of the eddies. Prasanna Kumar et al. (2007) observed an increase in nitrate (NO_3^-) and silicate (SiO_4) in the Bay of Bengal during both fall and spring and attributed this to the eddies. This resulted in higher concentrations of chlorophyll. They also observed that eddy-pumping shallowed the subsurface chlorophyll maximum (SCM), while primary production switches from 'regenerated' to 'new' production during episodic eddy events (Muraleedharan et al., 2007). Eddies can be identified with the help of Sea Surface Height Anomaly (SSHA) data.

Area averaged monthly time series of TMI (Tropical Microwave Imager) derived SST in the Western Arabian Sea (Prakash et al., 2012) for the years 1997 to 2011 indicates that SST varies from 24° to 31°C. Jochum and Murtugudde (2005) observed that the Indian Ocean is different from the Pacific and Atlantic, as bounded in the north and the prevailing equatorial winds are westerlies as a result of the Indonesian low, Therefore there is no equatorial upwelling. Further, because of the surrounding landmass the seasonal winds and currents are much stronger than in the Atlantic and Pacific.

2.4 Sea Surface Height Anomalies (SSHA)

Weekly TOPEX/Poseidon, ERS and Jason derived SSHA in the Western Arabian Sea during the third week of August (mid-monsoon) for the years 1997 to 2010 (Prakash et al., 2012) showed in some years (e.g., 2003) the presence of cold core eddies, identifiable as negative SSHA. As mentioned earlier, in this region the chl-*a* could reach up to 4 to 8 mg m^{-3} during the monsoon season. Sakova et al. (2006) presented SSH in a number of different locations in the Indian Ocean, and they also analyzed the corresponding Power Spectra. They identified five spectral band carrying most of the low frequency SSH variability in the Indian Ocean. These are semi-annual, annual, 18-20 months, 3 years and 4-6 years. The discovery of a strong 18-20 month signal was an important discovery.

2.5 Wind Patterns

Area averaged monthly time-series of CCMP (Cross Calibrated Multi Platform) and Quick Scat derived wind speed off the Somalia coast in the Western Arabian Sea for the years 1997 to 2003 (Prakash et al., 2012) indicate that wind speeds vary from 1 to 15 m s^{-1}, with an annual mean of 8 m s^{-1}. These high wind speeds occur during June to September, i.e., the monsoon season that causes coastal upwelling. As we saw in an earlier section, in this

region the chl-*a* could reach up to 4 to 8 mg m^{-3} in this season. Murakami et al. (2000) compared chl-*a* data for the equatorial Pacific from OCTS (Ocean Color Temperature Scanner) on board the ADEOS satellite with NSCAT derived wind stress. Compared to the values obtained in the Western Arabian Sea, the chl-*a* varied from 0.05 to 0.25 mg m^{-3} (smaller) and wind stress from 0 to 1.5 N m^{-2} (higher). Wind stress is related to the square of the wind speed. They found a significant negative correlation between wind stress and chl-*a*. Strutton et al. (2015) reported wind speed values for the Central Equatorial Indian Ocean in the range of -4 to +8 m s^{-1}. The corresponding wind stress values were -0.05 to +0.16 N m^{-2}, much less than in the Equatorial Pacific, due to lack of upwelling as explained earlier.

Chapter 3

Data and Methodology

3.1 Introduction

In this study, the variability of chl-*a*, SST, SSHA and WS over the Equatorial Indian Ocean (EIO) bounded by 5^{o}N – 5^{o}S and 45^{o}E – 95^{o}E is discussed. The following are the satellite platforms and the sources from where the data have been accessed/ downloaded.

Chl-*a* data from Ocean color sensor at 4 km spatial resolution for the period July 2002 – May 2014 were obtained from Level-3 Standard Mapped Images (SMI) of Aqua MODIS acquired by the National Aeronautics and Space Administration (NASA) Ocean color (http://oceancolor.gsfc.nasa.gov). SST sensor is Tropical Rainfall Measuring Machine (TRMM) Microwave Imager (TMI) with a pixel resolution of 0.25^{o}. SST data have been obtained from the Asia-Pacific Data Research Center of University of Hawaii (http://apdrc.soest.hawaii.edu). (http://las.incois.gov.in). Sea surface wind data was obtained from NCEP/NCAR (ftp.cdc.noaa.gov) are SSH data from Merged AVISO Altimetry and Niiler climatology (http://oceanwatch.pifsc.noaa.gov/las/servlets/constrain?var=15).

The datasets used and methods applied are presented in figure 3.1

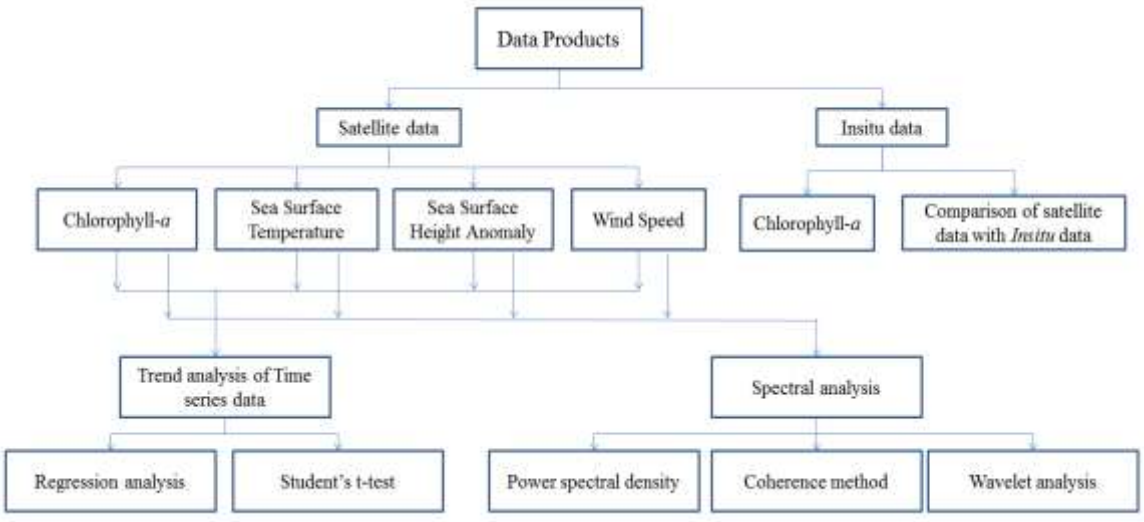

Figure 3.1 Flow chart showing used datasets of chlorophyll-*a*, Sea Surface Temperature, Sea Surface Height Anomaly and Wind Speed and applied methods.

3.2 Data Products

3.2.1 Satellite data

The spatial and temporal coverage of satellites provide a continuous data that can be assimilated from time into climate models to time and thus provide an estimate of errors in such models. Efforts have been made to utilize the available satellite observations of ocean in the numerical models, through assimilation, to generate ocean state which is near realistic.

The four parameters from satellite that are widely used for this purpose are the chl-*a*, SST, SSHA and WS. Various researchers (Kara et al. 2005, Babu et al. 2004, Millif et al. 1999) have shown the usefulness of satellite derived forcing over those available conventionally. These datasets are proven to be very accurate and are able to capture the natural variabilities in these parameters.

Moderate Resolution Imaging Spectro radiometer (MODIS) is a passive imaging spectro radiometer, its EOS satellites the Terra (10:30 a.m. descending node) and Aqua (1:30 p.m. ascending node) being in sun-synchronous, near-polar, circular orbit. The instrument scans across the track and has a swath of 2330 km. It uses 36 discrete spectral bands (visible, near and thermal infrared) between 0.41 and 14.2 μm, and provides a fairly comprehensive set of the land, oceans and atmospheric parameters in the visible and infrared regions of the spectrum. Aqua MODIS views the entire Earth's surface for every 1 - 2 days (vide MODIS Data and Technical Specifications, Table 3.2). The MODIS has many spectral bands onboard such as High resolution Infrared Radiation Sounder (HIRS) and NOAA/TOVS. Using MODIS spectral band nearer to HIRS-2, it is possible to get profiles of temperature and moisture as well as total perceptible water vapor, ozone, and atmospheric stability. A brief description of the MODIS channels is given in Table 3.1. In the present study, level 2 data have been used.

The MODIS instrument operates on both the Terra and Aqua spacecrafts. It acquires data at three spatial resolutions -- 250m, 500m, and 1,000m.

Accompanying with all the data sets from other instruments on board the Aqua and Terra Spacecrafts, MODIS data are conveyed to ground stations in White Sands, New Mexico, via the Tracking and Data Relay Satellite System (TDRSS). The data are then transferred to the EOS Data and Operations System (EDOS) at the Goddard Space Flight Center. The Level 1A, Level 1B, geolocation and cloud mask products and the Higher-level

MODIS land and atmosphere products are provided by the MODIS Adaptive Processing System (MODAPS), and then are transferred among three DAACs for sharing. Ocean color products are provided by the Ocean Color Data Processing System (OCDPS) and given to the science and applications community.

Several data products derived from MODIS observations illustrate characteristics of the atmosphere, oceans, land that can be utilised for analysing of methods and trends on regional to global scales. As just noted, MODIS products are obtainable from many references. LAASDS WEB providing MODIS Level 1 atmosphere products. U.S. Geological survey EROS data Center (EDC) providing Land Products. National Snow and Ice Data Center (NSIDC) in Boulder, Colorado providing Cryosphere data products (snow and sea ice cover) . sea surface temperature products and Ocean color products accompanying with information regarding these products are available at the OCDPS at GSFC. Users with an suitable x-band receiving system can obtain local data straightly from the spacecraft utilizing the MODIS Direct Broadcast signal (http://modis.gsfc.nasa.gov/data/ref).

Table 3.1 Technical Specifications of MODIS

Spatial Resolutioin	250 m (bands 1-2) 500 m (bands 3-7) 1000 m (bands 8-36)
Power	162.5 W (single orbit averge)
Weight	228.7 kg
Swath Dimensions	2330 km (cross track) by 10 km (along track at nadir)
Scan Rate	20.3 rpm, cross track
Quantization	12 bits
Data Rate	10.6 Mbps (peak daytime); 6.1 Mbps (orbital average)
Orbit	705 km

3.2.2 Retrieval of chlorophyll-*a* data from Aqua MODIS

Level-3 Standard Mapped Images (SMI) of Aqua MODIS acquired by the National Aeronautics and Space Administration (NASA) Ocean color (http://oceancolor.gsfc.nasa.gov) are used for the estimation of chl-*a* concentrations. To study the Ocean dynamics, NASA launched MODIS in 2002, on board the Aqua satellite platform. MODIS captures the data in 36 spectral bands ranging between 0.4 um to 14.4 um wavelength and varying at 1km in spatial resolutions. The Aqua platform comes under Sun-synchronous, near-polar orbit with the altitude of 705 km and every day the MODIS sensor captures images the complete globe. At the equator the level 3 standard mapped imaged (SMI) chl-a dataset has a spatial resolution of 4.6 km and a temporal resolution of 24 hours. The SMI dataset is an image binned representation of MODIS data (http://oceancolor.gsfc.nasa.gov). Quantitative data presented by MODIS Aqua device on entire marine biogeochemical characteristics to monitor oceanic circumstances that influence global change and to estimate the role of oceans in the global carbon cycle and other biogeochemical cycles. Detailed variations in CHL-a show several kinds and quantities of aquatic phytoplankton (microscopic plants), the information of which has both practical and scientific applications. This is a different dataset from the Ocean Biology Processing Group (OBPG), an official NASA data center that archives and distributes the ocean colour data to the users across the world. The concentration values are retrieved by using SEADAS software (source: NASA), and the monthly composite of chl-*a* concentrations from Ocean color for the period from July 2002 to May 2014 were obtained at 4 km spatial resolution.

3.2.3 TMI Sea Surface Temperature (SST) data

SST data was retrieved from Tropical Rainfall Measuring Mission/Microwave Imager (TRMM/TMI). The SST data with a pixel resolution of 0.25^{o} have been obtained from the Asia-Pacific Data Research Center of University of Hawaii (http://apdrc.soest.hawaii.edu) for the study period i.e., July 2002 – May 2014. TMI is a multi-channel, dual polarized, conical scanning passive microwave radiometer composed to calculate rain rates over a wide swath beneath the TRMM satellite. The purpose of the device was comparable to that the another satellite radiometers but the data resolution and its capacity are enough better, since the satellite orbital motion at a lower height. TRMM comprises a semi-equatorial track with an angle of 35 degrees. This kind of orbit maintains nearby 7 degrees per day, providing the TMI for testing the surface at all times of the day, in

contrast to the polar-orbiting radiometers, where the sampling is done twice in a day. In addition to rain rates, TMI also measures cloud liquid water, columnar water vapour, ocean surface WS and SST. The first satellite TMI SSTs, where microwave SSTs have demonstrated to be great value for several fields of research. TMI sensor performed on the TRMM satellite. Table 3.2 described 5 channels. Two outside calibration aims (one is hot and another one is cold) were utilized for consistency in measurements during the time span. TRMM experienced an orbital boost in orbit (from 350 – 400 km) in August 2001 in order to prolong the lifetime of the satellite and onboard instruments. However, the TRMM orbit began to sink in the middle of 2014 as there was lacking of fuel to sustain the orbit. Remote Sensing Sensor continued routing data processing until 6th April-2015 just before the TRMM satellite was close down on 8th April-2015. These gridded data are arranged according to inspection of date. All are regulated Universal Time (UTC), called as Zulu Time (Z), Greenwich Mean Time (GMT), and world Time. after launch, i.e., 7th December-1997 to 31st December-2014 TMI data products are ready for the time period. Other Satellite Remote Sensing data available in a gridded and binary format (www.remss.com).

TRMM is a low orbiting (~350 km till 2001 and ~403 km from 2001 onwards) satellite that provides global coverage of the tropical region (40^{o} N – 40^{o} S). TMI is a radiometer onboard the TRMM satellite with a 9 channels and 5 frequencies with linearly polarized, passive microwave radiometric system. TMI operates at 10.65, 19.35, 21.3, 37, and 85.5 GHz frequencies to measures atmospheric and surface brightness temperature. At each frequency the radiance is received in both vertical (V) and horizontal (H) polarizations, except the 21.3 GHz frequency, which is received only in vertical polarization. The swath width is 785.5 km, covered by 104 low-resolution pixels or 208 high-resolution pixels. A complete description of the TRMM sensor is provided by Kummerow et al. (1998). The spacecraft launch vehicle and TMI sensor specifications are given in Table 3.2.

Table 3.2: Characteristic features of TMI

Spacecraft	TRMM
Launcher	H-II Rocket
Launch date	Nov 28 1997
Inclination	Approx. 35 degrees

Orbit	Non Sun synchronous
Altitude	Approx. 350 km
Repeativity	46 day
Sensors	TMI, PR, VIRS, CERES, LIS
	TMI (Sensor Specification)
Frequency	10.65, 19.35, 21.3, 37 & 85.5 GHz
Polarization	V/H (21.3 V only)
Swath	~760 km (878 km after August 2001)
Resolution	6-50 km (VIRS, 24 km)
Scan mode	Conical scan (49 degrees)
Data Rate	8.8 kbps
Weight	50 kg
Power	39 Watts

The data sets provided by TMI include SST, surface wind speeds, atmospheric water vapor, cloud liquid water and precipitation rates.

3.2.4 Merged AVISO Altimetry and Niiler Climatology Sea-Surface Height Data

Ocean altimetry observation is carried out fundamentally by using data from the the JASON-1, JASON-2 satellite missions and NASA TOPEX/Poseidon including other satellite altimeters (e.g., Enivsat and ERS). It is feasible to ascertain a long history of SSH measurements throughout the world's oceans by combining the measurements from all the satellites. Moreover , as illustrated by Polovina et al. (1999), SSH data can be used for determining geostropic currents for obtaining additional insights concerning the marine surface circulation dynamics. The SSH data employed is the Delayed-Time of AVISO reference product of Mean Sea-Level Anomaly (MSLA) that merges data from Jason-1/Envisat , TOPEX/Poseidon/ERS and Jason-2/Envisat. Furhter, the Near Real-Time MSLA Jason-2 dataset of AVISO is also used for additional the unavailable data sets and the Delayed-Time products. The spatially dispersed SSH data includes MSLA data in extension

to the SSH climatology (Niiler, 2003). The dataset encompasses satellite-derived Sea Surface height measurements collected as mean values of the TOPEX/Poseidon/ERS, JASON-1/Envisat, and Jason-2/Envisat satellite sensors. Monthly sea surface height anomaly data are derived from Merged AVISO Altimetry and Niiler climatology (http://oceanwatch.pifsc.noaa.gov/las/servlets/ constrain?var=15). The spatial resolution is 1/3 degree. The geographic coverage is global, and temporal coverage ranges from 1992-2014. The data is combined with a Niiler Climatology (Niiler et al., 1994).

3.2.5 NCEP/NCAR Monthly Mean wind speed (WS) data

NCEP/NCAR Reanalysis of Monthly Means of WS data for July 2002 to May 2014 were obtained. The NCEP/NCAR Reanalysis mission has two unique characteristics: (i) the interval of the period covered, and (ii) the assembly of a very comprehensive observational database. The reanalysis covers the 60-year period 1957 – 2015. The observations are hoarded in the World Meteorological Organization (WMO) binary general format representation.

The length of the reanalysis and the desire to carry it out as quickly as possible to increase its utility, a system has been desired to perform one month of reanalysis per day. As a result, the NCEP/NCAR reanalysis system has many novel features not yet present in operational or research numerical weather forecasting systems (dss.ucar.edu).

3.3 *In situ* data: chlorophyll-*a*

In situ ocean observations come from different sources with varying degrees of quality. The highest quality data are collected during scientific research programs, by instrumented buoys (both moored and free drifting) and by ships. *In situ* observations were sparse enough to give a comprehensive coverage of these parameters which are needed at every point (Charles Troupin, 2011).

In order to produce the high quality data sets, *In situ* data were treated with rigorous quality control methods These methods are concerned to eliminate values with time or position problems (e.g., data on land), removal of identical copies, recognition and revision of depth reversal problems, range monitoring in the ocean pans, limits of descriptive statistics, and biased removal of orderly erratic data points collected from cruise (Conkright et al., 1994a, 1994b, 1998). The data were interpolated to approved levels using 3 to 4 point

Lagrangian interpolation (Reiniger and Ross, 1968). We have not analyzed $1^{o}x1^{o}$ gridded *in situ* chl-*a* mean values as advised by Conkright et al. (1998) in the merged analysis.

We used real time oceanographic data from *in situ* observing systems. *In situ* data are available from 09 January 2013 to 07 October 2015, at 104 locations with latitude, longitude and depth. For the Eastern Equatorial Indian Ocean region, it covered from 0^{o} – 5^{o}S Latitude, 78^{o}E – 95^{o}E Longitude, at 10 days intervals.

3.3.1 Chlorophyll-*a* (ARGO data)

Argo is an international project launched to collect information on the chl-*a* of the upper part of the world's oceans. Argo uses robotic floats that spend most of their life drifting below the ocean surface. They make chl-*a* measurements when they come up to the surface and transmit their data to satellites, and after that they return to depth to drift for 10 days. The drifting depth and the cycle period can be programmed *a priori* based on individual requirements. By 2007, proposed array of 3000 floats producing 100,000 chlorophyll profiles per year are deployed in the Global Ocean. In Indian Ocean there are about 500 floats deployed by various participating countries, including India (figure 3.2).

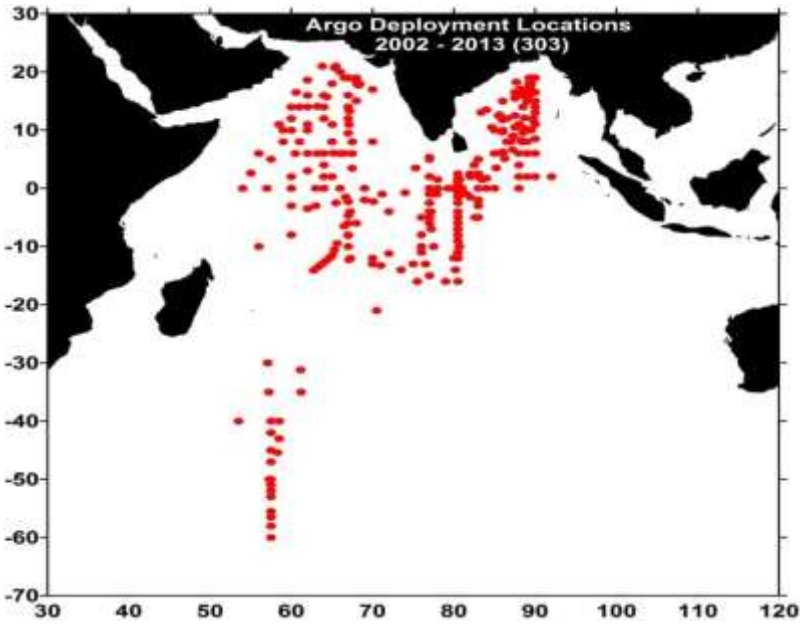

Figure 3.2 Map showing profiles of Argos deployed in the Indian Ocean.

Data from all these Indian floats upon transmission to ARGOS satellite are obtained from satellite data acquisition and processing system installed at INCOIS. Data is encoded in hexadecimal format, which is later decoded and individual profiles are obtained (figure 3.3). These profile data are subject to Real Time Quality Control (RTQC) and uploaded on to Global Data Centre (GDAC) within 24 hours. The profiles are also subject to Delayed Mode Quality Control (DMQC) and are made available to scientific community once in six months.

Argo is an universal mission to accumulate temperature data on the sea surface. It measures temperature when it come up to the surface of the ocean and transmits data to satellite, it drifts to ocean depth for ten days. Data from all the floats deployed by India upon transmission to ARGOS satellites are obtained from satellite data acquisition and processing system installed at INCOIS.

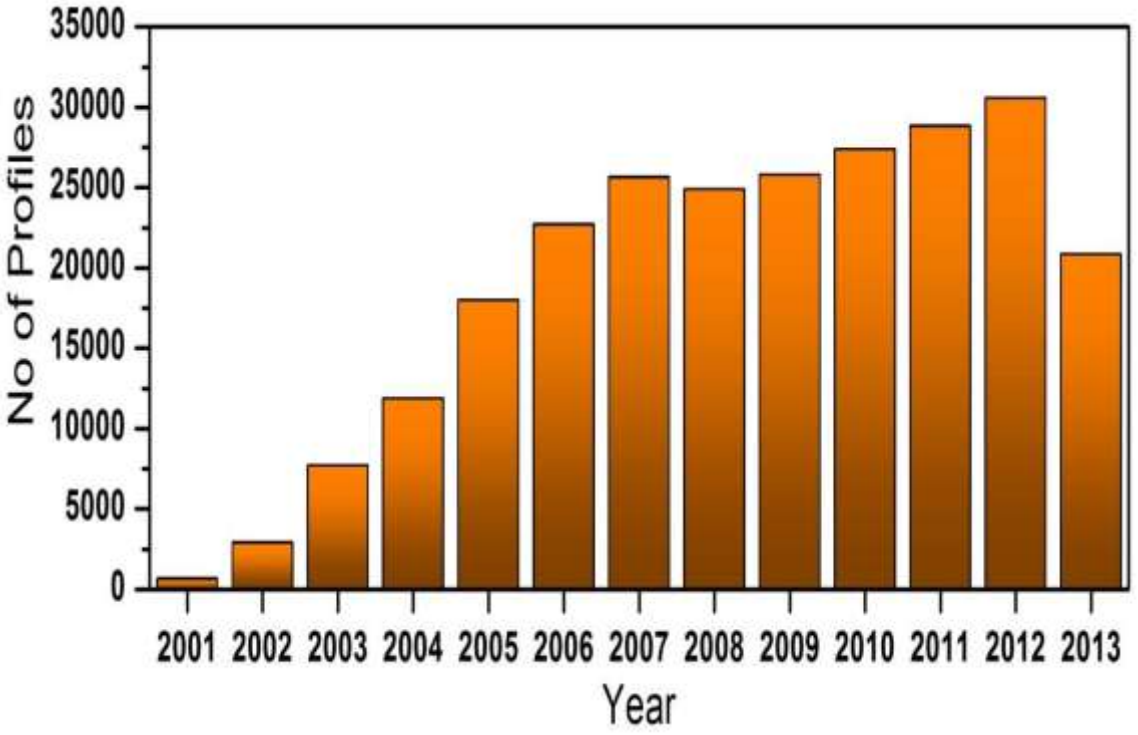

Figure 3.3 Year wise ARGO profiles constituting temperature and chl-*a*

Many value added products are generated utilizing these data sets. Value added products, based on individual float data are generated to access the performance of the float over a period of time. Data from all the floats are objectively analysed and spatial products ranging from ten days to month are generated. Data from all the floats along with the value

added products are made available on INCOIS website and also on INCOIS Live Access Server (LAS) for the access of users.

A new version of the "Argo Data and Products for Indian Ocean" is available for download. It is sequel to the version 2.1 developed by the Data Management and Information Group (DMG) of the Indian National Centre for Ocean Information Services (INCOIS), Hyderabad, India. The data can be interactively obtained by using the interface software developed in Java. This application works on Windows operating system and can be best viewed in 1024 X 768 screen resolution GUI for easy navigation, browsing, data extraction with user defined spatial and temporal Domains. Spatial Coverage is 45^{o} E – 95^{o} E and 5^{o}N – 5^{o}S and Temporal Coverage is January 2013 – December 2014 (http://www.incois.gov.in/argo/argo.jsp).

3.3.2 Comparison of satellite data with *in situ* data

Error estimate for an optimal combining data of *in situ* and satellite has been conducted. Provided with the less number of in situ observations contrasted to satellite measurements, the influence of the in situ data can be very inadequate in the final merged data. Due to this, in this section, in situ data data is compared with satellite data. The error statistics obtained in this section are decided using all in situ data by blending with either day-time or night-time satellite data, which is a proven method (Figure 3.4).

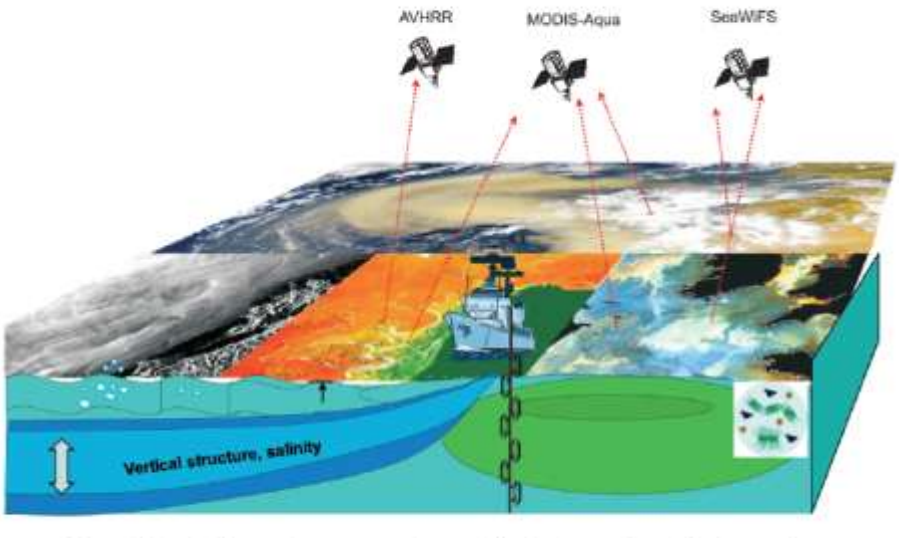

Figure 3.4 Schematic expression of comparison of *in situ* and remotely-sensed chl-*a* concentrations

Calculation of monthly anomalies

Monthly anomalies of Sea Surface Temperature and Sea Surface Heights are estimated by substracting the monthly climatology from the monthly observations in the study period (2002-2014).

3.4 Trend analysis of Time series data

We have done the Trend analysis by taking monthly data to find out the trend throughout the study period that is July 2002 to May 2014 for Indian Ocean region. To classify trend components in the time series data not approved "automatic" techniques. But, as long as the trend is single (consistently decreasing or increasing) consideration of such documents is not changed.. Smoothing forever includes few form of bounded averaging of data such that the If the time series data contain significant error, the primary step in the system of trend identification is smoothing nonsystematic parts of different views cancel every another out. The most general method is moving average smoothing which returns each element of the series by either the simple or weighted average of n surrounding elements, where n is the width of the smoothing "window" (Box and Jenkins, 1976; Velleman and Hoaglin, 1981). Medians can be utilised rather of means. The main advantage of median as compared to moving average smoothing is that its results are less biassed by outliers (within the smoothing window). Thus, if there are outliers in the data (e.g., due to measurement errors), median smoothing typically produces smoother or at least more "reliable" curves than moving average based on the same window width. The main disadvantage of median smoothing is that in the absence of clear outliers it may produce more "jagged" curves than moving average and it does not allow for weighting (ifg-izkf.uni-muenster.de).

In the moderately less general circumstances (in time series data), when the calculation failure is very high, distance weighted least squares smoothing or negative exponentially weighted smoothing methods can be applied. All those methods filter out the noise and change the data into a smooth curve that is moderately unbiased by outliers. A series with relatively few and systematically distributed points can be smoothed with bi-cubic splines.

Monotonous time series data can be adequately approximated by a linear function. The data need to be transformed first to remove the nonlinearity, if a clear monotonous

nonlinear component is present. Usually a logarithmic, exponential, or polynomial function is used.

3.4.1 Regression Analysis

We applied regression analysis method for chl-*a*, SST, SSHA and WS datasets to understand the correlation between chl-*a* and SST, chl-*a* and SSHA, chl-*a* and WS, also SST and SSHA throughout the study period that is July 2002 to May 2014 for weio region. The regression analysis tool performs linear regression by using the "least squares" method to fit a line through a set of observations. Rising regression analysis, we can understand that using the rising regression analysis, we can explain how a particular dependent variable is influenced by one or more independent variables. For instance, we can interpret how an automobile's performance is affected by factors such as weight, shape, and engine capacity. We can assign the share of each of the factor corresponding to the performance measure, based on a set of experimental data, and then use the effects to predict the performance of a new automobile.

The Regression analysis uses a sample from population generated by sampling analysis tool, treats the sample as input-range population. If the population is too big to process, we can use a characteristic sample. We can also produce a sample that comprises only the values from an appropriate part of a period whenever we assume that the input data is cyclic.

3.4.2 Student's t –test

The t-test measures for uniformity of the population means that carry individual sample. The tool operates on various assumptions: that the population variances are similar, that the population variances are not similar, and that the two samples describe after-treatment and before-treatment observations on the sample cases.

A t-test value,t, is calculated and presented as "t stat" in the output records. Based on the nature of data, t value can be negative or positive. Under the hypothesis of equal underlying population, which means, if $t<0$, "p(T<=t) on tail" provides the probability that a value of the t-stat would be observed which is more negative than t. The "t critical one-tail" gives the threshold value, so that the probability of finding a value of the t-stat is more than or equal to "t Critical one-tail" is Alpha.

A paired test is used when there is a natural pairing of observations i.e., when a sample group is tested before and after the experiment. This analysis is performed on a paired sample student's t-test to know whether observations are made before or after the treatment, which are expected to have come from distributions with equal population means. This t-test does not assume the variances of both populations as equal.

$$S^2 = \frac{n_1 S_1^2 + n_2 S_2^2}{n_1 + n_2 - 2}$$

S_1 = first Sample; S_2= second sample

n_1 = first observation; n_2= second observation

t-test: Assumption of Two-sample with equal variances

This anlaysis presents a two-sample student's t-test, assumes two data sets originated from distributions with the equal variance. This analysis is referred as a homoscedastic t-test. The t-test is used to decide if the two samples are expected to have originated from the equal population mean distributions.

t- test: Assumption of Two- sample with unequal variances

This t-test assumes that the two sets of data obtained from distributions of unequal variances. This analysis is referred as a heteroscedastic t-test. We can use this t-test to determine either of the two samples, expected to have appeared from distributions with same population means. This test can also be used when there are different subjects in the two samples. The paired test can also be used, as described in the following example, when there is a single set of subjects, two samples express measures for each subject before and after an experiment.

The following formula is used to determine the statistic t-value

$$t' = \frac{\bar{x} - \bar{y} - \Delta_0}{\sqrt{\frac{S_1^2}{m} + \frac{S_2^2}{n}}}$$

S1 = first Sample; S2= second sample

$\bar{x}$ = first sample mean; $\bar{y}$ = second sample mean

m = subject one; n = subject two

The formula given below is used to determine the degree of freedom (df). To obtain a critical value from the t-test of df, it is rounded to the nearest integer. It is due to the resultant of the calculation, which is usually not an integer. It is possible to compute a value for t-test with a non-integer df since the t-test uses the estimated df value without rounding. The results of t-test will differ in the unequal variances case due to different approaches in determing the degree of freedom.

$$df = \frac{\left(\frac{S_1^2}{m} + \frac{S_2^2}{n}\right)^2}{\frac{\left(S_1^2/m\right)^2}{m-1} + \frac{\left(S_2^2/n\right)^2}{n-1}}$$

S1 = first Sample; S2= second sample

$\bar{x}$ = first sample mean; $\bar{y}$ = second sample mean

m= subject one; n= subject two

All the data sets are subjected to t-test to find significance levels of the data using the the above formula.

3.5 Spectral analysis

We have applied spectral analysis methods for understanding the climate variations on regional and global scale for chl-*a*, SST, SSHA, and WS for WEIO. Spectral analysis is a method of decomposition of temporal signal into orthogonal periodic components with

different frequencies. For many oceanographic applications, the spectral representation of the signal (e.g. Chl-*a*, SST, SSH, WS) makes it possible to recognize and quantify the periodic or quasi-periodic components and distinct them from random and a episodic components. (A quasi-periodic module is characterized by a superposition of a number of periodic components with close frequencies). Apart from providing the spectral composition of a signal, spectral analysis makes it possible to filter the signal in a selected band (or bands) and analyze the filtered signal, as well as to estimate qualitatively the relative contribution of the variance of the signal in a particular band into the total variance of the signal. These procedures are based on specific properties of the spectral analysis such as orthogonality of the basic functions and demonstration of the energy of the signal through the spectral components via the Parseval's theorem.

Spectral analysis has certain limitations. The magnitude of a given spectral component describes the complete time period of the investigation. It does not contain evidence about the time variability of this component. Such information can be acquired by restoration of the signal in a interest frequency band, which is by summing up the spectral components in this band. On the other hand, one can evaluate a sequence of spectral decompositions of a signal in a moving time gap. In this case, the calculated spectral components can be attributed with the middle time of the corresponding time window, while the half width of the window can characterize the related uncertainty.

3.5.1 Detrending

To eliminate the trend from the time series of chl-*a*, SST, SSHA and WS datasets, we have done detrending. If a slow trend is seen in time series, there is a slow change in property of the variable over the whole interval under study. Trend is occasionally defined as a long term change in the mean value, but can also refer to change in other statistical parameters. For example, tree-ring series of evaluated ring size often have a trend in variance in addition to mean value. By tradition, periodic or seasonal components, and irregular oscillations, and the other parts were studied individually. Detrending is the mathematical or statistical operation of eliminating trend from the series and is regularly applied to remove a feature that distorts. In climatology, temperature trend might confound the relationship between solar radiation and air temperature due to urban heating. Detrending is also used as a preprocessing step to prepare time series for analysis in a systematic way. Several alternative approaches are available for detrending. Simple linear trend in the average can be removed by

substracting a least-squares-fit straight line. Additional complex trends might require different methods.

3.5.2 First Difference

Differencing can help stabilize the mean of a time series by moving changes in the level of a time series, and so eliminating trend and seasonality.

Auto Correlation Function (ACF) plot is useful to identify the non-stationary time series. The ACF is zero for stationary time series, while for the non-stationary data ACF decreases. Also, the value of r_1 is frequently positive and large for non-stationary data (https://www.otexts.org/fpp/8/1).

r_1 = difference between consecutive observations

The first difference of a time series is differences from one period to the subsequent. If Yt expresses the value of time series Y at period t, next the first difference of Y at period t is equal to Yt-Y-1. In statistics, DIFF(Y) is an expression of first Y difference and Y_DIFF1 in RegresIt. Y first difference is fixed and also entirely random (not auto-correlated), by a random walk model Y was described: every value is a random action apart from the previous value. When Y difference is stationary but not completely random – i.e., if its value at t period is auto-correlated with its value at previous times—then a further complicated forecasting model such as exponential smoothing or ARIMA can be appropriate.

(http://people.duke.edu/~rnau/411diff.html)

3.5.3 Seasonal differencing

To eliminate the seasonal and annual cycles from the time series of chl-*a*, SST, SSHA and WS datasets in order to understand the influence of IOD and ENSO, we have done seasonal differencing of the data. The difference between an observation and the corresponding observation from the previous year can be referred as a seasonal difference.

$Y'_t = y_t - y_{t-m}$ here m is number of seasons

also called "lag-*m* differences" as we substract the observation after a lag of *m* periods.

If seasonally differenced data seem to be white noise, then suitable model for the original data is

$$y_t = y_{t-m} + et$$

Forecasts from this model are equal to the last observation from the relevant season. That is, this model gives seasonal naïve forecasts.

3.5.4 Power Spectral Density

Power Spectral Density (PSD) is a measure of power intensity of a signal in the frequency domain. In practice, the PSD is computed from the FFT spectrum of a signal. The PSD helps way to characterize the amplitude versus frequency content of a random signal. PSDs are used to represent the control and input channel signals in the Random control system.

Random vibration is experienced every day in the real world. Motions are experienced every day in the real world. The motion experienced on the back of a truck, the hold of an airplane or ship, the bed of a flatcar during travel are all random vibrations. It is motion at many frequencies at the same time. The amplitude at these frequencies varies randomly with time. The usual way to describe random motion is in terms of its power spectral density.

The name "Power Spectral Density" comes from the study of random variations of the power absorbed in an electrical circuit. Although developed for electrical engineering applications, the same theory is applicable to mechanical vibration applications. Vibration testing typically uses acceleration measurements so "Acceleration Spectral Density" is a more apt name but "PSD" has been adopted by the industry.

3.5.5 Wavelet analysis

Applied the wavelet analysis to all the chl-*a*, SST, SSHA, and WS for understanding the climate variations on regional and global scale. To explore the stationary characteristics of the peaks obtained by the power spectrum of the SSA-RC time series, we have applied the Morlet based wavelet transform approach (Holschneider, 1995; Foufoula-Georgiou and Kumar, 1995; Torrence and Compo, 1998; Grinsted et al., 2004). Wavelet analysis is used for analyzing localized variations of power within a time series. By composing a time series into time-frequency space, one is able to determine both the dominant modes of variability and how those modes vary in time. The wavelet transform has been used for numerous studies in geophysics, tropical convection, including Physical Oceanography (Weng and Lau, 1994), the El Nino- Southern Oscillation (ENSO; Gu and Philander, 1995), atmospheric cold fronts

(Gamage and Blumen, 1993), central England temperature (Baliunas et al., 1997), the dispersion of ocean waves (Meyers et al., 1993), wave growth and breaking (Liu,1994), and coherent structures in turbulent flows (Farge, 1992). A complete description of geophysical applications can be found in Foufoula – Georgiou and Kumar (1995), while a theoretical treatment of wavelet analysis is given in Daubechies (1992). Many researchers regard wavelet transform as an interesting divesion that produces colorful pictures, but purely qualitative results.

To study the spatial temporal behavior of the spectral composition of the signal in time, one could apply DFT to the time restricted subsets of the signal, for example, by computing running Fourier spectra of the signal for a smaller time window. An alternative technique for studying the temporal dynamics of a time series that has became very popular in the last few decades is wavelet analysis (e.g. Emergy and Thomson, 2001, p. 500). This term refers to the application of the wavelet transform. In particular, it is not suitable for filtering the signal because the individual components of the decomposition of the signal are not, generally, orthogonal. Wavelet analysis is conducted by applying wavelet transform to the time series of the signal. We used software of C. Torrence and G. Compo (http://paos.colorado.edu/research/wavelet) and customized it for analysis of our data sets.

3.5.6 Cross wavelet transform

The cross wavelet transform (XWT) of two time series x_n and y_n is defined as $W^{xy} = W^x W^{y*}$, where * denotes complex conjugation. We further define the cross wavelet power as $|W^{XY}|$. The complex argument arg (W^{xy}) can be interpreted as the local relative phase between x_n and y_n in time frequency space. The theoretical distribution of the cross wavelet power of two time series with background power spectra P_k^y and P_k^y is given in Torrence and Compo (1998) as

$$D\left(\frac{\left|W_n^X(s)W_n^{Y*}(s)\right|}{\sigma_X\sigma_Y} < p\right) = \frac{Z_\nu(p)}{\nu}\sqrt{P_k^X P_k^Y},$$

Where Zv(p) is the confidence level associated with the probability p for a pdf defined by the square root of the product of two χ^2 distributions.

3.6 Software used

The data analysis and visualization has been done using Matlab scripts. The only exception are the scripts used for wavelet analysis, which are based on the Matlab code provided by C. Torrence and G. Compo (1998), and is publicly available at http://paos.colorado.edu/research/wavelets. The code was adapted for the current thesis needs.

3.7 Spatial autocorrelation

Spatial autocorrelation tests and interpret the degree of dependence with measurements in a geographic space. Model spatial autocorrelation statistics cover Moran's I, Geary's C, Getis's G and the standard deviational ellipse. These statistics require calculating a spatial loads matrix that replicates the strength of the geographic connection within observations in a neighbourhood, e.g., the distance between neighbours, the distances of shared boundary, or they fall into a stated directional class such as "west". Model spatial autocorrelation statistics examine the spatial weights to the covariance correlation at sets of places. Spatial autocorrelation that is extra positive than expected from random indicates the clustering of similar values across geographic space, during important negative spatial autocorrelation intimates that nearby values are major different than assumed by an outcome, proposing a spatial design associated with a chess board.

Spatial autocorrelation statistics such as Moran's I and Geary's C are global in the sense that they measure the overall degree of spatial autocorrelation for a dataset. The occurrence of spatial heterogeneity advises that the expected degree of autocorrelation can differ significantly beyond geographic space. Regional spatial autocorrelation statistics give assessments disaggregated to the level of the spatial separation units, allowing evaluation of the dependence correlations across space. G statistics compare neighbourhoods to a global standard and recognise limited areas of substantial autocorrelation. Local variants of the I and C statistics match neighbourhoods to a global standard and distinguish bounded regions of sharp autocorrelation. Bounded variants of the I and C statistics are also possible.

Lagged correlation is the correlation between two-time series delayed in time about other. Lagged correlation exhibits the correlation between time series for two regions. First, time series presents a delayed response to the another time series data, or possibly a delayed response to a general stimulus that influences both time series. Second, the response of first

time series to the second time series or an external stimulus can be "smeared" in time, sucha that a stimulus is confined to one detection obtains a response at various observations. For instance, because of storage in reservoirs, glaciers, etc., the volume discharge of a river in one year may depend on rainfall in the previous several years. Due to the changes in crown density and ate photosynthate storage; the width of a tree-ring within a year may depend on the climate of previous years. The simple correlation coefficient between the two time series aligned in time is insufficient to describe the relationship in such circumstances. As an alternative to the simple correlation coefficient, we examine the cross-correlation function and the impulse response function. The correlation between the time series shifted upon one another as a function of the number of observations of the offset is called as the cross-correlation function. The predicted cross-correlations function may be deformed and deceptive as a measure of the lagged relationship if the individual series are auto-correlated. We study two procedures to explain the pattern of cross-correlations. One is to remove the persistence of the two series before cross-correlation estimation. In this method, the two series are typically regarded on an "equal footing". The second method is the "system" approach, in which one series is observed as input and the other series as output from a dynamic linear system. The lagged response is evaluated from the "impulse response function", which is the response of the output at present and future to a hypothetical "pulse" of input limited to the present time. Calculation of the impulse response function involves use of the same filter and output series, succeeded by cross-correlation of the filtered series. The filter is designed to whiten the input series.

3.8 Composite analysis

The composite analysis is based on the assumption of monthly variations in data are relatively small and that for a given region data from a preceding month will represent the actual values quite well. The validity of this assumption may vary spatially and seasonally as oceanic and atmospheric forcing create higher frequency changes in variable and can be examined by measuring the accuracy of the data composite as a function of data potential. Several versions of the compositing method were evaluated during the development process.

There are a number of steps necessary to form composites of any given phenomenon. The first step is choosing a basis for the analysis, more specifically a positive and negative basis must be chosen. In prior work on ENSO composite analysis, generally the positive basis is used to describe El Niño events, and the negative basis is used to describe La Niña events.

In this study, a different basis has been applied to the various indices. For the Oceanic Nino Index (ONI), the basis used is the same used to determine events, or a five month period of overlapping three month seasons with an anomaly of greater than 0.4 degrees Celsius. For the Multivariate ENSO Index (MEI) and Southern Oscillation Index (SOI), a value of greater than 0.4 degrees Celsius. For the MEI and SOI, a value of greater than 0.5 standard deviations from the mean is used for the basis. Initially a basis of 1 standard deviation was used, but in the interest of achieving a complete period of ENSO events in each month, it was relaxed. Different time scales are used for composites depending on the index as well. Specifically, the MEI uses two month seasons, the ONI uses three month seasons.

Chapter 4

Chlorophyll-*a*, Sea Surface Temperature, Sea Surface Height and Wind Speed: Central Equatorial Indian Ocean

4.1 Introduction

The abundance of phytoplankton, microscopic marine plants that can convert inorganic carbon dioxide into organic carbon through photosynthesis in the upper layers of the ocean, plays an important role in the global carbon cycle through the biological pump and therefore, is of utmost importance in climate change studies (Behrenfeld et al., 2006). Its concentration (measured as the chl-*a* concentration) is a quantity of biomass at the stand of the oceanic food series and has been shown to influence the top-level predators such as fish (Lehodey et al., 1997). Planktonic ecosystems strip the nutrients such as nitrate, silicate and phosphate out of the surface layers of the ocean during the photosynthesis and thus they also contribute towards biogeochemical cycling of important chemical elements (Ravichandran et al., 2012). Among the various factors that regulate the growth of phytoplankton, presence of sunlight and nutrients are the most important factors; the latter is mainly controlled by the oceanic circulation pattern and mixed layer dynamics (Behrenfeld et al., 2006). These factors vary on inter and intra-annual scales and phytoplankton abundance also varies on similar scales. Though our understanding on variation in physical properties of the ocean has improved significantly over the last two decades, but the knowledge on phytoplankton distribution in relation to SST and wind dynamics is limited.

Wind is one of the major factors that govern upwelling and vertical mixing in the upper ocean. The large-scale correlation patterns between WS and chl-*a* concentration suggest different limiting factors for phytoplankton biomass in different parts of the world ocean. Monthly anomalies of WS and SST are mostly negatively correlated over the world ocean (Kahru et al., 2010), in most regions consistent with the hypothesis that increased wind speed cools the surface by vertical mixing that works by deepening the surface mixed layer and transferring nutrients from deep water to the surface. Areas with positive correlation between monthly SST anomalies and WS anomalies, e.g., in the eastern tropical Atlantic and Pacific, are controlled by the variation in interannual modes (Murtugudde et al., 1999;

Signorini et al., 1999). The spatial distribution of SST in the Indian Ocean is characterized by cooler water on the west which is in contrast to Pacific and Atlantic Oceans where it is warmer on the west. In fact, all characteristic properties of the ocean show marked east-west asymmetry in Indian Ocean. Freshwater input into the northern Indian Ocean is greater on eastern side because of monsoonal rains and river discharges causing the eastern part of the basin less saline than the west. A major upwelling system is located off the western boundary of the Arabian Sea and consequently biological productivity is higher in the west compared to the east. The thermocline also is deeper in the east than in the western Indian Ocean (Vinayachandran et al., 2009). Feng and Zue (2012), based on the observations during 2003-2009, state that the global ocean chl-*a* concentration is increasing while the SST is decreasing.

Equatorial Indian Ocean (EIO) is markedly different from other equatorial regions of the world ocean as the semiannual reversal of the wind system over the region causes reversal of the surface current. Another distinction of EIO is the lack of equatorial upwelling, unlike the equatorial Pacific and Atlantic Oceans (Schott et al., 2001). Therefore, biological productivity in the equatorial Atlantic and Pacific is usually higher than that in the EIO. It is also evident in the satellite-derived chl-*a* images where the chl-*a* concentration over EIO is very low compared to the northern Indian Ocean region, and therefore, has been referred as a 'biological desert' (Prasanna Kumar et al., 2009; Narvekar and Prasanna, 2010). Sorokin et al. (1985) observed high primary production in areas of divergence and in waters of the trade wind currents, whereas decreased primary production in areas of convergence. Vertical displacement of the thermocline due to local wind stress causes small scale phytoplankton bloom (chl-*a*>1 mg m^{-3}) in the latitudinal band of 5ºN to 10ºN in the central and western Indian Ocean (Murtugudde et al., 1999). Central Equatorial Indian Ocean powerfully affected by physical action on intraseasonal to interannual time scales. During inter-monsoon period semi-annually occurring eastward propagating Wyrtki jets, equatorial westerly winds are developed (Strutton et al., 2015).

The main objective of this work is to understand the monsoonal variability of chl-*a* concentration and SST and to evaluate their interrelationship over the Central Equatorial Indian Ocean (CEIO). We have analyzed Aqua MODIS satellite-derived time series data of ocean chl-*a* concentration, TMI SST, TOPEX SSHA, NCEP/NCAR derived WS to achieve this objective and the findings are reported in this chapter.

4.2 Time Series Trends

4.2.1 Chlorophyll-*a*

The area averaged chl-*a* concentration in the CEIO for the period 2002 - 2014 is shown in figure 4.1. The area averaged chl-*a* concentration varied from 0.09 mg m^{-3} to 0.22 mg m^{-3} during the study period. A minimum of areal average of chl-*a* concentration of 0.09 mg m^{-3} is recorded in June 2011 and a maximum of 0.22 mg m^{-3} recorded in December 2005. Five peaks of high concentrations of chl-*a* (0.22 mg m^{-3} in December 2005, 2010; 0.21 mg m^{-3} in October 2003, February 2014; 0.19 mg m^{-3} in September 2004) are observed.

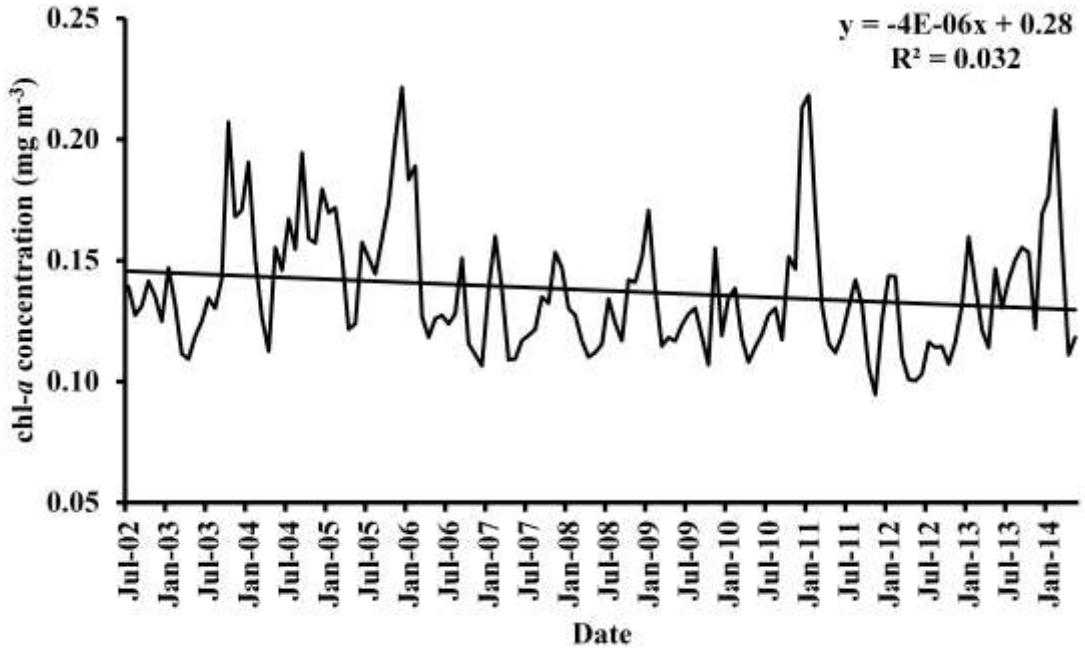

Figure 4.1 Area averaged monthly time-series of chlorophyll-*a* showing decreasing linear trend in the Central Equatorial Indian Ocean (Latitude $5^oN – 5^oS$, Longitude $65^oE – 80^oE$) study period 2002-2014.

It is clearly evident from the figure 4.1 that high chl-*a* concentration is found during months of October - December. This high chl-*a* concentration may be due to the triggering of enhanced horizontal advection generated near the Maldive Islands, which contributes to biological productivity along the EIO from the north. This enhanced biological production extends eastward from Maldives up to 80.5^o E during October - December; when the Wyrtki jets are well developed during fall (Sasamal, 2007). The second hypothesis on enhanced chl-*a* is that Wyrtki jets and wind stirring are responsible for the bringing up the mixed layer of

rich nutrients to the surface, and the enrichment of the mixed layer through cool thermocline water. This cooling event is responsible for the increase of surface chl-*a* concentration (Vinayachandran and Saji, 2008). Strutton et al. (2015) evaluated both the hypotheses using moored chl-*a* observations and modeled results and they found credence to both the hypotheses. However, the second hypothesis is supported by a positive correlation between wind speed and chl-*a* and a negative correlation between wind speed and mixed layer temperature (Strutton et al., 2015). But our results do not show positive correlation between wind speed and chl-*a*, and therefore, we suggest that the first hypothesis is at play in the CEIO. Chl-*a* concentration starts decreasing from March onwards and continues until the arrival of summer monsoon i.e., up to June. The cloud cover during the summer monsoon period i.e., from June to August, prohibits the satellite observations from capturing more accurately the chl-*a* variability as suggested by earlier researchers (Prasanna Kumar et al., 2009). In September the chl-*a* concentration is fairly high (but relatively less, compared to February/March) probably fuelled by the advection of nutrients upwelled in the southwestern region (Prasanna Kumar et al., 2001).

Surface chl-*a* concentration was significantly higher during the years 2003-2006 than the other years. Variability of chl-*a* plot (figure 4.1) for 2002 to 2014 period shows that the year 2005 has recorded highest value (0.22 mg m^{-3}) but tended to decrease from 2006 to 2009. It appears to increase again after December 2010. Interestingly, the highest chl-*a* concentration is observed during the month of December but these observations may be biased due to unavailability of clear satellite data during the summer monsoon months for better comparison. Nevertheless, this time of year would be the most appropriate to study chl-*a* concentration in EIO. In the southeastern Arabian Sea productivity is moderately significant during the summer monsoon season owing to the low intensity of upwelling in the region (Wiggert et al., 2005; Prakash et al., 2012), whereas during Northeast monsoon, the northern Arabian sea is more productive, when the convective mixing brings rich bottom nutrients to the ocean surface triggering high biological productivity (Madhupratap et al., 1996; Prakash et al., 2012). Further, water at the surface usually has higher concentrations of dissolved oxygen than the deeper water. This effect may be modified by the fact that warmer surface water cannot hold as much oxygen as deeper colder water. It is not well established whether these processes have a bearing on the productivity in the CEIO. Overall, no significant trend of chl-*a* was observed during 2002-2014 over the study region, which is evident from the regression analysis (R^2 = 0.03; significant at 0.05 level figure 4.1).

Increasing linear trend in the monthly mean chl-*a* for Equatorial Indian Ocean has been reported by Bureau of Meteorology Australian Government. The time series of chl-*a* in the Somali coast has two significantly distinct trends – consistent increase from 1998 to 2003 and decreasing trend after 2003 (Prakash et al., 2012), which is similar to our observations in the CEIO.

4.2.2 Sea Surface Temperature (SST)

To understand the observed variability of chl-*a* concentration, we also analyzed SST over the region. A sinusoidal variation of temperature was observed during the period 2002-2014 and varied in the range of 28.05^{o} - 31.05^{o} C. Time series of SST for the study period over the CEIO is shown in figure 4.2. The area averaged SST in the CEIO showed primary peak during April-May with a value of 30.5^{o}C and minimum SST of 27.6^{o}C during July-August. The high SST was also observed during October-November. Low SST values during December 2005 and December 2010 (28.05^{o}C), similar results already proved in his M.Tech thesis by Mohanty (2008) that is SST decreases due to cold fronts formation with north east monsoon winds during December and high peak of SSTs in the month of April 2010 (31.05^{o} C) were recorded. SST anomaly trend is positive, but not significant during the study period (figure 4.2), which is in contrary to the observations made by Prakash et al. (2012) over western Indian Ocean.

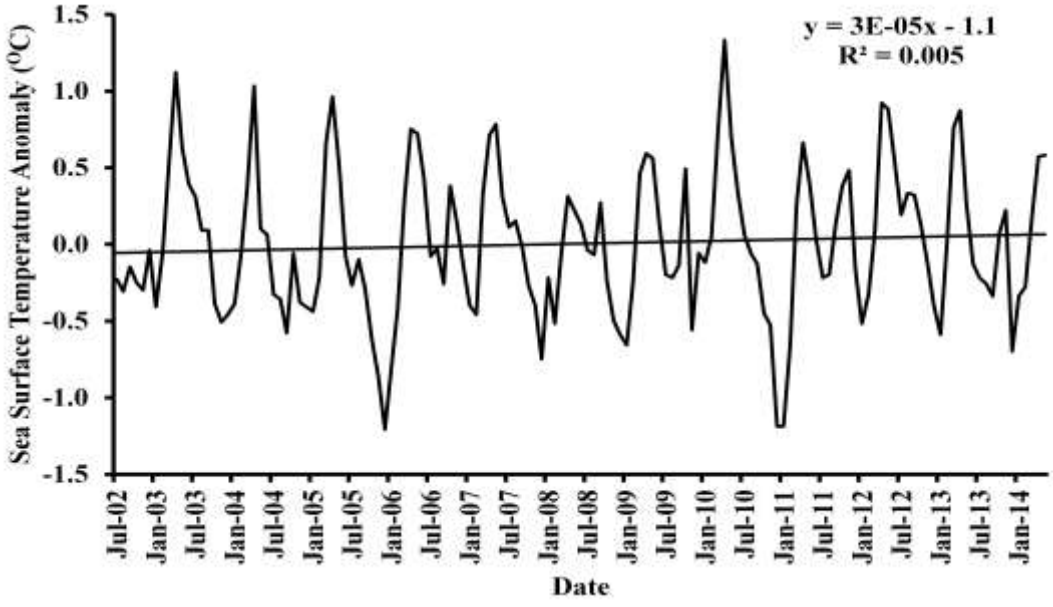

Figure 4.2 Area averaged monthly time-series of Sea Surface Temperature anomaly showing increasing linear trend in Central Equatorial Indian Ocean for the study period 2002 - 2014.

As SST is also an indicator of the vertical mixing and has remained almost the same over the past eight years which clearly indicates that there is no significant shift in terms of dynamics such as upwelling or winter mixing in this region. However, a significant fall in the SST (~3ºC) during winter and moderate decrease during the summer (~1-2ºC) occurs in this zone (20°N to 25°N and 62°E to 75°E) which explains the presence of relatively high surface chl-*a* during the winter monsoon i.e., in December month. It is well established that mixing of deeper water with the surface water causes decrease in SST and supplies nutrients to the upper layers which enhances the productivity and hence the high surface chl-*a* (Prakash and Ramesh, 2007).

4.2.3 Sea Surface Height Anomalies (SSHA)

The area averaged SSHA in the CEIO for the period 2002 - 2014 is shown in figure 4.3. The area averaged SSHA varied from -6.7 cm to 8.4 cm during the study period. A minimum of areal average of SSHA of -6.7 cm is recorded in December 2003 and a maximum of 8.4 cm recorded in July 2012. Four peaks of high SSHA values are (8.4 cm in July 2012; 8.0 cm in June 2008; 7.9 cm in July 2013; 6.9 cm in June 2007). Overall, increasing linear trend of SSHA was observed during 2002-2014 over the study region, which is evident from the correlation analysis of SSHA (R^2=0.22) for CEIO.

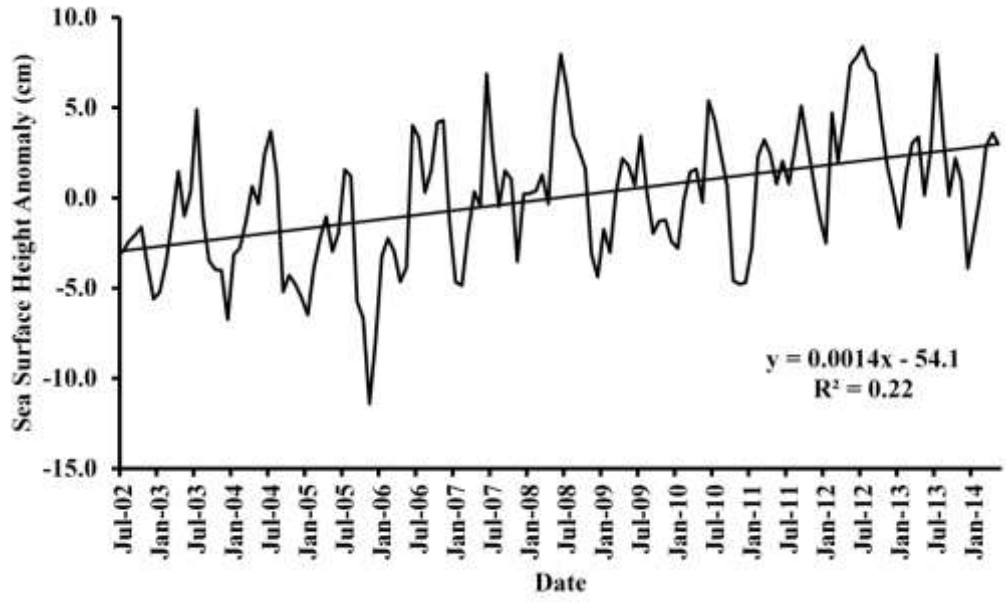

Figure 4.3 Area averaged monthly time-series of Sea Surface Height anomalies showing increasing linear trend in the Central Equatorial Indian Ocean for the study period 2002- 2014.

Climate-change consequences on the Indo-Pacific warm pool influences the islands in the middle of the Indian Ocean to experience significantly increased Sea Surface Height than the global mean. Consequently, several islands and coasts in the Indian Ocean also coastal population suffer from elevated environmental stress (http://www.unep.org/).

4.2.4 Wind Speed (WS)

The area averaged WS in the CEIO for the period 2002 - 2014 is shown in figure 4.4. The area averaged ws varied from 3.18 m s^{-1} to 7 m s^{-1} during the study period. A minimum of areal average of ws is 3.18 m s^{-1} is recorded in May 2007 and a maximum of 7 m s^{-1} recorded in November 2004. Three high peak ws values are (7 m s^{-1} in November 2004; 6.2 m s^{-1} in November 2013; 5.62 m s^{-1} in April 2011; 5.6 cm in February 2005). Overall, no significant linear trend of WS was observed during 2002-2014 over the study region, which is evident from the regression analysis of ws (R^2=0.0008) for Central Equatorial Indian Ocean (Figure 4.4).

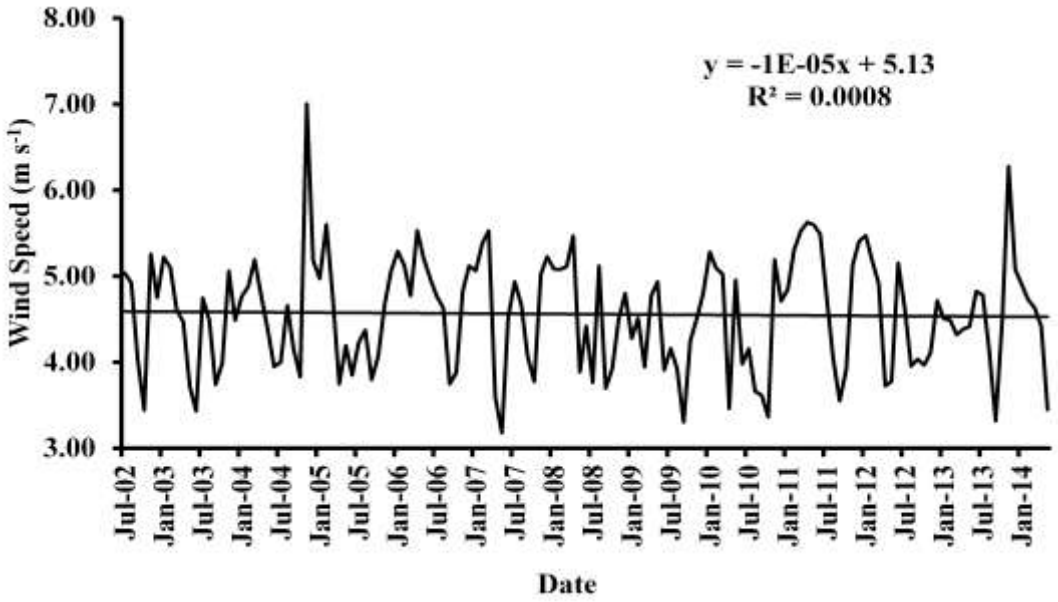

Figure 4.4 Area averaged monthly time-series of Wind Speed in the Central Equatorial Indian Ocean. The decreasing trend is clearly seen.

4.3 Inter-relationships

We found reasonable correlation between SST and surface chl-*a* concentration (R^2= 0.57; p<0.05) (figure 4.5). Statistical test ('student's *t*-value') shows that correlation between chl-*a* and SST is significant at 0.05 level. Unlike in WEIO, here the relationship is more or less linear, as upwelling seldom occurs.

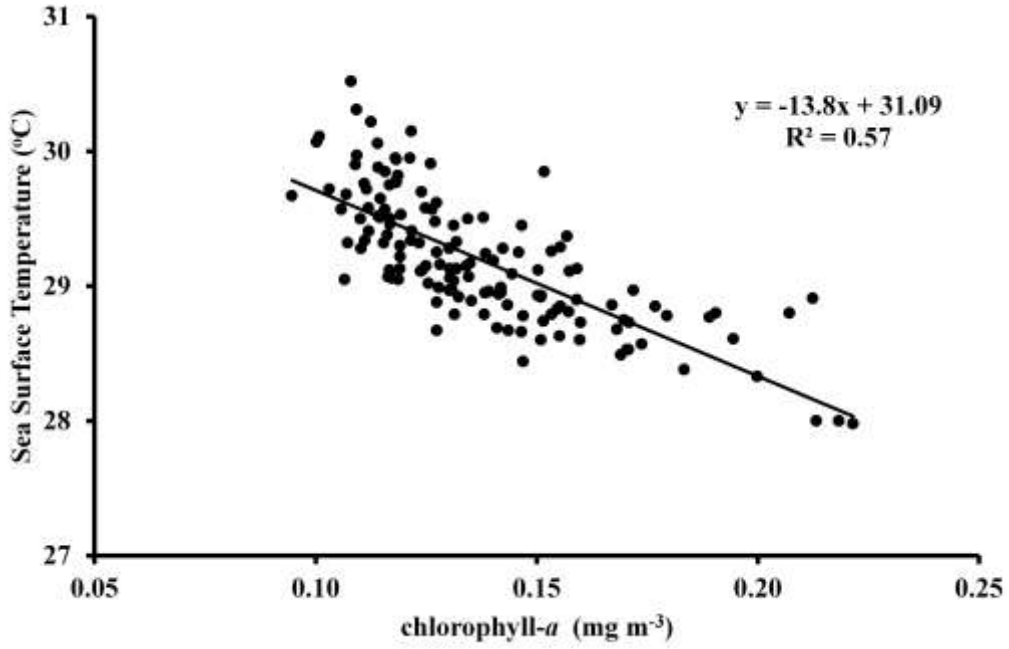

Figure 4.5 Scatter plot of the monthly chlorophyll-*a* concentrations versus SST showing strong (R^2=0.57) (p<0.05) significant at 0.05 level. The straight line represents least squares linear fit with slope (-) 13.8 and intercept at 31.1.

Similar relationship has earlier been reported from the northern Indian Ocean (Goes et al., 2005; Prakash and Ramesh, 2007). There appears to be lag of one month's time between SST and enhancement in surface chl-*a* concentration as indicated by the negative correlation (R^2=0.42). This lag may be due to the triggering of enhanced horizontal advection and Wyrtki jets. Open ocean chl-*a* concentration may play key role in controlling SST by trapping the surface layer solar radiation. When the open ocean chlorophyll-*a* concentration is high, SST can be increased (Mohanty, 2008).

Also we have seen weak correlation (R^2=0.01; not significant at 0.05 level) between chl-*a* concentration and wind speed from the 'student's *t*-value' (figure 4.6).

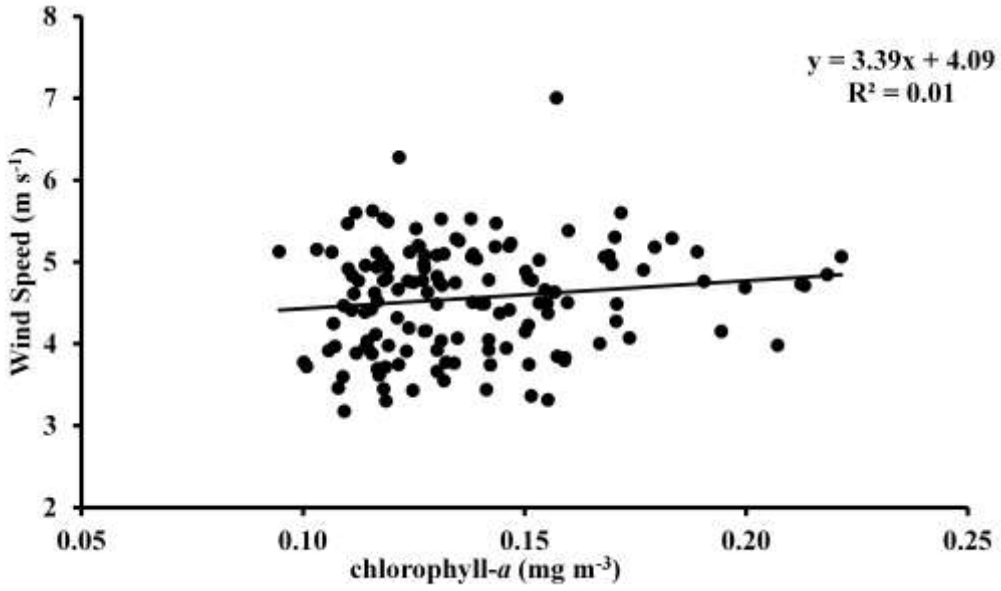

Figure 4.6 Scatter plot of monthly chlorophyll-*a* concentrations versus wind speeds showing weak insignificant correlation R^2=0.01. The straight line represents least square linear fit with slope 3.39 and intercept at 4.09 in the central equatorial Indian Ocean for the period 2002-2014.

4.4 Discussion

The variability at different time scales is evidenced and the focus of this study is to highlight the variability in each parameter and coherence among them and discuss the dynamics behind such coherence. We have applied the power mathematical tools of Fast Fourier Transform (FFT) and wavelet analysis for understanding the climatic variations on regional and global scale. As a preliminary step, we have applied the power spectrum analysis to all the four data sets. Power spectrum plots of the data sets which clearly indicate two dominant peaks at 54 and 25 weeks cyclicity corresponding to 12 and 6 months respectively. These peaks are coherent and found to be common in all our data sets suggesting the presence of annual and semi-annual cycles.

In order to study the periodicities on inter-annual scale, we have done de-seasonalization of the data. This becomes essential as the temporal extended term and medium term trends in the dataset can be affected by the seasonal oscillations. In order to avoid the spurious signals triggered due to these seasonal variations in the long term trend analysis, de-seasonalization is done. De-seasonalization has been done by using moving average. Based on the cyclical nature of dataset, the moving average window size function is

chosen. Generally, the datasets tend to have one year cycle. Hence the moving mean function gap is 12 time steps (since the dataset is monthly). Linear regression trend analysis is repeated on the de-seasonalized dataset. This may or may not have different trends when compared with the trend analysis done on the original anomaly dataset.

The power spectral density plots for SST, chl-*a*, SSHA and WS are shown in Figure 4.7. The power spectral density (PSD) plot of SST shows two strong low-frequency maxima corresponding to ~ 32, and 16-18 month periods i.e., 3 and 2 years respectively (Figure 4.7a). This clearly suggests the presence of quasi-biennial signals (2-3 years periodicity) in SST anomalies of the Central Equatorial Indian Ocean (CEIO) (e.g. Meehl and Arablaster, 2001).

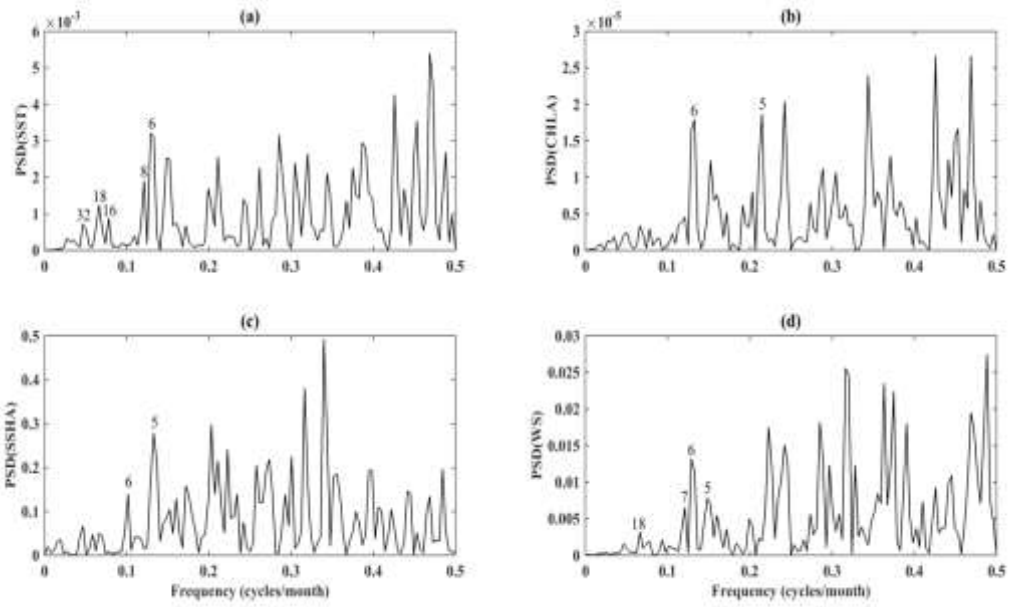

Figure 4.7 Power Spectrum plots of (a) Sea Surface Temperature, (b) chlorophyll-*a*, (c) Sea Surface Height anomaly, and (d) Wind Speed for the Central Equatorial Indian Ocean. A high power at 32, 16-18, and 6- 8 months is observed suggesting the implication of quasi biennial oscillations and also semi-annual variability in power spectrum of SST (figure 4.7a). The power spectrum of chl-*a* (figure 4.7b) data shows strong and well separated peaks at 5 and 6 months. Power spectrum of SSHA (figure 4.7c) shows significant peaks at 5 and 6 months, and WS (figure 4.7d) shows a high power at 18 and 5- 7 months period.

A strong peak at 4 months period is also observed from the power spectrum suggesting the implication of semi-annual variability in the SST anomalies (figure 4.7a). The PSD of chl-*a* data (figure 4.7b) shows peaks at 12-13, 5-8 and 5 months, whereas SSHA

shows peaks at 7-8, 5-6 and 4 months (figure 4.7c). The PSD of Wind Speed data (figure 4.7d) shows peaks at 18 and 5-7 months period emphasizing the influence of semi-annual variability in the data.

To explore the stationary characteristics of the peaks obtained by the power spectrum of the reconstructed (RC) time series, we have applied the Morlet based wavelet transform approach (Holschneider, 1995; Foufoula-Georgiou and Kumar, 1995; Torrence and Compo, 1998; Grinsted et al., 2004). The wavelet spectrum identifies the main periodicities in the time series and helps to analyze the periodicities with respect to time (figure 4.8). Three consecutive positive IO Dipoles (pIODs) during 2006-2008 have been demonstrated by Cai et al. (2009). Semi-annual signal is weaker during IOD events (i.e., in 2006-2008) due to the absence of Wyrtki jet in fall and probably in spring as well. Joseph et al. (2012) show clear evidence of weakening of spring Wyrtki jets during the years 2006–2011, which apparently reflects the strengthening of easterly wind anomalies associated with IOD events occurred during the period of study.

Here we can clearly observe the occurrence of very strong IOD during the fall of 2006, and also the interference of the signal of 18 months and 32 months period for the constructive formation of IOD in 2008. The wavelet power spectrum of the SST data (figure 4.8a) shows high power around 32 months (January 2006 to June 2010) and 16 months (June 2010 to September 2012) suggesting the influence of ENSO and IOD on chl-*a* respectively. The wavelet spectrum of the chl-*a* data (figure 4.8b) shows high peak at 12 months (October 2003 to September 2004) clearly suggesting the annual cycle influence. The wavelet power spectrum of the SSHA-RC data (figure 4.8c) shows high power around 4-8 months period. The WS-RC data (figure 4.8d) show a strong signal at 36 months suggesting the influence of ENSO in the data.

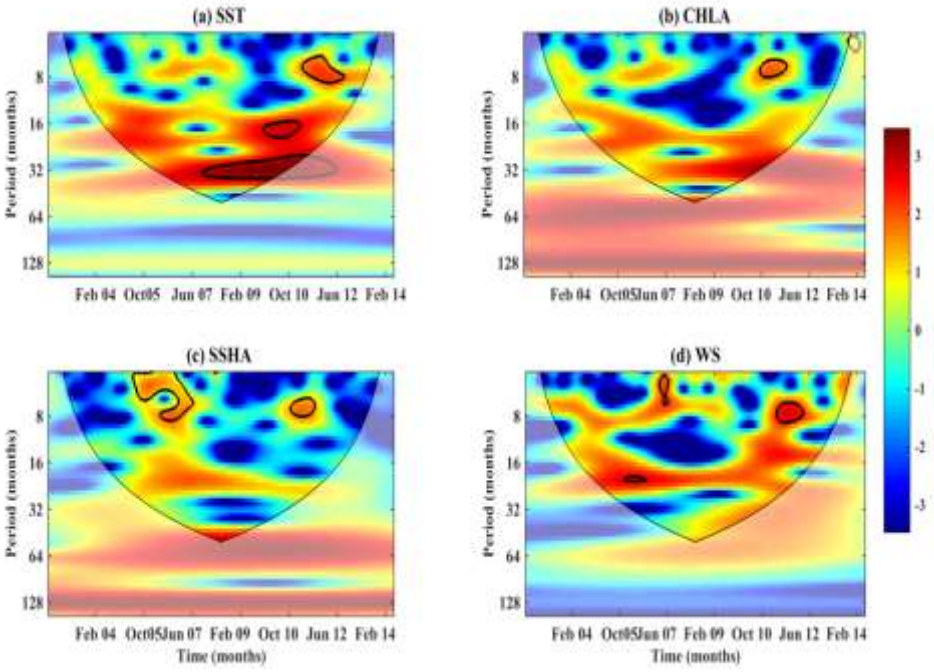

Figure 4.8 Wavelet spectrum of (a) Sea Surface Temperature, (b) chlorophyll-*a*, (c) Sea Surface Height Anomaly, and (d) Wind Speed for the Central Equatorial Indian Ocean.

The wavelet spectrum of SST-SSHA-chl-*a* depicts a statistically significant power at around 32, 16-18 and 6-12 months at > 95% significance level, and suggests a clear imprint of ENSO-IOD on the SST-SSHA-chl-*a* data.

In order to have the better visualization of time series for two similar periods and for the interpretation of the results, cross wavelet spectrum is applied. Figure 4.9 shows the cross wavelet spectrum of (a) chl-*a*-SST, (b) chl-*a*- SSHA, (c) SST-SSHA and (d) chl-*a*–Wind Speed data. The contours (dark black lines) are the enclosing regions where the wavelet cross power is significantly higher at 95% confidence level. The phase relationship is shown in arrows with inphase pointing to right, antiphase pointing to left.

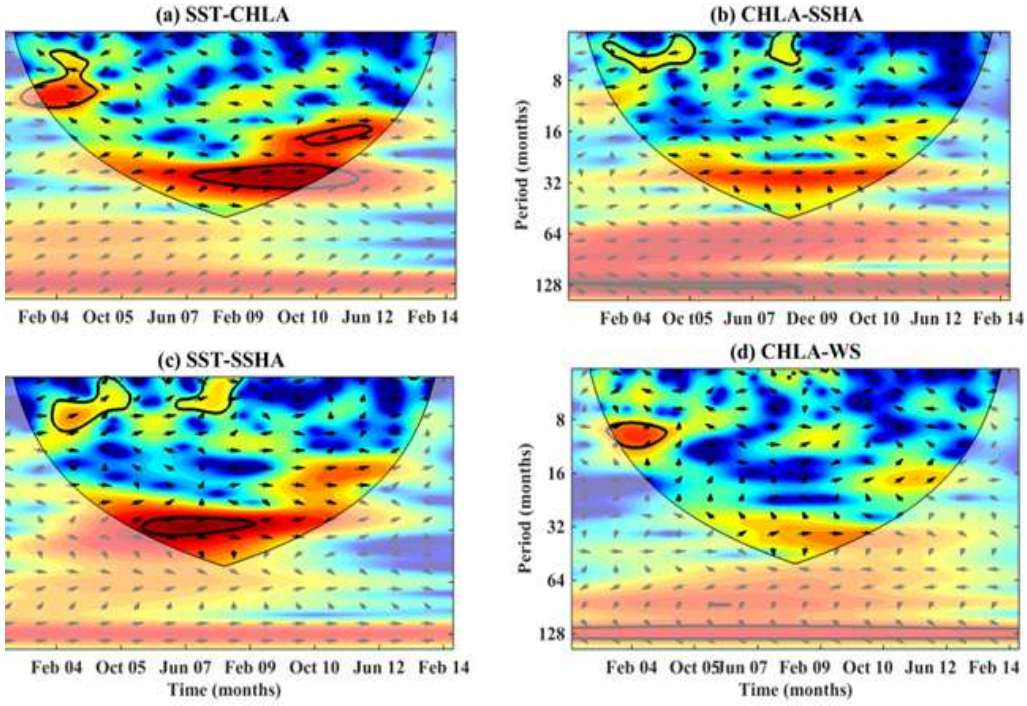

Figure 4.9 Cross wavelet spectrum of (a) SST-chl-*a*, (b) chl-*a*-SSHA, (c) SST-SSHA, and (d) chl-*a*-WS. The contours (black lines) exhibit significant cross power at 95% confidence level in the central equatorial Indian Ocean region. The relative phase relationship is shown by arrows (in-phase points to the right and anti-phase points to the left).

The SST and chl-*a* cross wavelet spectrum (figure 4.9a) shows similar features as that of chl-*a* and SSHA cross wavelet plot (figure 4.9b), which clearly indicates the trend relation between SST-SSHA-chl-*a* in the WEIO. The cross spectrum plot of chl-*a* and SSHA (figure 4.9b) shows the significant power around 6 months, and cross wavelet spectrum of SST and chl-*a* shows strong power at 32-36 months from August 2007 to March 2012 . The wavelet cross spectra of SST and SSHA (figure 4.9c) shows a high power at 28-32 months period from October 2005 to December 2009. From the figure 4.9 we can see the change in phase for periods around 4 to 6 months with SSHA leading SST. The chl-*a* and wind speed cross spectrum (figure 4.9d) shows that wind speed leads chl-*a* by 6 and 14 months.

4.5 Summary

Monthly chl-*a* concentrations show no significant trend during the years 2002-2014 over the Central Equatorial Indian Ocean, which is evident from the regression analysis (R^2=0.03; 'student's t- value at 0.05 level). Monthly averaged time series data of SST also show no significant trend during study period over the region. Increasing linear trend of

SSHA was observed during 2002-2014, which is evident from the correlation analysis of SSHA (R^2=0.21). Climate-change consequences on the Indo-Pacific warm pool influences the islands in the middle of the Indian Ocean to experience significantly raised sea-level than the global mean. Overall, no significant trend of WS was observed during 2002-2014 over the study region, which is evident from the regression analysis (R^2=0.0008) for CEIO. The Power Spectral Density plots of SST, chl-*a*, SSHA and WS show ~32, 16-18, 12-13, 5-8, 4 months periodicity, which suggest the presence of Quasi-Biennial signal (2-3 years periodicity) and semi-annual signal. The Wavelet power spectrum plots suggest the influence of IOD-ENSO on SST and WS respectively. The reasonable correlation is observed between SST and surface chl-*a* concentrations (R^2= 0.57; $p<0.05$). Statistical test ('student's t-value') shows that correlation between chl-*a* and SST is significant at 0.05 level. Unlike in WEIO, the relationship is more or less linear in CEIO, as upwelling seldom occurs. We have also observed weak correlation (R^2= 0.01) between chl-*a* concentration and WS.

Chapter 5

Western Equatorial Indian Ocean

5.1 Introduction

Air-sea interactions and Ocean dynamic forces play a key role in governing the biological, chemical and physical processes. Variations in the biological and chemical processes can influence the climate variability (Murtugudde et al., 2000; Xiu and Liu, 2006). The biological action in the sea involves the single-celled microscopic marine plants called phytoplanktons, which contain small packets of chlorophyll-*a* (chl-*a*) in their cells and absorb energy and use for photosynthesis. Hence, the phytoplanktons are considered to be a primary source responsible for determining the photosensitive properties near the ocean surface (Nakamoto et al., 2001). Primary production has a significant influence on the climate cycle, and, however, it is difficult to measure due to changing climate on various time scales. Hence, sea surface chl-*a* is frequently used in models of ocean primary production, as it can be measured easily from the world ocean database and satellite evaluations. Understanding the unevenness in chl-*a* concentrations can provide evidence indirectly on other associated physical processes. Well known climate modes (e.g., Indian Ocean Dipole (IOD), El Nino Southern Oscillation (ENSO), Madden Jullian Oscillation (MJO) etc.) work out in the equatorial regions as strong coupling between atmosphere and ocean takes place in these areas. Compared to the other ocean basins the Equatorial Indian Ocean (EIO) is unique in various aspects such as the presence of Wyrtki jets due to strong reversal of monsoon winds, IOD and intraseasonal oscillations of currents (Murthy et al., 2000; Saji et al., 1999; Vinayachandran et al., 2009). Another aspect of EIO is the deficiency of equatorial upwelling, unlike in the equatorial Pacific and Atlantic Oceans where the biological productivity is usually higher than that in the EIO (Prakash et al., 2015). Further, EIO is evidently different from other equatorial regions of the world ocean as the semiannual reversal of the wind system over the region causes reversal of the surface current. It is also evident in the satellite-derived chl-*a* values that the chl-*a* concentration over EIO is very low compared to any other region in the northern Indian Ocean and, therefore, has been mentioned as a ‘biological desert’ (Narvekar and Prasanna, 2010; Vidya et al., 2013).

The Western Equatorial Indian Ocean (WEIO) is well known for primary productivity during normal years, its interannual variability is less and little attention has been paid to the WEIO region during positive IOD years as the region experiences down-welling during these years and hence reduction in chl-*a* concentration. The positive IOD events are unusually initiated with stronger equatorial easterly winds, with anomalous upwelling in the eastern Indian Ocean (e.g. Saji et al., 1999; Murtugudde et al., 2000; Vinayachandran et al., 2009). Therefore, the WEIO region supports the abundant biological activity and dynamically active due to seasonal reversal of winds, upwelling/downwelling etc.

A number of studies demonstrate that the variations in circulation linked with the IOD events have an impact on the climate variability in Asia and Africa (Saji and Yamagata, 2003a, b; Ashok et al., 2001, 2004, 2007; Behera et al., 2005). The IOD events are considered as a key to the fundamental mechanisms responsible for climate change and biochemical processes in the tropical Indian Ocean. Sarma (2006) observed a close relationship between SST anomalies and chl-*a*, and between SSH anomalies and chl-*a* in the Arabian Sea during IOD events. Reddy and Salvekar (2008) and Wiggert et al. (2009) demonstrated the close relationship between chl-*a* concentration in the southeast tropical Indian Ocean and IOD events. Although many studies have focused on chl-*a* in the tropical Indian Ocean by direct observations as well as remote sensing outputs (Murtugudde et al., 1999; Sarma, 2006; Vinayachandran and Mathew, 2003; Wiggert et al., 2009; Currie et al., 2013), the studies over the WEIO on chl-*a* in relation to SST and SSHA are rather scanty. Moreover, the Indian Ocean is a complex and highly variable system under the dynamics of monsoon. Although a number of works have addressed the physical dynamics of climate system in the Indian Ocean (eg., Strutton et al., 2014), very little is known about the chl-*a* variability in the WEIO.

The present study evaluates the importance of chl-*a* and its relation with the SST, SSHA, and WS in the WEIO, which in turn influences productivity. The studies on productivity in WEIO in space and time are limited, and therefore the present study throws light on dynamics and productivity of the region.

5.2 Time Series Trend

5.2.1 Chlorophyll-*a*

The area averaged chl-*a* concentration in the WEIO for the period 2002 - 2014 is shown in figure 5.1. The area averaged chl-*a* concentration varied from 0.09 mg m^{-3} to 0.62

mg m^{-3} during the study period. A minimum of areal average of chl-*a* concentration of 0.09 mg m^{-3} is recorded in April 2007 and a maximum of 0.62 mg m^{-3} recorded in July 2003. Five peaks of high concentrations of chl-*a* (0.39 mg m^{-3} in August 2002; 0.52 mg m^{-3} in July 2004; 0.37 mg m^{-3} in June 2005; 0.41 mg m^{-3} in August 2010; 0.38 mg m^{-3} in August 2013) are recorded.

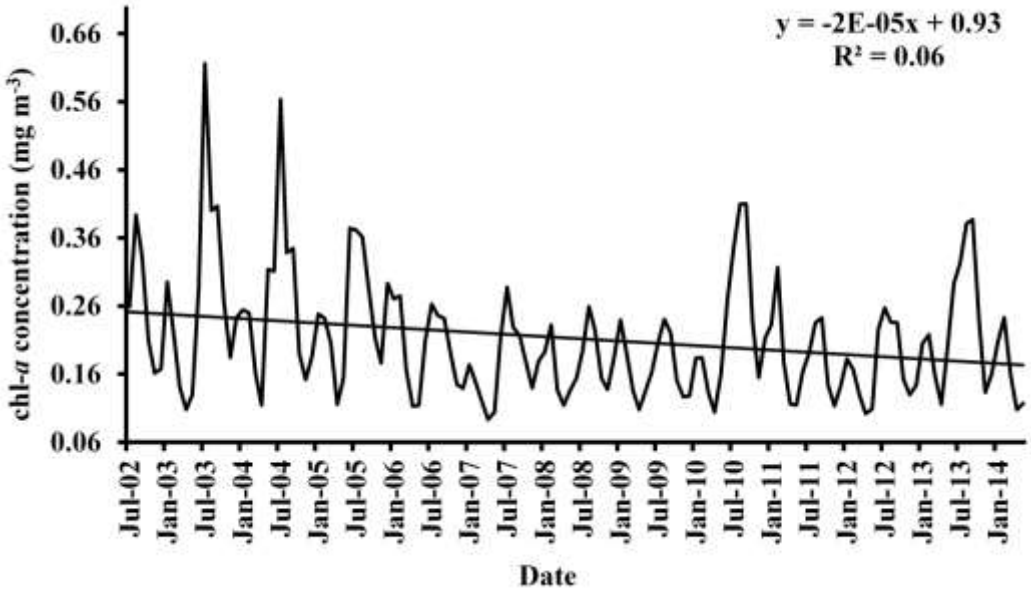

Figure 5.1 Area averaged monthly time-series of chlorophyll-*a* showing decreasing linear trend for in the Western Equatorial Indian Ocean (Latitude $5^oN – 5^oS$, Longitude $45^oE – 65^oE$) study period 2002-2014.

Among the tropical oceans, the Western Indian Ocean receives highest chl-*a* concentrations during Southewest monsoon (Naqvi et l., 2003; Prasanna Kumar et al., 2001; Ryther and Menzel, 1965; Wiggert et al., 2005). In the Western Indian Ocean, the monsoonal wind forcing is the substantial and leads to a strong open ocean and coastal upwelling emerging from the coastal divergence of Ekman transport and Ekman pumping, a supply of nutrients to the surface and carrying high rates of primary productivity (Prasanna Kumar et al., 2001; Wiggert et al., 2005; Levy et al., 2007; McCreary et al., 2009; Resplandy et al., 2011). High upwelling regions gets high nutrients and therefore high chl-*a* concentrations and highly productive area (Mohanty, 2008). Overall, decreasing linear trend of chl-*a* was observed during 2002-2014 over the study region, which is evident from the correlation analysis of chl-*a* ($R^2 = 0.06$) significant at 0.05 level for WEIO.

5.2.2 Sea Surface Temperature (SST)

Time series of SST anomalies for the study period over the WEIO is shown in figure 5.2. A sinusoidal variation of temperature was observed during the period 2002-2014 and varied in the range of 26.59^{o} - 30.73^{o} C. The area averaged SST in the WEIO showed maximum SSTs during April with a value of 30.73^{o} C and minimum SST of 26.59^{o} C during July. The high SST during April, low SST values during July 2005 (26.59^{o} C) and July 2004 (26.65^{o} C), and high peak of SSTs in the month of April 2010 (30.73^{o} C) were recorded. During May inter-annual variation in SST is significant in the WEIO which is a standard deviation of 3^{o}C and a significant variation of 1.5 standard deviation existed in WEIO in December (Mohanty, 2008). Overall, no linear trend of SST was observed during 2002-2014 over the study region, which is evident from the low correlation coefficient of SST (R^2 = 0.00006) for WEIO. No significant trend of SST observed during the present study period (figure 5.2) is in contrast to the observations made by Prakash et al. (2012) over western Indian Ocean for a 6 years period i.e., from 1998 to 2003. It is known that upwelling along the western boundary drives the low SST during July-August.

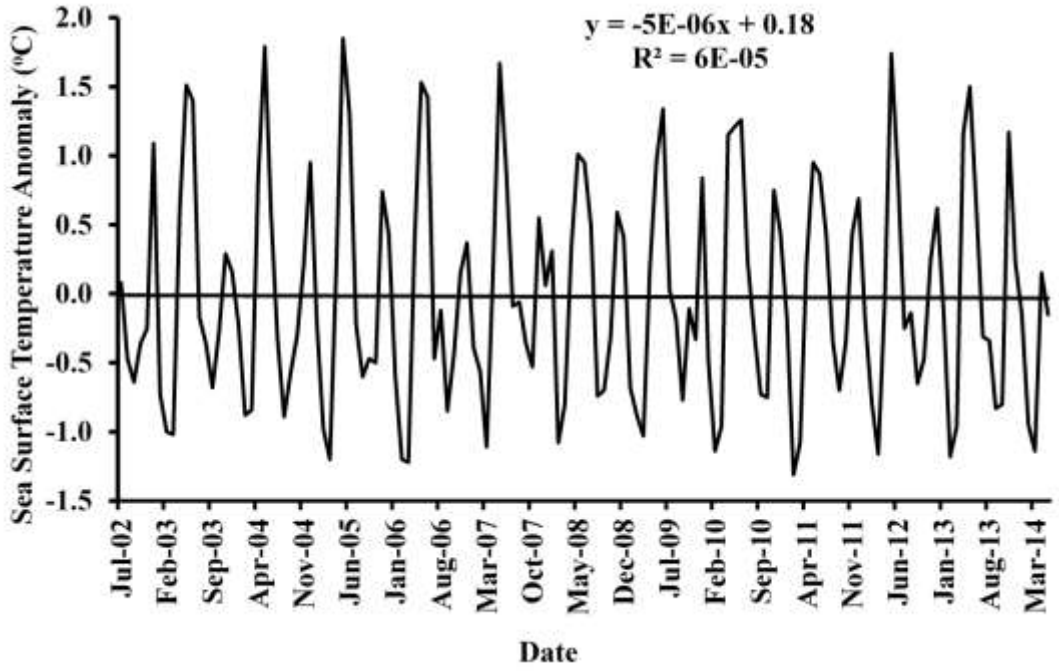

Figure 5.2 Area averaged monthly time-series of Sea Surface Temperature anomalies showing decreasing linear trend in Western Equatorial Indian Ocean for the study period 2002-2014.

As SST is also an indicator of the vertical mixing and has remained almost the same over the past eight years which clearly indicates that there is no significant shift in terms of dynamics such as upwelling or winter mixing in this region. However, a significant fall in the SST (~3º C) during winter and moderate decrease during the summer (~1-2º C) occurs in this zone (20^oN to 25^oN and 62^oE to 75^oE) which explains the presence of relatively high surface chl-*a* during the winter monsoon i.e., in December month. It is well established that mixing of deeper water with the surface water causes decrease in SST and supplies nutrients to the upper layers which enhances the productivity and hence the high surface chl-*a* (Prakash and Ramesh, 2007).

5.2.3 Sea Surface Height anomaly (SSHA)

The area averaged SSHA in the WEIO for the period 2002 - 2014 is shown in figure 5.3. The area averaged SSHA varied from -14.09 cm to 9.35 cm during the study period. A minimum of areal average of SSHA of -14.09 cm is recorded in December 2005 and a maximum of 9.35 cm recorded in March 2010. Four peaks of high SSHA values are (9.35 cm in March 2010; 9.15 cm in August 2012; 9.10 cm in March 2014; 8.95 cm in August 2013) are recorded. Overall, increasing linear trend of SSHA was observed during 2002-2014 over the study region, which is evident from the correlation analysis of SSHA ($R^2 = 0.13$). Over the past few decades, sea level in WEIO has risen because of the expansion of warming (Climate Institute, 2010).

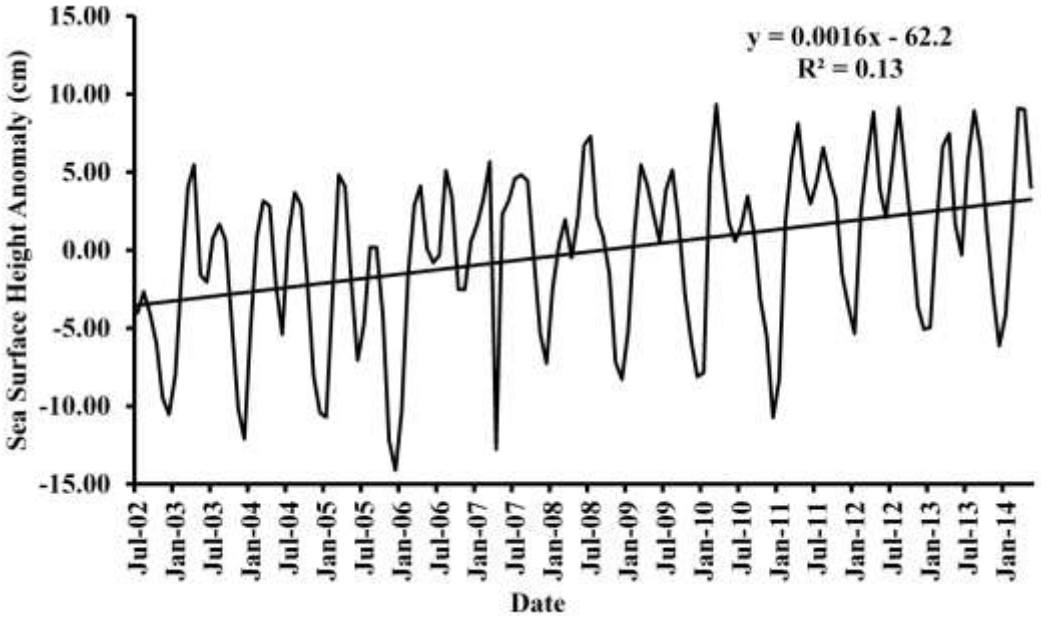

Figure 5.3 Area averaged monthly time-series of Sea Surface Height Anomalies showing increasing linear trend in the Western Equatorial Indian Ocean for the study period 2002- 2014.

Han (2010) studied ground and satellite observations of Indian Ocean sea levels with simulated models of climate change and identified a clear spatial pattern in sea surface height anomaly rise since the 1960s. Other researchers have also reported increased sea levels in the tropical Indian Ocean. These changes in regional ocean patterns and sea levels could exacerbate flooding due to monsoon in Bangladesh and India and lead to increased rainfall in the eastern tropical Indian Ocean and drought in the WEIO. Areal and satellite images are taken over the past 60 years, a time during which the sea levels have risen (UNEP, 2010).

5.2.4 Wind Speed (WS)

The area averaged WS in the WEIO for the period 2002 - 2014 is shown in figure 5.4. The area averaged WS varied from 3.1 m s^{-1} to 8.95 m s^{-1} during the study period. A minimum of areal average of WS is 3.1 m s^{-1} is recorded in November 2006 and a maximum of 8.5 m s^{-1} recorded in June 2007. Four high peaks of WS values are (8.5 m s^{-1} in June 2007; 8.2 m s^{-1} in July 2008; 8.1 m s^{-1} in July 2013; 8.95 cm in August 2013) are recorded. Overall, no significant trend of WS was observed during the years 2002-2014, which is evident from the regression analysis of WS (R^2=0.002) in the WEIO.

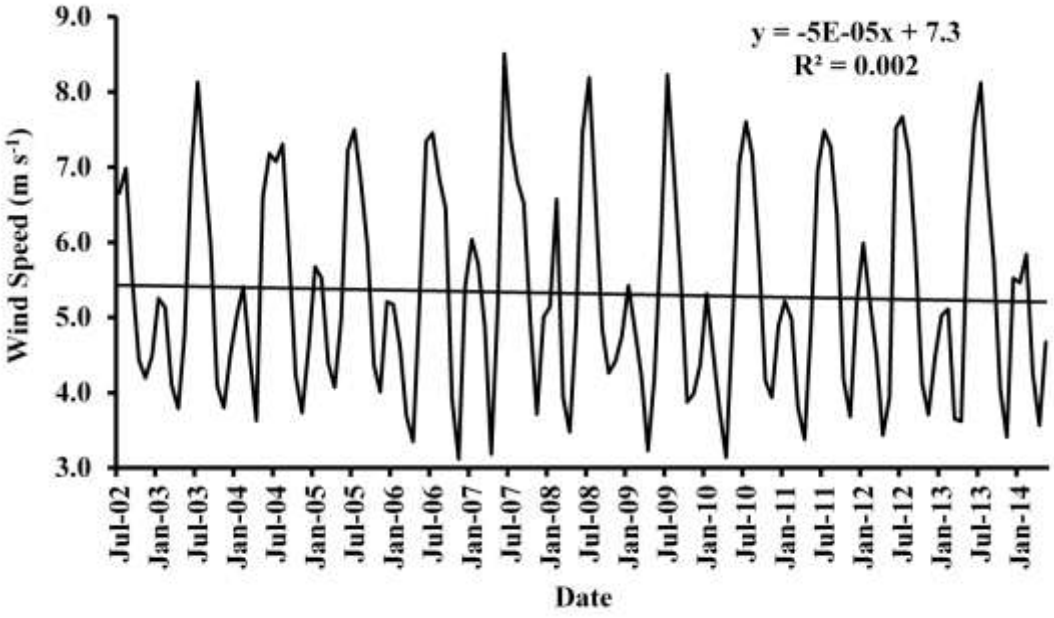

Figure 5.4 Area averaged monthly time-series of wind speed in the Western Equatorial Indian Ocean. No significant trend is detected.

5.3 Inter-relationships

Scatter plots of chl-*a*, SST, SSHA, and WS are prepared to understand the relationship between each variable and shown in figure 5.5. We found strong correlation between SST and surface chl-*a* concentration: ($R^2 = 0.61$; $p < 0.05$) (figure 5.5a). Statistical test ('student's *t*-value') shows that correlation between chl-*a* and SST is significant at 95% confidence level. Here least squares linear fit with slope -8.12 and intercept 30.1 represented by straight line.

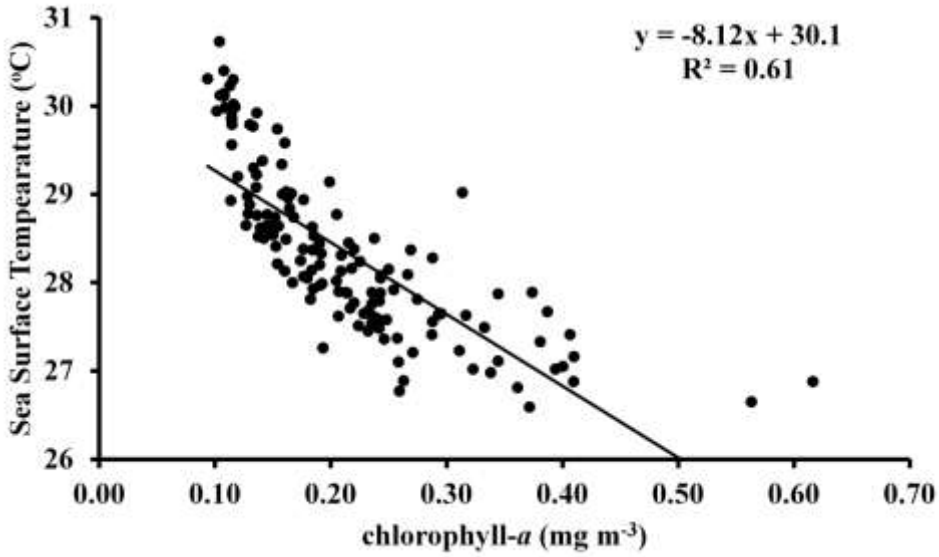

Figure 5.5a Scatter plot of the monthly chlorophyll-*a* concentrations versus SST showing strong correlation (R^2=0.61) ($p<0.05$) in the Western Equatorial Indian Ocean for the period 2002-2014.

The correlation improves when a parabolic fit is done ($y=24.49x^2-21.71x+31.7$; R^2 =0.74) (Figure 5.5b). This is because when the upwelling increases, temperature decreases because of the supply of nutrient-rich bottom cold water, leading to a greater increase in chl-*a*. Chl-*a* and SST during the earlier decades present a significant trend, and a good correlation between these two datasets, describing the substantial role of SST trends in the Western Indian Ocean being harmful to marine primary production. increasing SST can reduce chl-*a* concentrations hence, they are the sign of intensified surface stratification and therefore overcome vertical mixing of rich-nutrient subsurface waters (Roxy et al., 2015; Behrenfeld et al., 2016). Open ocean chl-*a* concentration may play a key role in the control of SST by trapping the surface layer solar radiation.

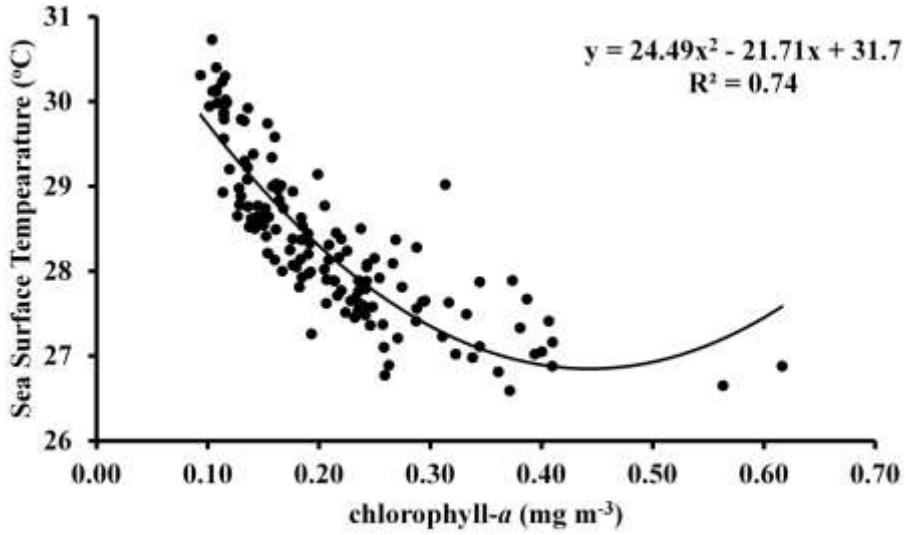

Figure 5.5b Scatter plot of the monthly chlorophyll-*a* concentrations versus SST showing strong correlation (R^2=0.74; p<0.05) in the Western Equatorial Indian Ocean for the period 2002-2014.

When the open ocean chl-*a* concentration is high, SST of the oceans can be increased (Mohanty, 2008). But Murakami et al. (2000) suggests that when chl-*a* increases, SST will decrease in the western equatorial Pacific because of coastal upwelling and vertical mixing around the islands caused by local WS bursts.

We found reasonable correlation between WS and chl-*a* concentration (R^2 = 0.42; p <0.05) (figure 5.6). Statistical test ('student's *t*-value') shows that correlation between chl-*a* and WS is significant at 0.05 level. Here the least squares linear fit with slope 9.8 and intercept 3.23 represented by straight line. The relation between WS and chl-*a* does not seem to be linear. This is because, at high Wind Speeds the chl-*a* gets scattered in the surface ocean. Chl-*a* shows good positive correlation with Wind Speed. The most complex features including the highest correlations between chl-*a* and winds can be seen in the equatorial regions.

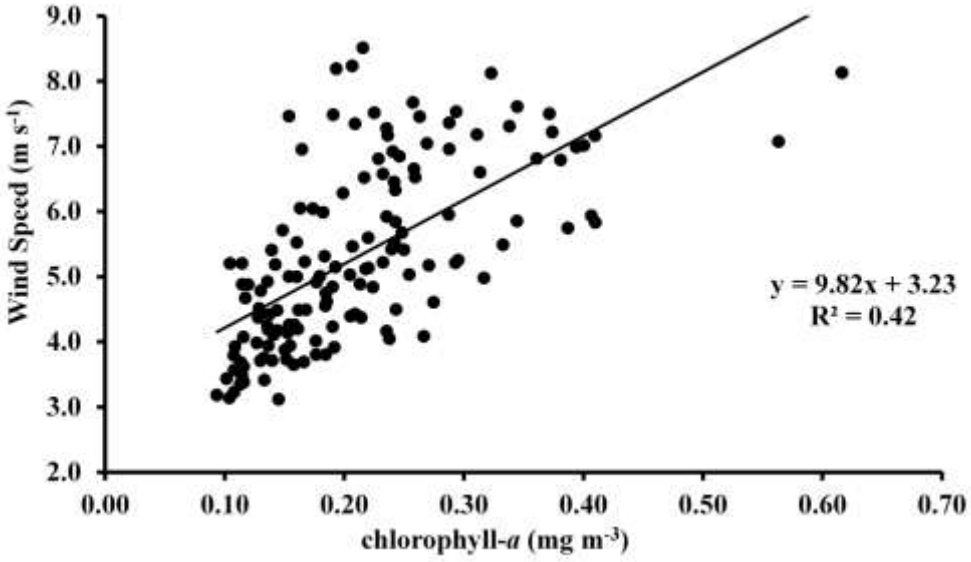

Figure 5.6 Scatter plot of the monthly chlorophyll-*a* concentration versus Wind Speed in the WEIO for the period 2002-2014.

Kahru et al. (2010) demonstrated similar results i.e., the highest positive correlation between chl-*a* and Wind Speed in the western Pacific (WEPAC).

In order to understand the dynamics involved in providing strong coherence between SST-chl-*a* and SSH-chl-*a*, we have plotted lag-lead correlations between SST-chl-*a* (figure 5.7) and SSH-chl-*a* (figure 5.8) in the WEIO.

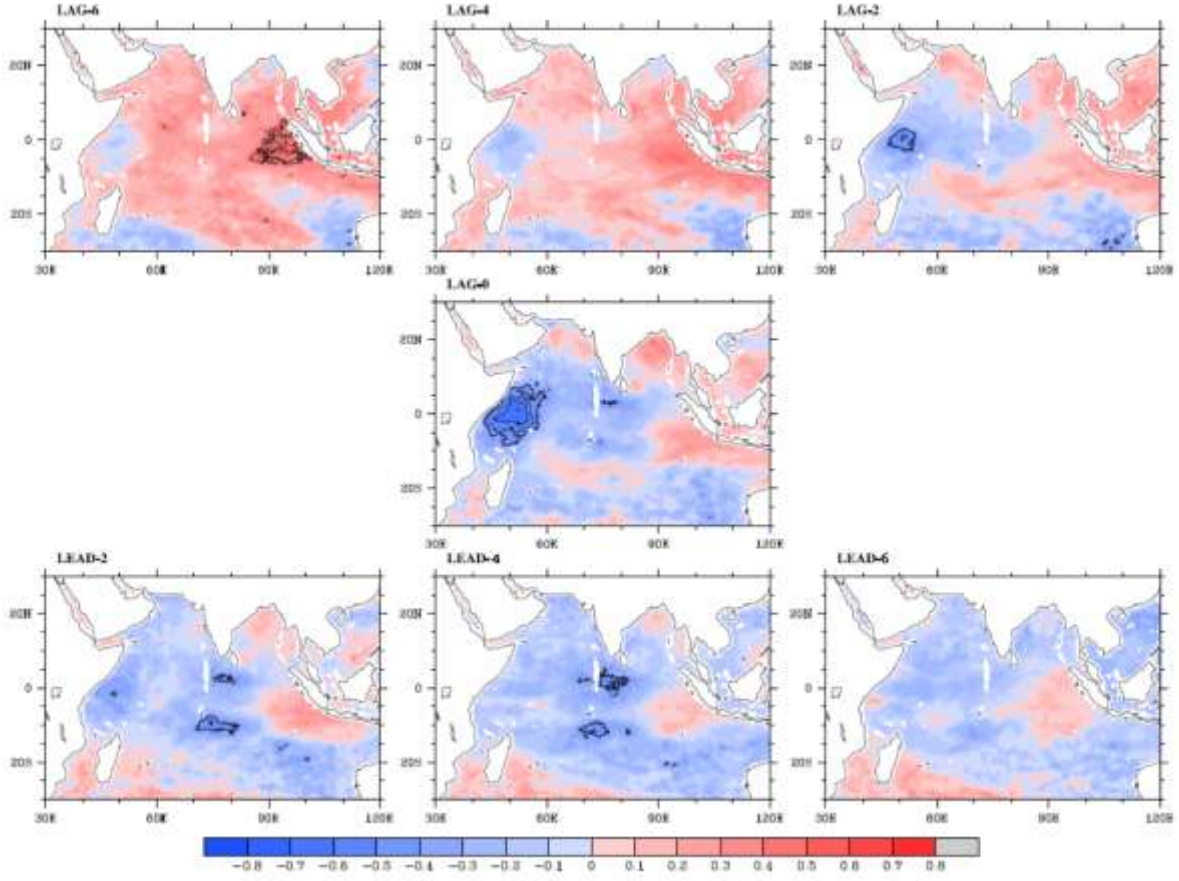

Figure 5.7 Correlation map between Sea Surface Temperature and chlorophyll-*a* at (a) Lag-6 (b) Lag-4 (c) Lag-2 (d) Lag-0 (e) Lead-2 (f) Lead-4 (g) Lead-6 in the Western Equatorial Indian Ocean for the study period 2002-2014. Dotted areas denote 95% confidence regions.

As expected significant negative correlations are noticed between SSH-chl-*a* over Central Equatorial Indian Ocean at four months lead, over West-Central Equatorial Indian Ocean over two months lead and at WEIO at lead zero. These patterns clearly say that Rossby waves close to the equator play a very important role in modulating the variations of chl-*a* in WEIO. At lead-0 strong IOD pattern is seen in correlation between SST-chl-*a*, which clearly suggests that chl-*a* anomalies and EEIO chl-*a* anomalies are strongly correlated to IOD dynamics in WEIO. Unlike in WEIO, we don't see significant negative correlations of chl-*a* variability with SSH anomalies at different lags in EEIO.

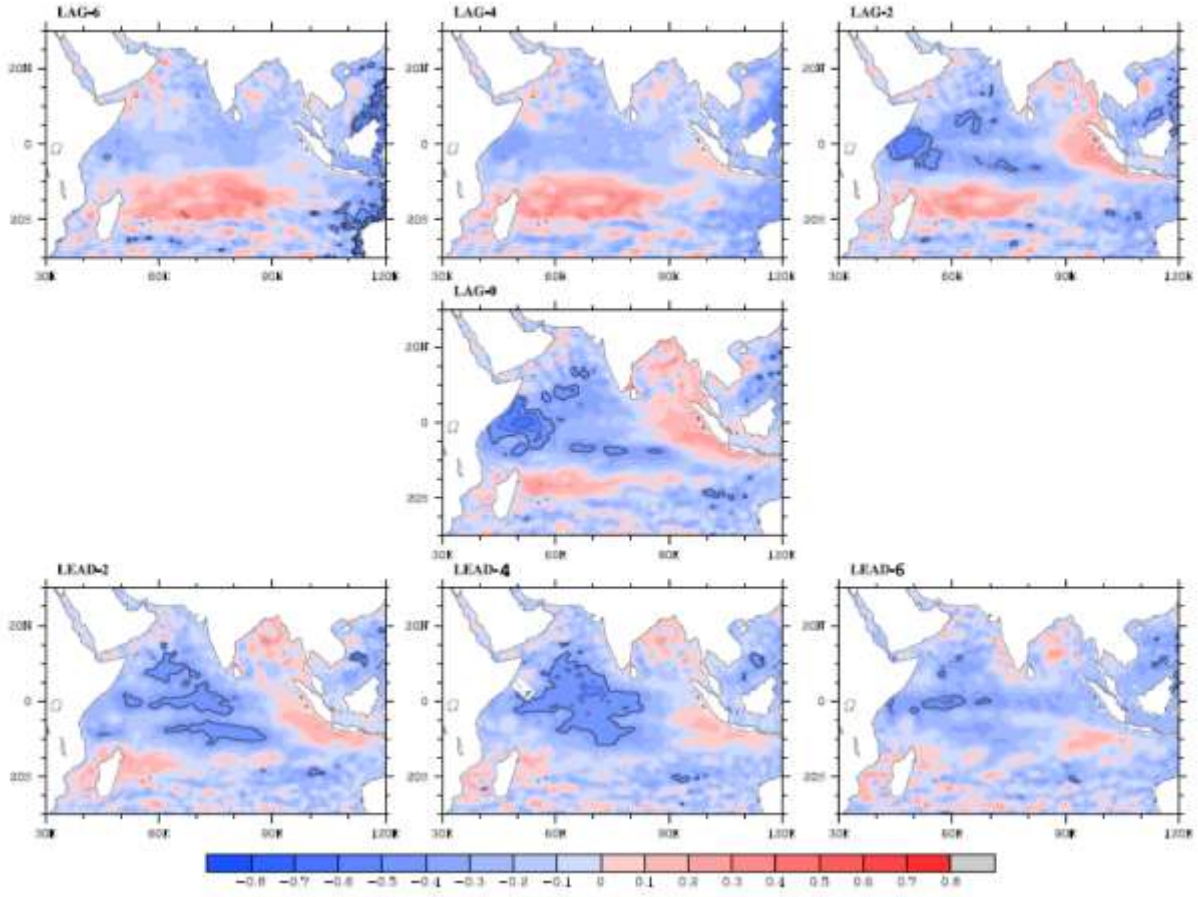

Figure 5.8 Correlation map between Sea Surface Height and chlorophyll-*a* at (a) Lag-6 (b) Lag-4 (c) Lag-2 (d) Lag-0 (e) Lead-2 (f) Lead-4 (g) Lead-6 in the Western Equatorial Indian Ocean for the study period 2002-2014. Dotted areas denote 95% confidence regions.

This is probably due to the fast response to equatorial Kelvin waves as explained in Iskandar et al. (2005). One of the strong contrasts between WEIO and EEIO is that WEIO dynamics are a response to fast moving equatorial Kelvin waves. Therefore WEIO chl-*a* variability has a strong predictable component due to the slow propagating near Equator Rossby waves. This is the figure study shows that the WEIO chl-*a* variability has a strong predictable component due to the slow near equator Rossby wave.

5.4 Discussion

The variability at different time scales is evidenced and the focus of this study is to highlight the variability in each parameter and coherence among them and discuss the dynamics behind such coherence. The power mathematical tools of Fast Fourier Transform (FFT) and wavelet analysis are applied for understanding the climatic variations on regional and global scale. We have applied the power spectrum analysis to all the four data sets. Power spectrum plots of the data sets which clearly indicate two dominant peaks at 54 and 25 weeks cyclicity corresponding to 12 and 6 months respectively. These peaks are coherent and found to be common in all our data sets suggesting the presence of annual and semi-annual cycles.

De-seasonalisation of data has been carried out to understand the periodicities on inter-annual scale. This becomes essential as the temporal extended term and medium term trends in the dataset can be affected by the seasonal oscillations. In order to avoid spurious signals triggered by these seasonal variations in the long term trend analysis, de-seasonalization is done using a moving average. Based on the cyclical nature of dataset, the moving average window size function is chosen as discussed in the previous chapter. Generally, the datasets tend to have one year cycle. Hence the moving mean function gap is 12 time steps (since the dataset is monthly). Linear regression trend analysis is repeated on the de-seasonalized dataset.

The power spectral density (PSD) plots for SST, chl-*a*, SSHA and WS are shown in figure 5.9. The power spectral density (PSD) plot of RC-SST shows two strong low-frequency maxima corresponding to ~ 32, and 16-18 month periods i.e., 3 and 2 years respectively (figure 5.9a). This clearly suggests the presence of Quasi-Biennial signals (2-3 years periodicity) in SST anomalies of the WEIO (e.g. Meehl and Arablaster, 2001). The PSD of RC-chl-*a* data (figure 5.9b) shows powers at 12-13, 5-8 and 5 months. The power spectrum of the RC-SSHA (figure 5.9c) shows peaks at 7-8, 5-6 and 4 months. The RC-PSD of wind speed data (figure 5.9d) shows peaks at 10-12, 4-5, and strong maxima at 3 months period emphasizing the influence of semi-annual variability in the data.

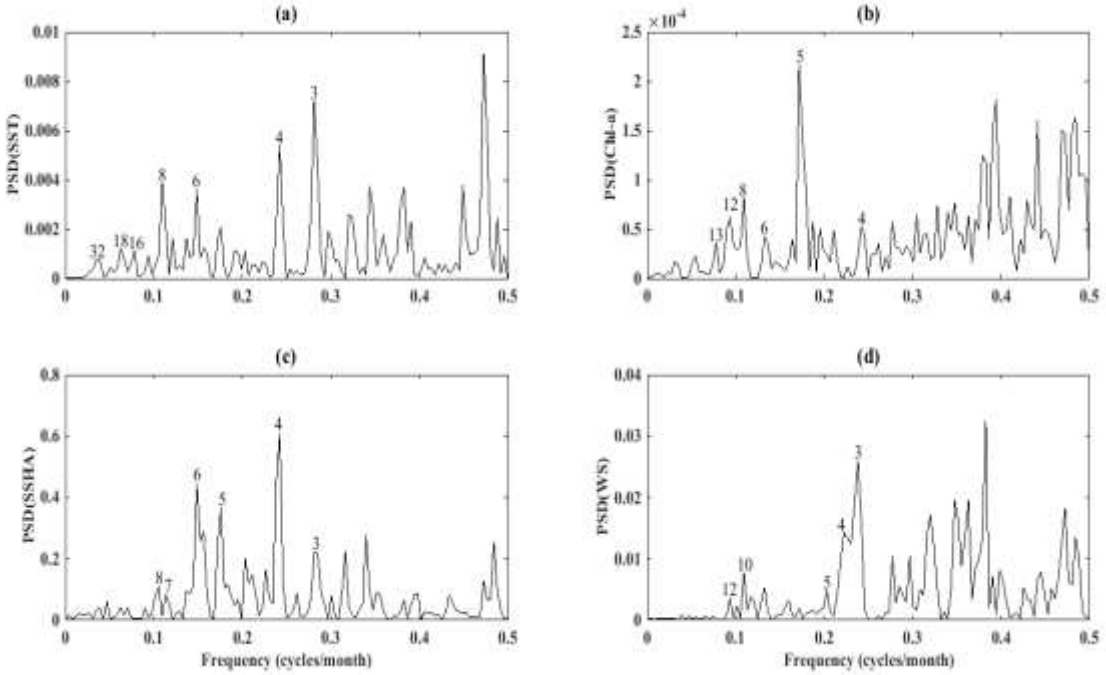

Figure 5.9 Power Spectrum plots of (a) Sea Surface Temperature, (b) chlorophyll-*a*, (c) Sea Surface Height anomaly, and (d) Wind Speed for the Western Equatorial Indian Ocean. A high power at 32, 16, and 4- 8 months is observed suggesting the implication of quasi biennial oscillations and also semi-annual variability in power spectrum of SST (figure 5.9a). The power spectrum of chl-*a* (figure 5.9b) data shows strong and well separated maxima at 13, 12, 4- 8 months. Power spectrum of SSHA (figure 5.9c) shows strong peaks between 4- 8 months cyclicity, and ws (figure 5.9d) shows a high power at 10- 12 and 3- 5 months period.

To explore the stationary characteristics of the peaks obtained by the power spectrum of the RC time series, the Morlet based wavelet transform approach is used as suggested by various researchers (Holschneider, 1995; Foufoula-Georgiou and Kumar, 1995; Torrence and Compo, 1998; Grinsted et al., 2004). The wavelet spectrum identifies the main periodicities in the time series and helps to analyze the periodicities with respect to time (figure 5.10). Semi-annual signal is weaker during IOD events (i.e., in 2006-2008) due to the absence of Wyrtki jet in fall and probably in spring as well (Cai et al., 2009). Joseph et al. (2012) show clear evidence of weakening of spring Wyrtki jets during the years 2006–2011, which apparently reflects the strengthening of easterly wind anomalies associated with IOD events occurred during the period of study.

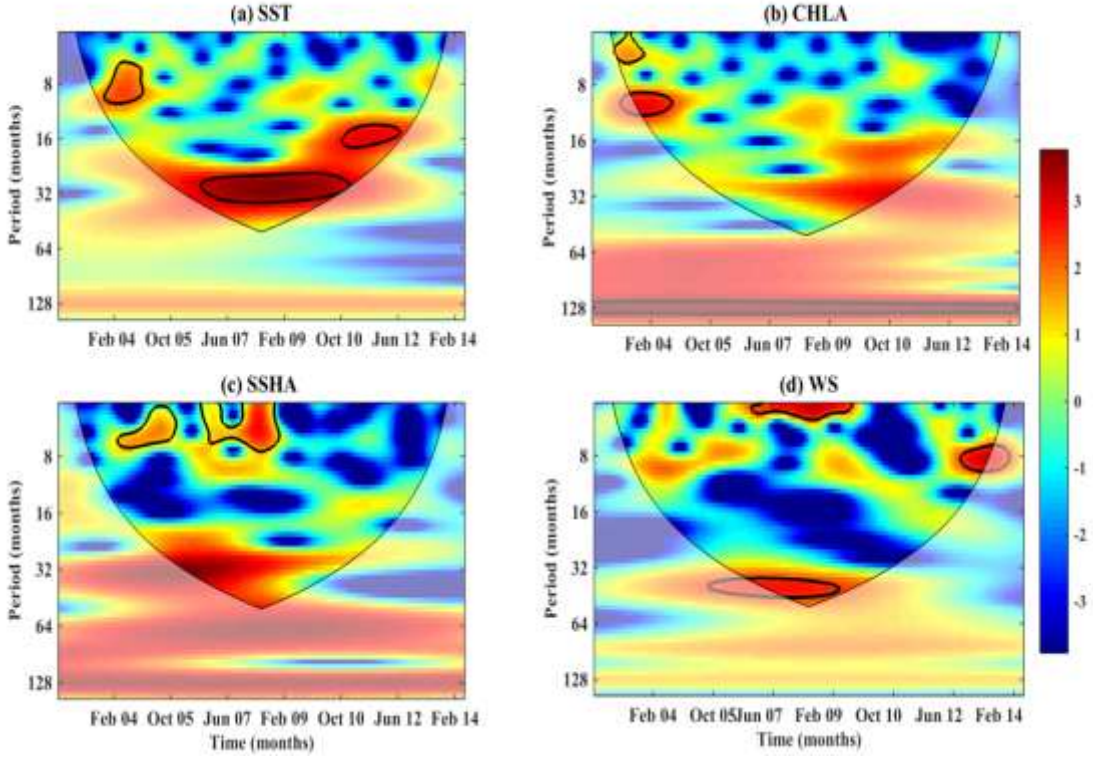

Figure 5.10 wavelet spectrum of (a) SST, (b) chl-*a*, (c) SSHA, and (d) WS for the study period from 2002 to 2014.

Here we can clearly observe the occurrence of very strong IOD during the fall of 2006, and also the interference of the signal of 18 months and 32 months period for the constructive formation of IOD in 2008. The wavelet power spectrum of the SST data (figure 5.10a) shows high power around 32 months (January 2006 to June 2010) and 16 months (June 2010 to September 2012) suggesting the influence of ENSO and IOD on chl-*a* respectively. The wavelet spectrum of the chl-*a* data (figure 5.10b) shows high peak at 12 months (October 2003 to September 2004) clearly suggesting the annual cycle influence. The wavelet power spectrum of the SSHA-RC data (figure 5.10c) shows high power around 4-8 months period. The WS data (figure 5.10d) show strong signal at 36 months suggesting the influence of ENSO in the data.

Cross wavelet spectrum is applied to have the better visualization of time series for two similar periods and for the interpretation of the results, Figure 5.11 shows the cross wavelet spectrum of (a) chl-*a*-SSHA, (b) chl-*a*-SST, (c) SST-SSHA and (d) chl-*a*–WS data. The contours (dark black lines) are the enclosing regions where the wavelet cross power is

significantly higher at 95% confidence level. The phase relationship is shown in arrows with inphase pointing to right, antiphase pointing to left. The chl-*a* and SST cross wavelet spectrum (figure 5.11a) shows similar features as that of chl-*a* and SSHA cross wavelet plot (figure 5.11b), which clearly indicates the trend relation between SST-SSHA-chl-*a* in the WEIO. The cross spectrum plot of chl-*a* and SSHA shows the significant power around 6 months, and cross wavelet spectrum of SST and chl-*a* shows strong power at 32-36 months from August 2007 to March 2012. The wavelet cross spectra of SST and SSHA (figure 5.11c) shows a high power at 28-32 months period from October 2005 to December 2009.

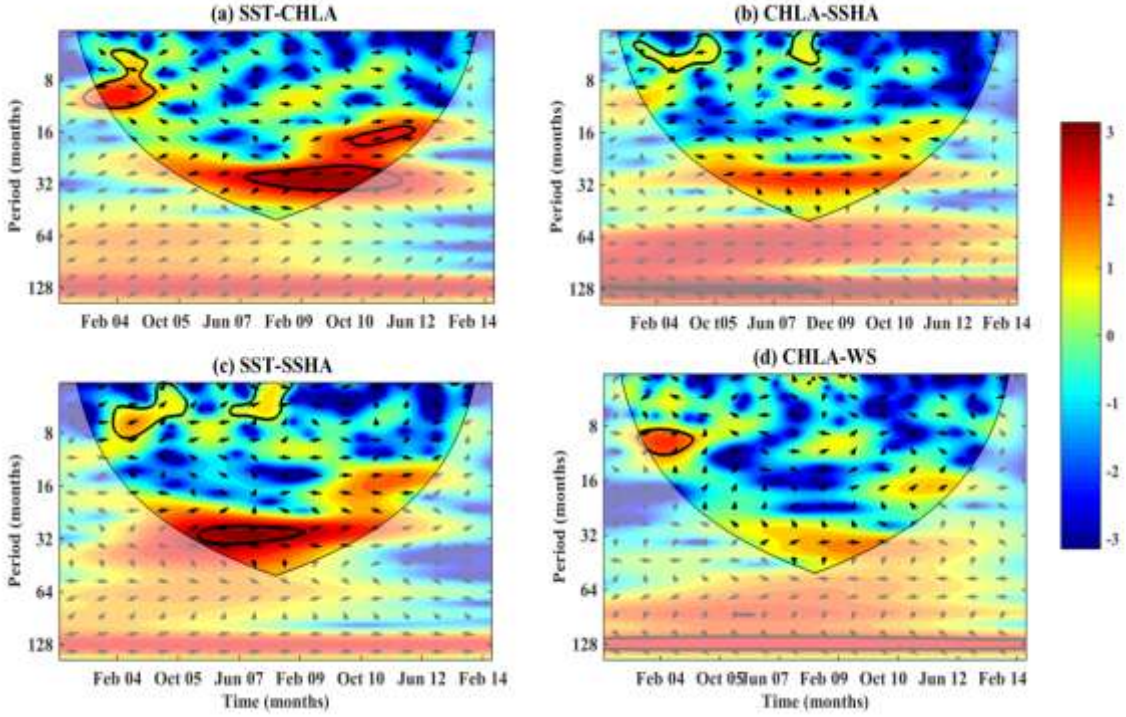

Figure 5.11 Cross wavelet spectrum of (a) SST-chl-*a*, (b) chl-*a*-SSHA, (c) SST-SSHA, and (d) chl-*a*-WS. The contours (black lines) exhibit significant cross power at 95% confidence level in the Western Equatorial Indian Ocean region. The relative phase relationship is shown by arrows (in-phase points to the right and anti-phase points to the left).

The wavelet spectrum of SST-SSHA-chl-*a* depicts a statistically significant power at around 32, 16-18 and 6-12 months at > 95% significance level, and suggests a clear imprint of ENSO-IOD on the SST-SSHA-chl-*a* data. From the figure 5.11 we can also see the change in phase for periods around 4 to 6 months with SSHA leading SST. The chl-*a* and wind speed cross spectrum (figure 5.11d) shows that wind speed leads chl-*a* by 6 and 14 months.

5.5 Summary

Monthly chl-*a* concentrations show decreasing linear trend during the years 2002-2014 over the WEIO, which is evident from the regression analysis (R^2=0.06; 'student's t-value at 0.05 level) as observed in the central EIO. Monthly averaged time series data of SST show no trend (R^2 = 0.00006) during the study period over the region. Increasing linear trend of SSHA was observed during 2002-2014 over the study region, which was evident from the correlation analysis of SSHA (R^2 = 0.13). Satellite observations of Equatorial Indian Ocean with simulated models of climate change has identified spatial patterns in sea surface height anomaly rise since the 1960s. Overall, no trend in WS is observed during the years 2002-2014 over the study region, which is evident from the regression analysis of WS (R^2 = 0.002). The better correlation is observed in a parabolic fit ($y = 24.49x^2-21.71x+31.7$; R^2 = 0.74). The good correlation shows due to increase in upwelling and decrease in temperature by the supply of cold nutrient-rich water from the bottom leading to increase in chl-*a*. A reasonable correlation between WS and chl-*a* concentration (R^2=0.42; $p<0.05$) is recorded. Statistical test ('student's t-value') shows that correlation between chl-*a* and WS is significant at 0.05 confidence level. Spatial correlation plot between Sea Surface Height and chl-*a* significant shows negative correlations in the WEIO at lead zero., This pattern clearly shows that Rossby waves close to the Equator play a very important role in modulating the variations of chl-*a*. From this spatial correlation plot it can be understood that WEIO chl-*a* variability has a strong predictable component due to the slow propagating Rossby waves near the Equator. The power spectral density plots of SST, chl-*a*, SSHA and WS show ~32, 16-18, 12-13, 5-8, 4 months periodicity, which suggest the presence of Quasi-Biennial signal (2-3 years periodicity) and semi-annual signal in the EIO. The wavelet power spectrum plots suggest the influence of IOD and ENSO on SST and WS respectively.

Chapter 6

Eastern Equatorial Indian Ocean

6.1 Introduction

Active ocean-atmosphere interactions occur in the Eastern Equatorial Indian Ocean (EEIO), which affects the monsoon system. Surface waters of the EIO are mostly warmer than 28^{o}C, providing the necessary condition for active interaction between the ocean and atmosphere. Over the EEIO upwelling process modulates the upper-ocean conditions within a warm water pool region (Masumato et al., 2005). A distinct semiannual signal of the eastward swift of ocean surface currents, known as the Wyrtki jets is or equatorial jets are observed. The seminal work of Wyrtki (1973), suggested that monthly surface currents, which propagate eastward as equatorial jets along the equator in the Indian Ocean. These jets occur twice a year during the monsoon transition periods (April/May and October/November) and the surface zonal current with a typical amplitude of about 80 cm/s along the equator (Han et al., 1999). Variability in the surface temperature and salinity affects physical and biogeochemical/ecological phenomena within the region as well as globally. The chl-a concentrations reveal its largest intra-seasonal variability of chl-a revealed during May-October when the mean thermocline is shallow. During summer-fall and winter-spring seasons upwelling occurs.

Eastward equatorial undercurrents are transient features related to wave dynamics in the Indian Ocean (Schott and McCreary 2001). Earlier studies of equatorial Indian Ocean circulation refer to the seasonal cycle (e.g. Gent et al. 1983; McCreary et al. 1993; Anderson and Carrington 1993) or inter-annual variability of climate (Reverdin et al. 1986; Saji et al. 1999; Murtugudde et al. 1999; Schiller et al. 2000). The seasonal cycle of surface zonal current, is determined by the phase relation between wind-driven flow and flow associated with waves (Han et al. 1999).

El Nino/Southern Oscillation (ENSO) is defined as the inter-annual climate variability in the tropical Pacific (McPhaden et al., 2006; Currie et al., 2013). In 1990s, the Indian Ocean was considered to be largely unresponsive to the inter-annual forcing of ENSO (Murtugudde and Busalachi, 1999; Saji et al., 1999; Webster et al., 1999). But now we know

that the Indian Ocean dipole mode is an independent mode not associated with the El-Nino southern oscillation (ENSO) (Saji et al., 1999; Webster et al., 1999).

The Indian Ocean Dipole is normally characterized by anomalous cooling of SST in the Eastern Equatorial Indian Ocean (EEIO) and anomalous warming of SST in the western equatorial. It is associated with the changes in the normal convection situated over the eastern Indian Ocean (JAMSTEC, 2009). At the time of IOD, which happens during September – October, the EEIO becomes unusually cold, whereas the Western Equatorial Indian Ocean becomes warm. In the eastern Indian ocean correlations between SSTA and ENSO indices suggest that IOD events are driven by ENSO (Allan et al., 2001; Baquero-Bernal et al., 2002; Xie et al., 2002; Hastenrath 2002; Krishnamurthy and Kirtman, 2003; Annamalai et al., 2003). During 1997, it was found out that a strong IOD event occurred with a strong ENSO. During IOD, ENSO lacks the dipole pattern due to SSTA (Tozuka et al., 2008; Vinayachandran et al., 2009). Several researchers have made efforts to understand the chl-*a* variability in the Eastern Equatorial Indian Ocean (EEIO) during positive IOD years as it is connected with the upwelling during these years (Murtugudde et al., 1999; Susanto and Marra, 2005; Currie et al., 2013).

In the present chapter, variability of SST, chl-*a*, SSHA and WS over a period of 13 years (2002 – 2014) in EEIO (Latitude 5^oN-5^oS, Longitude 80^oE-95^oE) is discussed.

6.2 Time Series Trends

6.2.1 Chlorophyll-*a*

The area averaged chl-*a* concentration in the EEIO for the period 2002 - 2014 is shown in figure 6.1. It varied from 0.09 mg m^{-3} to 0.19 mg m^{-3} during the study period. A minimum of areal average of chl-*a* concentration of 0.09 mg m^{-3} is recorded in March 2003 and a maximum of 0.19 mg m^{-3} recorded in September 2004 and October 2010. Five peaks of high concentrations of chl-*a* (0.17 mg m^{-3} in October 2003; 0.19 mg m^{-3} in September 2004; 0.18 mg m^{-3} in September 2005; 0.19 mg m^{-3} in October 2010; 0.18 mg m^{-3} in August 2013) are recorded. Monthly chl-a concentrations show decreasing trend during the years 2002-2014 over the EEIO, which is evident from the regression analysis (R^2 = 0.01; 'student's t-value at 0.05 level).

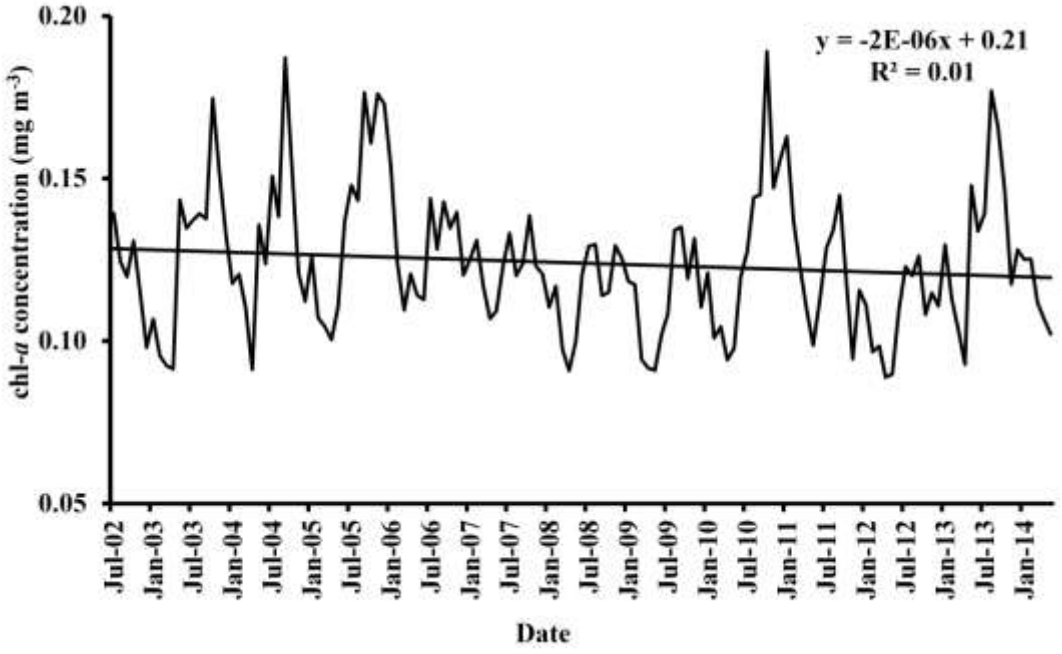

Figure 6.1 Area averaged monthly time-series of chlorophyll-*a* showing decreasing linear trend in the Eastern Equatorial Indian Ocean (Latitude $5^oN - 5^oS$, Longitude $80^oE - 95^oE$) study period 2002-2014.

6.2.2 Sea Surface Temperature (SST)

Area averaged time series of SST over EEIO was analyzed and presented in figure 6.2. A sinusoidal variation of temperature was observed during the period 2002-2014 and varied in the range of 28.35^oC - 30.38^oC. The area averaged SST in the EEIO showed high peaks during April-May with a value of 30.38^oC and minimum of 28.35^oC during July-August. Low SST values occurred during September 2006 (28.43) and November 2010 (28.35^oC). The peaks of SST were recorded in April 2010 (30.05^oC). Monthly averaged time series data of SST show no trend ($R^2 = 0.001$) during the study period over the EEIO (figure 6.2). Mohanty (2008) also observed similar trends. Very minimal decrease of SST may be due to the formation of cold fronts by north east monsoon winds during December.

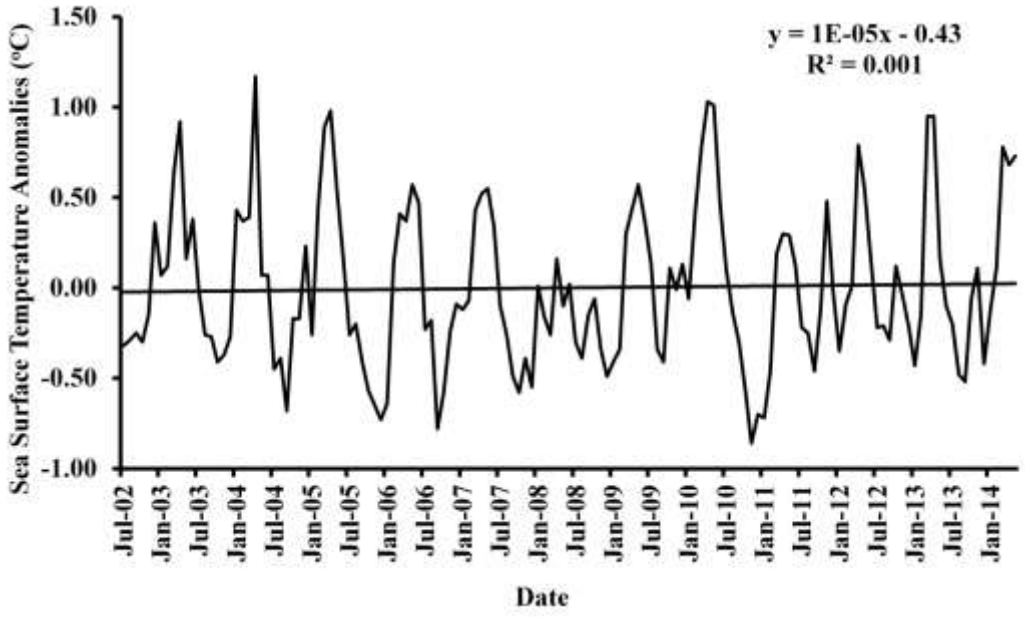

Figure 6.2 Area averaged monthly time-series of Sea Surface Temperature Anomalies showing no significant trend in the Eastern Equatorial Indian Ocean for the study period 2002-2014.

6.2.3 Sea Surface Height Anomaly (SSHA)

The area averaged SSHA in the EEIO for the period 2002 - 2014 is shown in figure 6.3. The SSHA varied from (-)11.24 cm to 10.89 cm during the study period. A minimum of SSHA of (-)11.24 cm is recorded in January 2007 and a maximum of 10.89 cm recorded in May 2012. Five peaks of high SSHA values (9.12 cm in June 2004; 6.61 cm in June 2005; 7.39 cm in May 2009; 10.89 cm in May 2012; 9.03 cm in May 2013) are recorded. Overall, increasing linear trend of SSHA was observed during 2002-2014 over the EEIO, which is evident from the correlation analysis of SSHA ($R^2 = 0.15$) for EEIO.

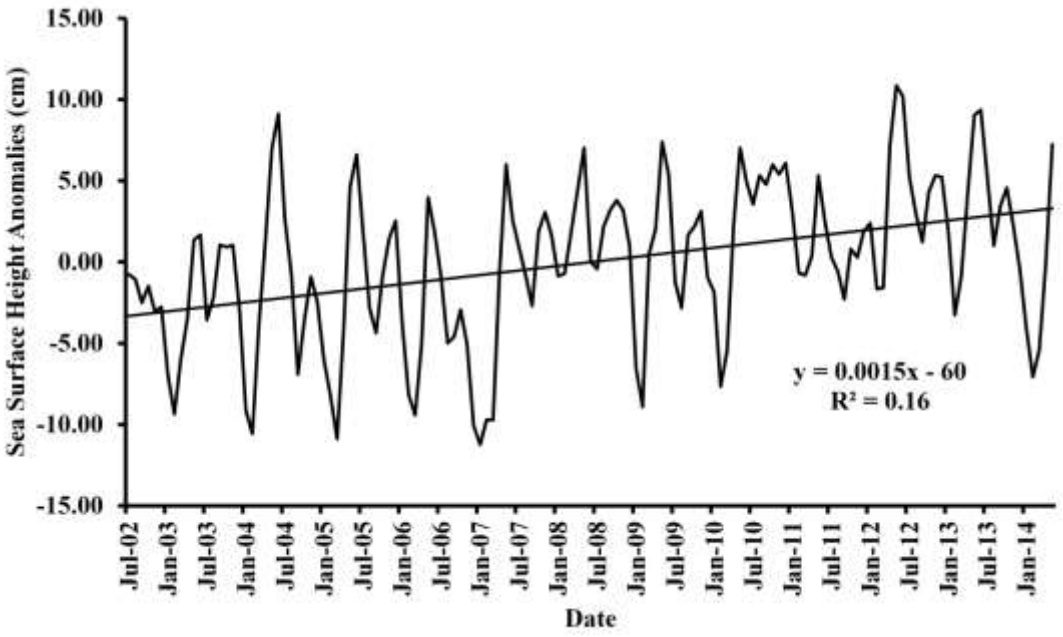

Figure 6.3 Area averaged monthly time-series of Sea Surface Height anomalies showing increasing linear trend in the Eastern Equatorial Indian Ocean for the study period 2002- 2014.

Based on satellite and terrestrial views of Indian Ocean Sea Surface Height, Han et al. (2010) and UNEP (2010) have observed a apparent spatial design of rise in Surface Height anomaly since the 1960s. These differences in regional ocean designs and Surface Height may lead to flooding in monsoons in India, and enhanced rainfall over Tropical Eastern Indian Ocean and drought in the WEIO.

6.2.4 Wind Speed (WS)

The area averaged WS in the EEIO for the period 2002 - 2014 is shown in Figure 6.4. It is observed that the area averaged WS varied from 2.88 m s^{-1} to 6.56 m s^{-1} during the study period. A minimum of areal average of WS is 2.88 m s^{-1} is recorded in March 2013 and a maximum of 6.56 m s^{-1} recorded in September 2006. Five high peaks of WS values (6.23 m s^{-1} in May 2004; 6.21 m s^{-1} in July 2005; 6.56 m s^{-1} in September 2006; 6.34 m s^{-1} in October 2010; 6.18 m s^{-1} in June 2013) are recorded. Overall, no significant trend of WS was observed during 2002-2014, which is evident from the regression analysis of WS (R^2=0.00003) in the EEIO.

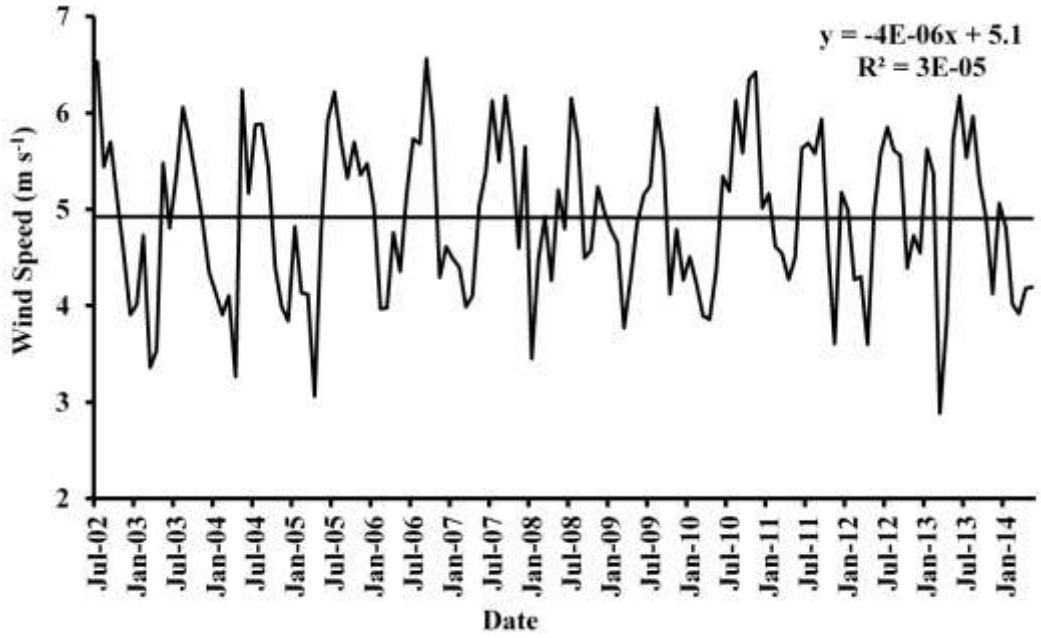

Figure 6.4 Area averaged monthly time-series of Wind Speed showing decreasing trend in the Eastern Equatorial Indian Ocean for the study period 2002-2014.

6.3 Inter-relationships

Scatter plots of chl-*a*, SST, SSHA, and WS are prepared to understand the relationship between each variable and shown in figure 6.5. We found strong correlation between SST and Surface Chl-*a* concentration: (R^2=0.52; $p<0.05$) (Figure 6.5a). Statistical test ('student's t-value') shows that correlation between chl-*a* and SST is significant at 0.05 level. Here least squares linear fit with slope (-)14.87x and intercept 31.05 represented by the straight line.

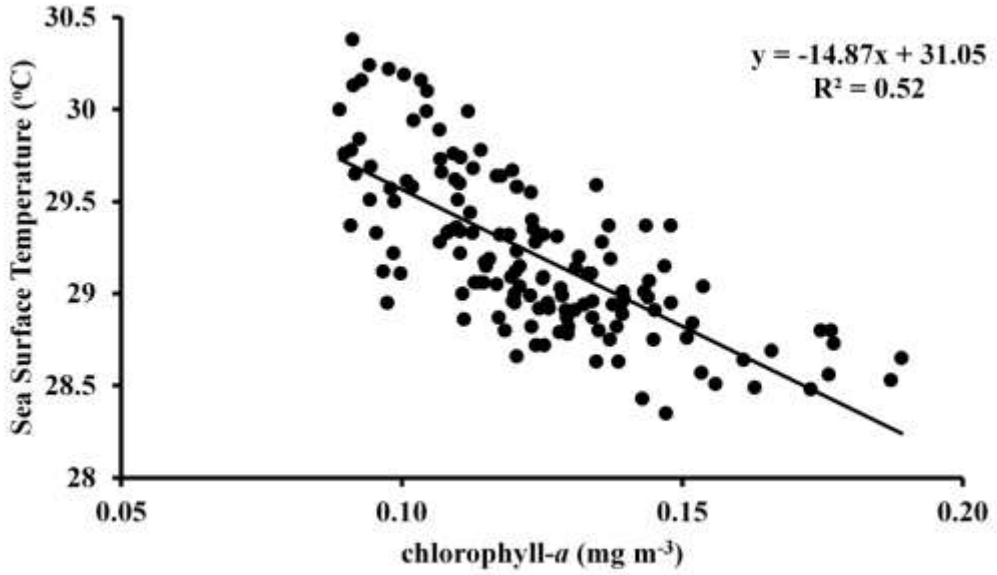

Figure 6.5a Scatter plot of the monthly chlorophyll-*a* concentrations versus Sea Surface Temperature in the Eastern Equatorial Indian Ocean (Latitude $5^oN - 5^oS$, Longitude $80^oE - 95^oE$) for the period 2002-2014.

A parabolic fit (figure 6.5b) shows good correlation between SST and chl-*a* ($y=144x^2-52.76x+33.47$; $R^2=0.57$). In general, when the upwelling occurs, temperature decreases because of the supply of nutrient-rich bottom cold water, leading to a greater increase in chl-*a*. Numerical model study indicated that the presence of phytoplankton may result in cooler SST over the Eastern Equatorial Pacific Ocean due to the upwelling (Nakamoto et al., 2001; Lin et al., 2007, 2008; Anderson et al., 2007).

During positive IOD events significant upwelling occurs to the west of Sumatra (1^oC temperature or more cools (Liu et al., 2016).

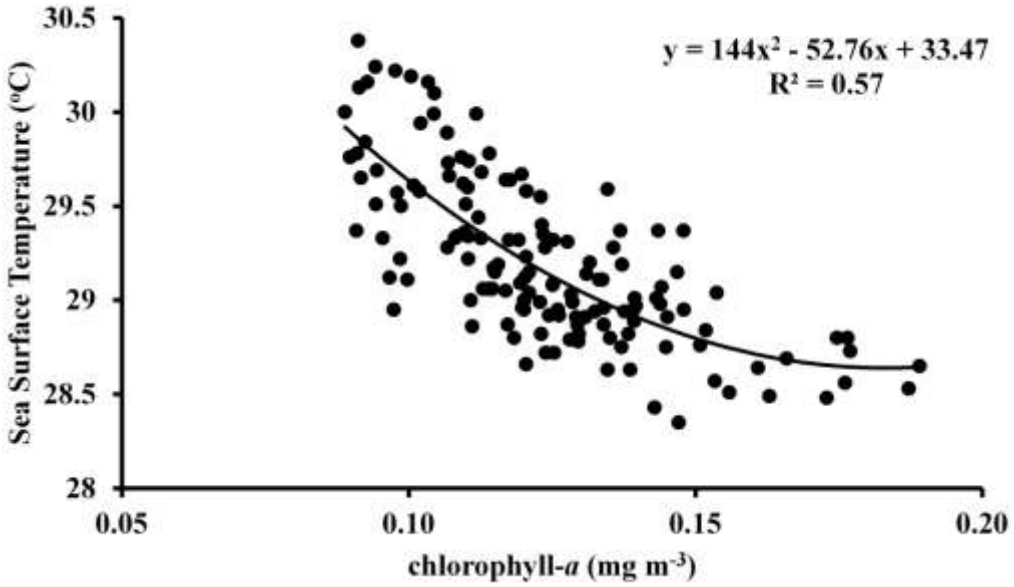

Figure 6.5b Scatter plot of the monthly chlorophyll-*a* concentrations versus sea surface temperature in the eastern equatorial Indian Ocean (Latitude $5^oN – 5^oS$, Longitude $80^oE - 95^oE$) for the period 2002-2014.

Open ocean chl-*a* concentration may play key role in the control of SST by trapping the surface layer solar radiation. When the open ocean chlorophyll-*a* concentration is high, SST ocean can be increased (Mohanty, 2008).

Reasonable good correlation is found between WS and chl-*a* concentration (R^2=0.38; $p<0.05$) (figure 6.6). Statistical test ('student's t-value') shows that correlation between chl-*a* and WS is significant at 0.05 level. Here least squares linear fit with slope 23.24 and intercept 2.03 represented by the straight line. The significant correlation occcurs because the Eastern Equatorial Indian Ocean experiences upwelling during boreal fall, due to the prevailing of southeast winds (Susanto et al., 2001).

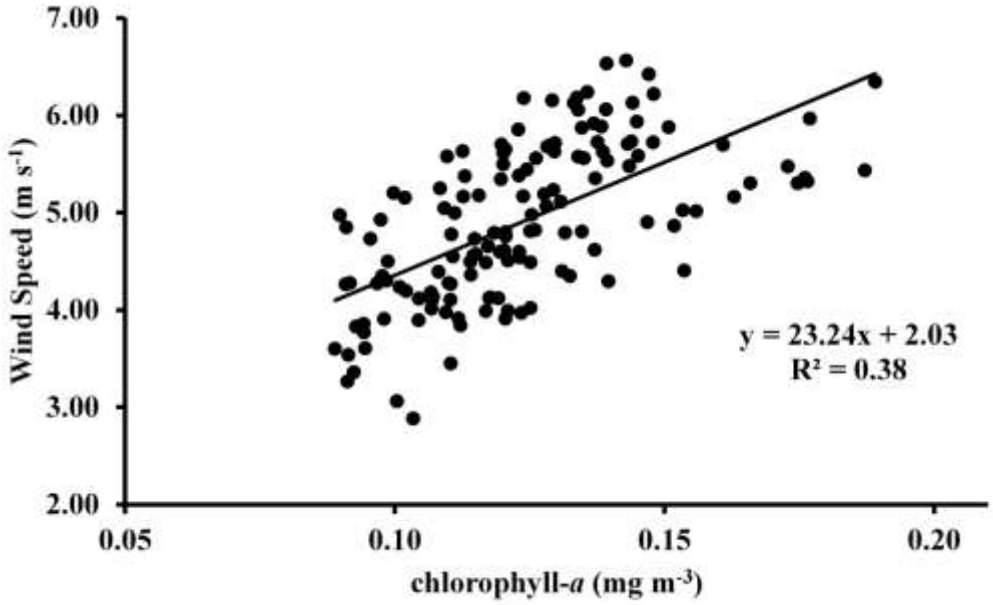

Figure 6.6 Scatter plot of the monthly chlorophyll-*a* concentrations versus wind speeds showing reasonable positive correlation R^2= 0.38 ($p<0.05$) significant at 0.05 level. The straight line represents least squares linear fit with slope 23.2 and intercept 2.0 in the Eastern Equatorial Indian Ocean for the period 2002-2014.

In order to understand the dynamics involved in providing strong coherence between SST-chl-*a* and SSH-chl-*a*, we have plotted lag-lead correlations between SST-chl-*a* (figure 6.7) and SSH-chl-*a* (figure 6.8) in the EEIO. Significant negative correlations are noticed between SSH-chl-*a* at zero months lag over the Eastern Equatorial Indian Ocean; whereas in WEIO we found correlation with two months lead. These patterns clearly suggest that Rossby waves close to the Equator play a very important role in modulating the variations of chl-*a* in EEIO.

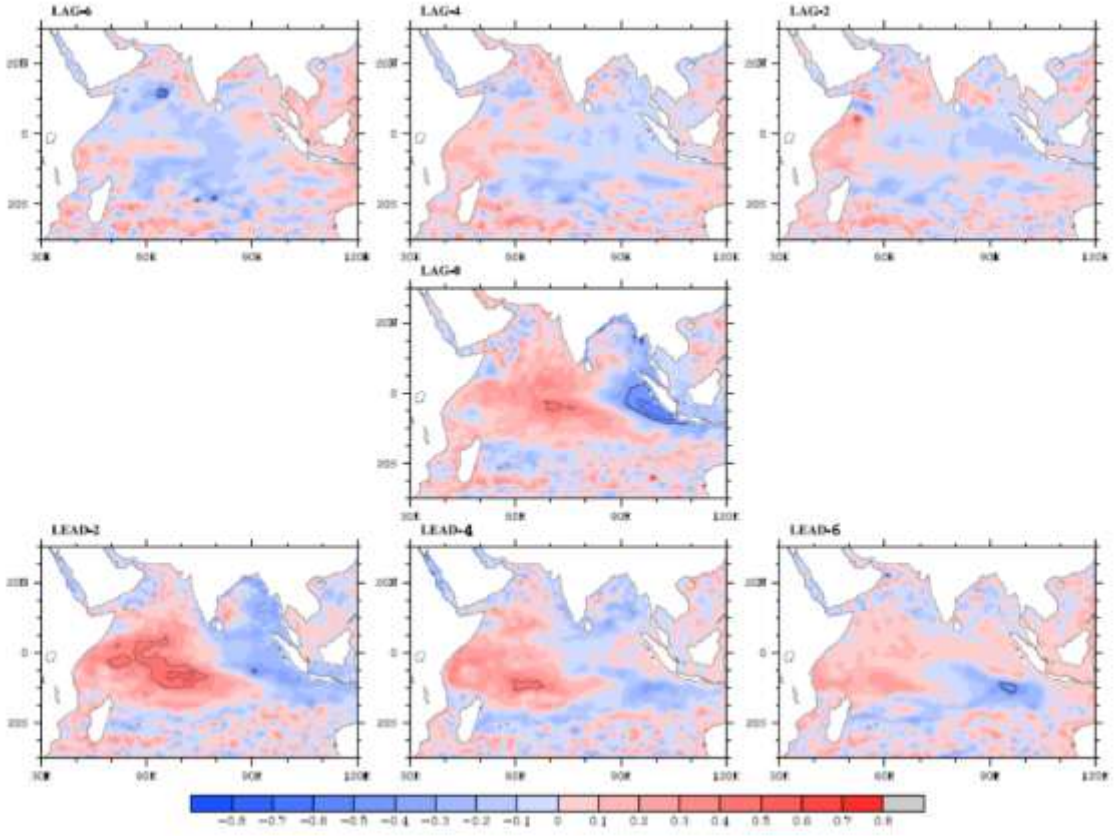

Figure 6.7 Correlation map between Sea Surface Height and chlorophyll-*a* at (a) Lag-6 (b) Lag-4 (c) Lag-2 (d) Lag-0 (e) Lead-2 (f) Lead-4 (g) Lead-6 in the Eastern Equatorial Indian Ocean. Dotted areas denote 95% confidence regions.

At lead-0 strong IOD pattern, a correlation between SST-chl-*a* is seen, which clearly suggests that EEIO chl-*a* anomalies and WEIO chl-*a* anomalies are strongly correlated to IOD dynamics in response to fast moving equatorial Kelvin waves. Therefore EEIO chl-*a* variability has a predictable component due to the slow propagating near equator Rossby waves.

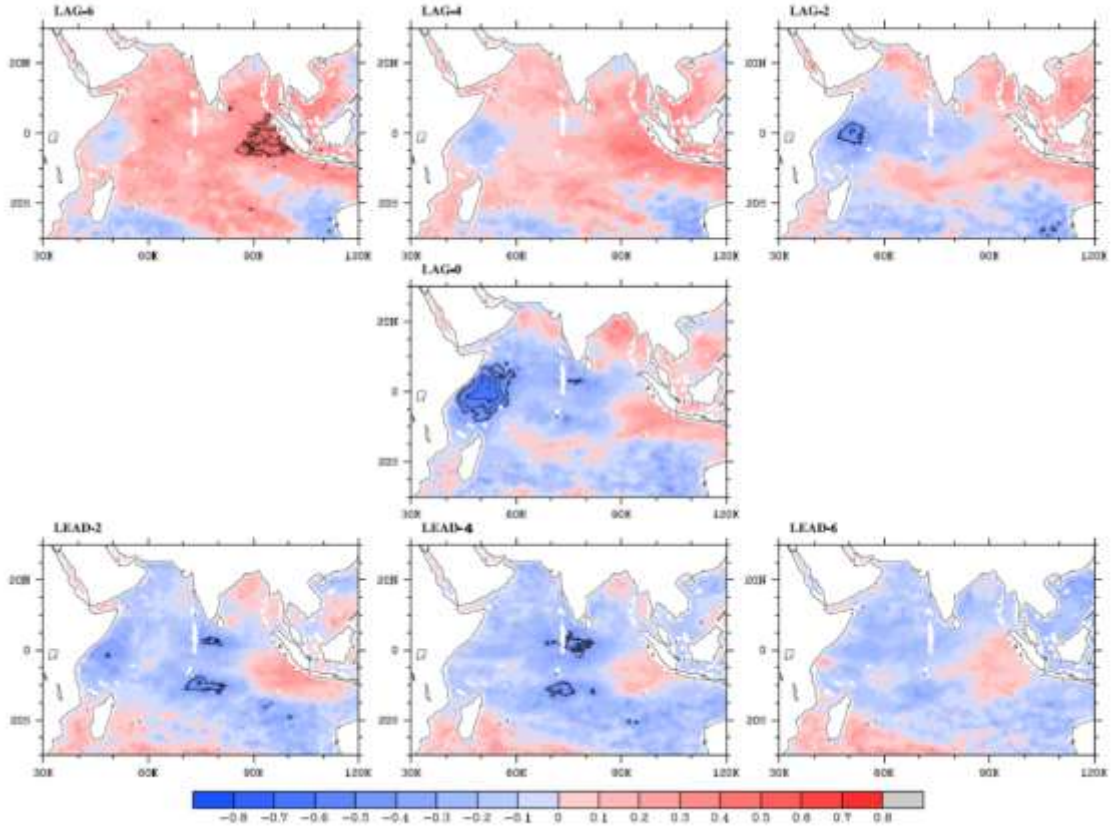

Figure 6.8 Correlation map between Sea Surface Temperature and chlorophyll-*a* at (a) Lag-6 (b) Lag-4 (c) Lag-2 (d) Lag-0 (e) Lead-2 (f) Lead-4 (g) Lead-6 in the Eastern Equatorial Indian Ocean. Dotted areas denote 95% confidence regions.

6.4 Discussion

The variability at different time scales is evidenced and the variability in each parameter and coherence among them are presented and discussed the dynamics behind such coherence. The power mathematical tools of Fast Fourier Transform (FFT) and wavelet analysis are applied for understanding the climatic variations on regional and global scale. We have applied the power spectrum analysis to all the four data sets of EEIO. Figure 6.5 shows the power spectrum plots of the data sets which clearly indicate two dominant peaks at 54 and 25 weeks cyclicity corresponding to 12 and 6 months respectively. These peaks are coherent and found to be common in all our data sets suggesting the presence of annual and semi-annual cycles.

The power spectral density (PSD) plots for SST, chl-*a*, SSHA and WS are shown in figure 6.9. The power spectral density (PSD) plot of RC-SST (figure 6.9a) shows strong peaks at 32, and 13-16 month periods i.e., 3 and 2 years respectively and the power spectrum of the RC-chl-*a* (figure 6.9b) Shows peaks at 32 and 5-6 months period. This clearly suggests the presence of Quasi-Biennial signals (2-3 years periodicity) in SST anomalies and chl-*a* for the EEIO (e.g., Meehl and Arablaster, 2001). The power spectrum of the RC-SSHA (figure 6.9c) shows peaks at 6-8 months is observed because of intra-seasonal cycle influence. The PSD of wind speed data (figure 6.9d) shows peaks at 28 and 6 months.

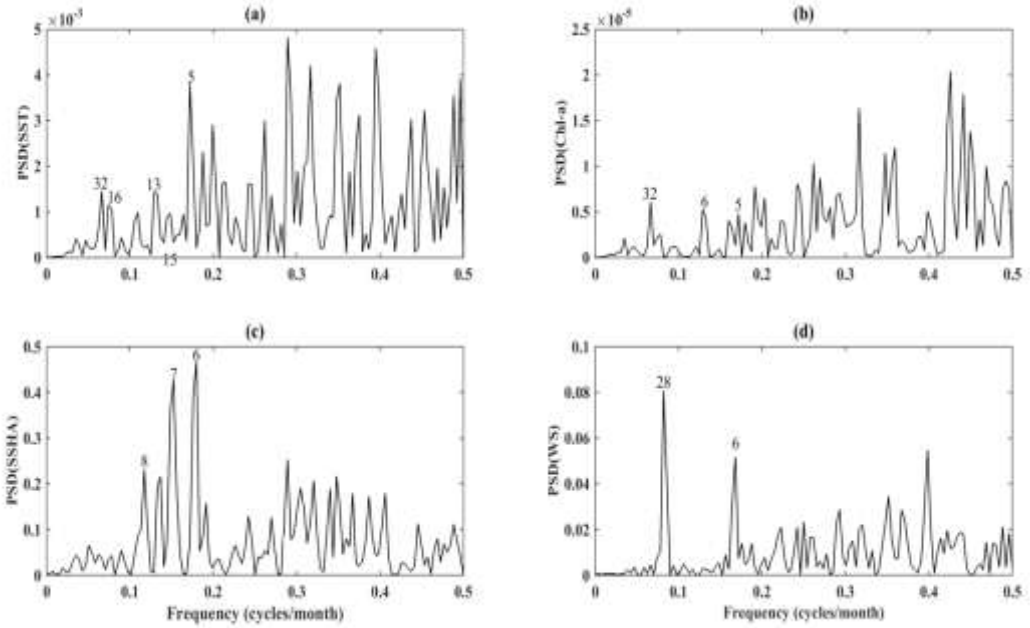

Figure 6.9 Power Spectrum plots of (a) Sea Surface Temperature, (b) chlorophyll-*a*, (c) Sea Surface Height anomaly, and (d) Wind Speed for the Eastern Equatorial Indian Ocean. High speaks found at 32, 16, 13 and 5 months is observed suggesting the implication of Quasi Biennial oscillations and also semi-annual variability in power spectrum of SST (figure 6.9a). The power spectrum of Chl-*a* (figure 6.9b) data shows strong and well separated maxima at 32, 5-6 months. Power spectrum SSHA (figure 6.9c) shows strong peaks at 6-8 months cyclicity, and ws (figure 6.9d) shows a high power at strong peaks between 28 and 6 months.

To explore the stationary characteristics of the peaks obtained by the power spectrum of RC time series, the Morlet based wavelet transform approach is used as discussed in the previous chapter. The wavelet spectrum identifies the main periodicities in the time series and helps to analyze the periodicities with respect to time (figure 6.10). Semi-annual signal is

weaker during IOD events (i.e., in 2006-2008) due to the absence of Wyrtki jet in fall and probably in spring as well (Cai et al., 2009). Joseph et al. (2012) also exhibited weakening of spring Wyrtki jets during the years 2006- 2011, which apparently reflects the strengthening of easterly wind anomalies associated with IOD events occurred during this period.

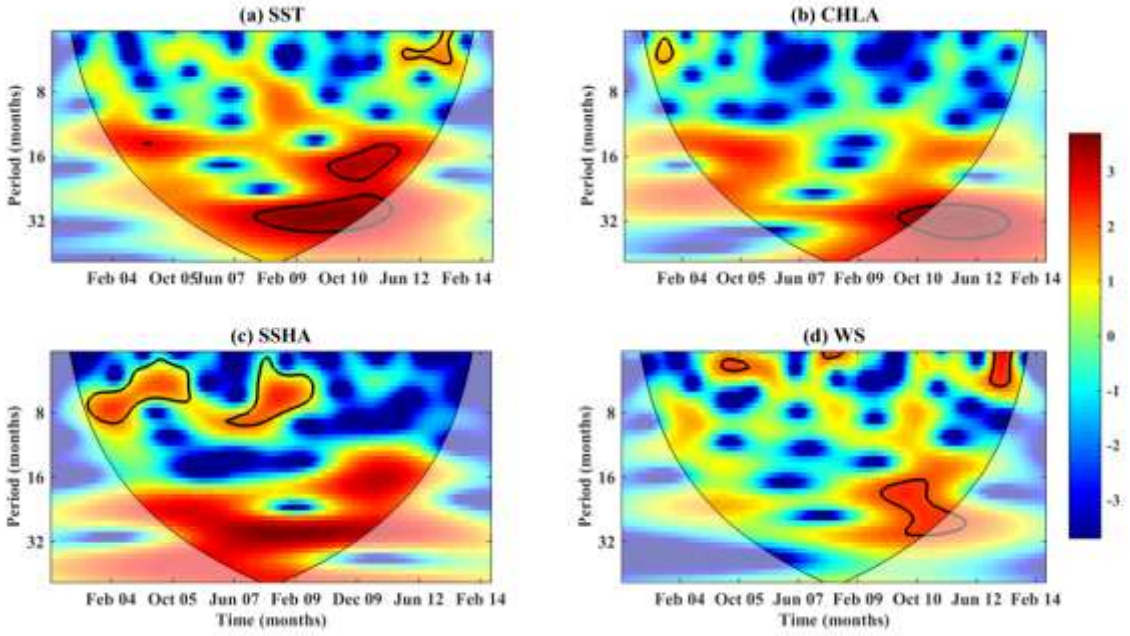

Figure 6.10 Wavelet analysis spectrum of (a) SST, (b) chl-*a*, (c) SSHA, and (d) WS for the study period from 2002 to 2014.

To investigate the temporal behavior of chl-*a* and SST signals, we have conducted the Wavelet analysis to the chl-*a*, SST, SSHA and WS data sets. We observed the occurrence of very strong IOD during the fall of 2006, and also the interference of the signal of 18 and 32 months period for the constructive formation of IOD in 2008. The wavelet power spectrum of the SST data (figure 6.10a) shows well separated high power at 36 months (June 2010 to August 2013) suggesting the influence of ENSO and IOD on chl-*a* respectively in EEIO. The wavelet spectrum of the chl-*a* (figure 6.10b) data depicts a statistically significant power at 32 months cyclicity throughout the data period of 2002-2014 and well separated strong peak at 32 months (October 2010 to August 2013). The wavelet spectrum of the chl-*a* data suggests the presence of Quasi-Biennial oscillation (QBO) in the data. The SSHA wavelet spectrum (figure 6.10c) shows high power at periods of 4 months and 8 months. The WS wavelet spectrum (figure 6.10d) shows peaks at 28 and 8 months periodicity. During positive

IOD enhanced upwelling could bring rich nutrient cold bottom water to the surface, causing increase chl-*a* concentrations, also SSH negative anomalies appear in the EEIO and coincide with SST negative anomalies (Liu et al., 2016). The wavelet spectrum of SST-chl-*a*-WS depicts a statistically significant power at around 32 and 16 months significant, and suggest a clear imprint of ENSO-IOD on the SST-chl-*a*-WS data.

Cross wavelet spectrum is applied to get better visualization of time series for two similar periods and for the interpretation of the results, Figure 6.11 shows the cross wavelet spectrum of (a) SST-chl-*a*, (b) chl-*a*-SSHA, (c) SST-SSHA, and (d) chl-*a*-WS data. The contours (dark blue lines) are the enclosing regions where the wavelet cross power is significant. The phase relationship, with in phase pointing to right and antiphase pointing to left, is shown by arrows. The cross spectrum plot of SST-chl-*a* (Figure 6.11a) shows the significant power at 28-38 months from September 2008 to December 2012. Similar features chl-*a* and WS also reflect the same from September 2008 to December 2012. The chl-*a*-SSHA cross spectrum (Figure 6.11b) showing peaks at 28, 16 and 6 months, whereas cross spectrum of SST-SSHA (Figure 6.11c) shows significant peaks at 32, 16, 8 months.

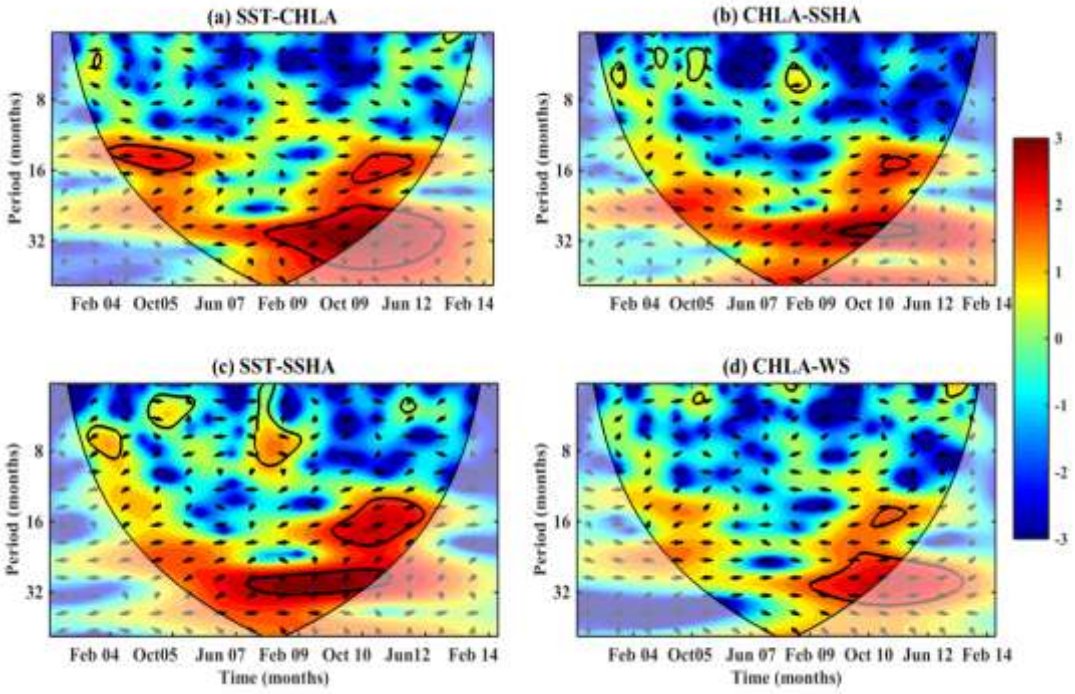

Figure 6.11 Cross wavelet spectrum of (a) SST-chl-*a*, (b) chl-*a*-SSHA (c) SST-SSHA (d) chl-*a* –WS in the Eastern Equatorial Indian Ocean.

6.5 Summary

Monthly chl-*a* concentrations show decreasing trend during the years 2002-2014 over the EEIO, which is evident from the regression analysis (R^2 = 0.01; 'student's t-value at 0.05 level).

Monthly averaged time series data of SST show no trend (R^2 = 0.001) during the study period over the EEIO. Increasing linear trend of SSHA was observed during 2002-2014, which was evident from the correlation analysis of SSHA (R^2 = 0.15). Overall, no trend in WS is observed during the years 2002-2014, which is evident from the regression analysis of WS (R^2=0.00003) for the EEIO. The better correlation is observed when a parabolic fit is done ($y=144x^2-52.76x+33.47$; R^2=0.57). A reasonable correlation between WS and chl-*a* concentration (R^2=0.38; $p<0.05$) is observed. Statistical test ('student's t-value') shows that correlation between chl-*a* and WS is significant at 0.05 level. Here least squares linear fit with slope 23.24 and intercept 2.03 represented by the straight line. From the spatial correlation plot, significant negative correlations are noticed between SSH-chl-*a* at zero months lag. This clearly suggests that Rossby waves close to the Equator play a very important role in modulating the variations of chl-*a*. At lead-0 strong IOD pattern correlations between SST-chl-*a* clearly suggest that chl-*a* anomalies in EEIO and WEIO are strongly correlated to IOD dynamics. EEIO chl-*a* variability has a predictable component due to the slow propagating near Equator Rossby waves. The power spectral density plots of SST, chl-*a*, SSHA and WS show 32, 13-16, 5-6 months periodicity, which suggest the presence of Quasi-Biennial signal (2-3 years periodicity) and semi-annual signal in the Eastern Equatorial Indian Ocean. The wavelet power spectrum plots suggest the influence of IOD and ENSO on SST and WS respectively in whole of Equatorial Indian Ocean.

Chapter 7

Summary of Results and Conclusions

In this chapter the main results obtained in this thesis are summarized.

7.1 Central Equatorial Indian Ocean

The area averaged chl-*a* concentration, SST and WS in the CEIO for the period 2002 - 2014 did not show any significant trend. High chl-*a* concentration is found during months of October-December due to the triggering of enhanced horizontal advection generated near the Maldives, contributing to productivity along the EIO from the north. This enhanced production extends eastwards from Maldives up to 80.5^{o} E during October – December, as the Wyrtki jets are well developed. The second hypothesis on enhanced chl-*a* is that Wyrtki jets and wind stirring are responsible for the bringing up the mixed layer of rich nutrients to the surface, and the enrichment of the mixed layer through cooler thermocline water. This hypothesis is ruled out here, as our results do not show positive correlation between wind speed and chl-*a*. Therefore, we suggest that the first hypothesis is more likely at play in the CEIO.

Chl-*a* concentration starts decreasing from March onwards and continues until the onset of summer monsoon i.e., up to June. The cloud cover during the summer monsoon i.e., from June to August, prohibits the satellite observations from capturing more accurately the chl-*a* variability as also suggested by earlier researchers (Prasanna Kumar et al., 2009). In September the chl-*a* concentration is fairly high (but relatively less, compared to February/March) probably fuelled by the advection of nutrients upwelled in the southwest (Prasanna Kumar et al., 2001).

The area averaged SSHA in the CEIO for the period 2002 - 2014 showed an increasing linear trend evident from the correlation analysis (R^2=0.21). Climate-change consequences on the Indo-Pacific warm pool influences the islands in the middle of the Indian Ocean to experience significantly raised sea-level than the global mean. Consequently, some coasts and islands in the Indian Ocean also coastal population suffer from elevated environmental stress (http://www.unep.org/).

We applied the Fast Fourier Transform (FFT) and wavelet analysis to all the four data sets. Power spectra clearly indicate two dominant peaks at 54 and 25 weeks cyclicity corresponding to 12 and 6 months, respectively. These peaks are coherent and found to be common in all our data sets suggesting the presence of annual and semi-annual cycles. The power spectral density (PSD) plot of SST showed two strong low-frequency maxima corresponding to~ 32, 16-18 and 6-8month periods i.e., 2 and 3 years respectively. This clearly suggests the presence of quasi-biennial signals (2-3 years periodicity) in SST anomalies of the central equatorial Indian Ocean (CEIO). A strong peak at 4 months period was also observed from the power spectrum suggesting semi-annual variability in the SST anomalies. The power spectrum of the SSHA showed peaks at 7-8, 5-6 and 4 months. The PSD of chl-*a* data showed powers at 12-13, 5-8 and 5 months. The PSD of wind speed data showed peaks at 18, 5-7 months period emphasizing the influence of semi-annual variability in the data.

In the wavelet spectra we can clearly observe the occurrence of very strong IOD during the fall of 2006, and also the interference of the signal of 18 months and 32 months period for the constructive formation of IOD in 2008. The wavelet power spectrum of the SST data showed high power around 32 months (January 2006 to June 2010) and 16 months (June 2010 to September 2012) suggesting the influence of ENSO and IOD on chl-*a*, respectively. The wavelet spectrum of the chl-*a* showed high peak at 12 months (October 2003 to September 2004) clearly suggesting the annual cycle. The wavelet power spectrum of the SSHA-RC data showed high power around 4-8 months period. The WS-RC data showed strong signal at 36 months suggesting the influence of ENSO.

The wavelet spectra of SST,SSHA and chl-*a* depicts a statistically significant power at around 32, 16-18 and 6-12 months at > 95% significance level, and suggests a clear imprint of ENSO-IOD on the SST-SSHA-chl-*a* data. The cross wavelet spectrum of chl-*a* and SSHA showed significant power around 6 months, and cross wavelet spectrum of SST and chl-*a* showed strong power at 32-36 months from August 2007 to March 2012 . The chl-*a* and SST cross wavelet spectrum showed similar features as that of chl-*a* and SSHA cross wavelet plot, which clearly indicates the trend relation between SST-SSHA-chl-*a* in the WEIO. The wavelet cross spectra of SST and SSHA showed a high power at 28-32 months period from October 2005 to December 2009. From the figure 5.8 we can see the change in phase for periods around 4 to 6 months with SSHA leading SST. The Chl-*a* and wind speed cross spectrum showed that wind speed leads chl-*a* by 6 and 14 months with phase value of 130^{o}

– 140^{o}. A reasonable correlation between SST and surface chl-*a* concentration: R^2=0.57 was found. Statistical test ('student's *t*-value') showed that the correlation between chl-*a* and SST is significant at 0.05 confidence level. Similar relationship was reported earlier from the northern Indian Ocean (Goes et al., 2005; Prakash and Ramesh, 2007). There appears to be lag of one month's time between SST and enhancement in surface chl-*a* concentrations indicated by the negative correlation of 0.4. This lag may be due to the triggering of enhanced horizontal advection and Wyrtki jets. Open ocean chl-*a* concentration may play key role in the control of SST by trapping the surface layer solar radiation. When the open ocean chlorophyll-*a* concentration is high, SST ocean can be increased (Mohanty, 2008). There was no significant correlation between chl-*a* concentration and Wind Speed.

7.2 Western Equatorial Indian Ocean

The area averaged chl-*a* concentration in the WEIO for the period 2002 - 2014 showed a decreasing linear trend of chl-*a*, but not in SST and WS. An increasing linear trend of SSHA was observed. Over the past few decades, sea levels in Western Equatorial Indian Ocean have risen because of the expansion of warming WEIO (Climate Institute, 2010). A new study (Han and others, 2010) that the satellite and terrestrial investigations of the Indian Ocean Sea Surface Height aided with climate change related simulated models have found an apparent spatial pattern in Sea Surface Height Anomaly increase since the 1960s. Researchers have also reported the increase in sea levels over the tropical Indian Ocean. These fluctuations in localised sea surface height and Ocean structures could intensify flooding due to monsoons in Bangladesh and India, leading to enhanced rainfall in the tropical eastern Indian Ocean and drought in the WEIO. Previous 60 years of Areal and satellite photographs received, a time during which there is proof that Sea Surface Height has increased.

We have applied Fast Fourier Transform (FFT) and wavelet analysis to all the four data sets. Power spectra clearly indicate two dominant peaks at 54 and 25 weeks cyclicity corresponding to 12 and 6 months, respectively. These peaks are coherent and found to be common in all our data sets suggesting the presence of annual and semi-annual cycles. Power spectra of de-seasonalized data (called RC data, i.e., reconstructed data) show high power at 32, 16, and 4- 8 months is observed suggesting quasi biennial oscillations and also semi-annual variability in SST. The power spectrum of chl-*a* shows strong and well separated maxima at 13, 12, 4- 8 months. Power spectrum of SSHA shows strong peaks between 4- 8 months cyclicity, and WS shows a high power at 10- 12 and 3- 5 months period. The power

spectral density (PSD) plot of RC-SST shows two strong low-frequency maxima corresponding to~32, 16-18 and 4-8 month periods i.e., 3 and 2 years, respectively. This clearly suggests the presence of quasi-biennial signals (2-3 years periodicity) in SST anomalies of WEIO. The power spectrum of the RC-SSHA shows peaks at 7-8, 5-6 and 4 months. The PSD of chl-*a* data shows powers at 12-13, 5-8 and 5 months. The PSD of Wind Speed data shows peaks at 10-12, 4-5, and strong maxima at 3 months period emphasizing the influence of semi-annual variability in the data. The wavelet power spectrum of the SST data shows high power around 32 months (January 2006 to June 2010) and 16 months (June 2010 to September 2012) suggesting the influence of ENSO and IOD on chl-*a*, respectively. The wavelet spectrum of the chl-*a* data shows high peak at 12 months (October 2003 to September 2004) clearly suggesting the annual cycle influence. The wavelet power spectrum of the SSHA-RC data shows high power around 4-8 months period. The WS-RC data show strong signal at 36 months suggesting the influence of ENSO in the data. The wavelet spectra of SST, SSHA, and chl-*a* depict statistically significant power at around 32, 16-18 and6-12 months at > 95% significance level, and suggests a clear imprint of ENSO-IOD on the SST-SSHA-chl-*a* data The cross wavelet spectrum of Chl-*a* and SSHA shows the significant power around 6 months, and cross wavelet spectrum of SST and chl-*a* shows strong power at 32-36 months from August 2007 to March 2012. The chl-*a* and SST cross wavelet spectrum shows similar features as that of chl-*a* and SSHA cross wavelet plot, which clearly indicates the trend relation between SST-SSHA-chl-*a* in the WEIO. The wavelet cross spectra of SST and SSHA shows a high power at 28-32 months period from October 2005 to December 2009. The change in phase for periods around 4 to 6 months is such that SSHA leads SST by 120^{o} - 150^{o}. The Chl-*a* and wind speed cross spectrum shows that wind speed leads chl-*a* by 6 and 14 months.

A strong negative correlation between SST and surface chl-a concentration was observed. Rising SST can reduce chl-*a* since they are a indication of enhanced surface stratification and therefore suppressed vertical mixing of nutrient-rich subsurface waters. Open ocean chlorophyll-a concentration may play key role in the control of SST by trapping the surface layer solar radiation. When the open ocean chlorophyll-a concentration is high, SST ocean can be increased. A reasonably good correlation between WS and chl-a concentration was observed. In order to understand the dynamics involved in providing strong coherence between SST-chl-*a* and SSH-chl-*a*, we plotted lag-lead correlations between SST-chl-*a* and SSH-chl-*a* in the WEIO. As expected significant negative

correlations are noticed between SSH-chl-*a* over Central Equatorial Indian Ocean at four months lead, over west-central equatorial Indian Ocean over two months lead and at WEIO at lead zero. These patterns clearly indicate that that Rossby waves closed to equator play a very important role in modulating the variations of chl-*a* in WEIO. This study for the first time shows that the WEIO chl-*a* variability has a strong predictable component due to the slow near equator Rossby wave.

7.3 Eastern Equatorial Indian Ocean

The area averaged chl-*a* concentrations, wind speed and SST in the EEIO for the period 2002 – 2014 did not show any significant trend, but a significant linear trend was seen in SSHA, as in the Central and Western Equatorial Indian Oceans. This is expected as Global Warming is common to all the three regions as is the consequent thermal expansion of the oceans.

Fast Fourier Transform (FFT) and wavelet analysis were applied all the four data sets. Power spectra clearly indicate two dominant peaks at 54 and 25 weeks cyclicity corresponding to 12 and 6 months, respectively. These peaks are coherent and found to be common in all our data sets suggesting the presence of annual and semi-annual cycles.

Data were de-seasonalized (called RC data, e.g., reconstructed data). The power spectrum density (PSD) plot of RC-SST shows strong peaks at 32, 16, 13 month periods i.e., 2 and 3 years respectively and the power spectrum of the RC-chl-*a* shows peaks at 32 and 5-6 months periods. This clearly suggests the presence of quasi-biennial signals (2-3 years periodicity) in SST anomalies and chl-*a* in the EEIO The power spectrum of the RC-SSHA shows peaks at 6-8 months probably because of intra-seasonal cycle influence. The PSD of wind speed data shows peaks at 28 and 6 months.

The wavelet power spectrum of the SST shows well separated high power at 36 months (June 2010 to August 2013) suggesting the influence of ENSO and IOD on chl-*a* respectively. The wavelet spectrum of the chl-*a* depicts a statistically significant power at 32 months cyclicity throughout the data period of 2002-2014, with a well separated strong peak at 32 months (October 2010 to August 2013). The wavelet spectrum of the chl-*a* suggests the presence of quasi-biennial oscillation (QBO). The SSHA wavelet spectrum shows high power at periods of 4 months and 8 months. The WS wavelet spectrum shows peaks at 28 and 8 months periodicities. During positive IOD enhanced upwelling could bring rich nutrient cold

bottom water to the surface, causing increase chl-*a* concentrations, also SSH negative anomalies appear in the Eastern Equatorial Indian Ocean and coincide with SST negative anomalies (Liu et al., 2016).

The wavelet spectrum of SST, chl-*a*, and WS depicts statistically significant power at around 32 and 16 months that suggests a clear imprint of ENSO-IOD on them. The cross wavelet spectrum of SST-chl-*a* shows significant power at 28-38 months from September 2008 to December 2012; similar features are also seen in the cross wavelet spectra of chl-*a* and WS duration the same period. The chl-*a*-SSHA cross wavelet spectrum shows peaks at 28, 16 and 6 months. Cross spectrum of SST-SSHA shows significant peaks at 32, 16, 8 months.

We found strong correlation between SST and surface chl-*a* concentration: R^2=0.52 ($p<0.05$) (Figure 6.8). Statistical test ('student's t-value') shows that correlation between chl-*a* and SST is significant at 0.05 level. Here least squares linear fit with slope (-)52.76 and intercept 33.47 represented by the straight line. The correlation uniform when a parabolic fit is done ($y=24.49\ x^2-21.71x+31.66$ R^2=0.57). This is became when the upwelling occurs, temperature decreases by the nutrient supply increases much more, leading to a greater increase in chl-*a*. Numerical model study indicated the presence of phytoplankton may result in cooling SST over the eastern equatorial Pacific Ocean due to the upwelling (Nakamoto et al., 2001; Lin et al., 2007, 2008; Anderson et al., 2007).

During positive IOD events significant upwelling occurs to the west of Sumatra; 1^oC temperature or more cools (Liu et al., 2016).

Open ocean chlorophyll-*a* concentration may play key role in the control of SST by trapping the surface layer solar radiation. When the open ocean chlorophyll-*a* concentration is high, SST ocean can be increased (Mohanty, 2008).

A good positive correlation between WS and chl-*a* concentration: R^2 = 0.38, significant at 0.05 level is seen. During the boreal fall. EEIO experiences upwelling, due to the prevailing of southeast winds (Susanto et al., 2001).

Significant negative correlations are noticed between SSH-chl-*a* over Eastern Equatorial Indian Ocean at zero months Lag, over Eastern Equatorial Indian Ocean moving towards WEIO and found at two months lead. These patterns clearly indicate that Rossby waves close to the equator play a very important role in modulating the variations of chl-*a* in

EEIO. Similar analysis is done for WEO. At lead-0 strong IOD pattern in correlations between SST-chl-*a* are seen, which clearly suggests that EEIO chl-*a* anomalies and WEIO chl-*a* anomalies are strongly correlated to IOD dynamics is a response to fast moving equatorial Kelvin waves. Therefore EEIO chl-*a* variability has a predictable component due to the slow propagating near equator Rossby waves.

Unlike WEIO chl-*a* variability, for EEIO we don't see significant negative correlations with SSH anomalies at different lags. This is probably due to the fast response to equatorial Kelvin waves. One of the strong contrasts between WEIO and EEIO is that WEIO dynamics is a response to fast moving equatorial Kelvin waves. Therefore WEIO chl-*a* variability has a strong predictable component due to the slow propagating near equator Rossby waves. This study for the first time shows that the WEIO chl-*a* variability has a strong predictable component due to the slow near equator Rossby wave.

References

Allan, R.J., Chambers, D., Drosdowsky, W., Hendon, H., Latif, M., Nicholls, N., Smith, I., Stone, R., Tourre, Y., 2001. Is there an Indian Ocean dipole independent of the El Nino-southern oscillation. Clivar exchanges 6, 4-8.

Anderson, T.R., 1993. A spectrally averaged model of light penetration and photosynthesis. Limnol. Oceanogr. 38, 1403–1419.

Annamalai, H., Murtugudde, R., Potemra, J., Xie, S.P., Liu, P., Wang, B., 2003. Coupled dynamics over the Indian Ocean: Spring initiation of the zonal mode. Deep Sea Research 50, 2305-2330.

Arief, D., Murray, P., 1996. Low-frequency fluctuations in the Indonesian throughflow through Lombok Strait. Journal of Geophysical Research 101, 12,455-12,464.

Ashok, K., Guan, Z., Yamagata, T., 2001. Impact of the Indian Ocean Dipole on the relationship between the Indian Monsoon rainfall and ENSO. Geophysical Research Letters 26, 4499- 4502.

Ashok, K., Weng, H.S., Behera, S., Rao, S. A., Yamagata, T., 2007. El Nino Modoki and its Teleconnection. Journal of Geophysical Research 112, C11007, doi: 10.1029/2006JC003798.

Ashok, K., Wing-Le Chan, Tatsuo Motoi, Yamagata, T. 2004. Decadal variability of the Indian Ocean Dipole. Geophysical Reserarch Letters 31, L24207, doi:10.1029/2004GL 021345.

Babu, K.N., Sharma, R., Agarwal, N., Agarwal, V.K., Weller, R.A., 2004. Study of the mixed layer variations within the north Indian Ocean using a 1-D model. Journal of Geophys. Res.109, C08016, doi: 10.1029/003JC002024.

Baliunas, S., Frick, P., Sokoloff, D., Soon, W., 1997. Time scales and trends in the central England temperature data (1659-1990): a wavelet analysi. Geophys. Res. Lett. 24, 1351-1354.

Banse, K., McClain, C. R., 1986. Winter blooms of phytoplankton in the Arabian Sea as observed by the Coastal Zone Colour Scanner. J. Mar. Ecol. Prog. Series 34, 201–211.

Barber, R.T., Marra, J., Bidigare, R.C., Codispoti, L. A., Halpern, D., Johnson, Z., Latara, M., Goericke, R., Smith, S. L., 2001. Primary productivity and its regulation in the Arabian Sea during 1995. Deep-Sea Res. II 48, 1127–1172.

Behera, S.K., Luo, J.J., Masson, S., Delecluse, P., Gualdi, S., Navarra, A., Yamagata, T., 2005. Paramount impact of the Indian Ocean dipole on the East African short rains: A CGCM study. Journal of Climate 18, 45114-4530

Beherenfeld, M.J., Robert, T. O'Malley., Siegel, D.A., Charles, R. McClain., Sarmiento, J. L., Feldman, G. C., Milligan, A.J., Falkowski,P.G., Letelier, R.M., Boss, E.S., 2006. Climate-driven trends in Contemporary Ocean Productivity. Nature 444, doi: 10.1038/nature05317.

Benquero-Bernal, A., Latif, M., Legutke M., 2002. On dipole like variability of sea surface temperature in the tropical Indian Ocean. Journal of Climate 15, 1358-1368.

Bhattathiri, P. M. A., Devassy, V. P., and Radhakrishna, K., 1980. Primary production in the Bay of Bengal during southwest monsoon of 1978, Mahasagar- Bulletin of the National Institute of Oceanography13, 315-323.

Box, G.E.P., Jenkins, G. M., 1976. Time Series Analysis: Forecasting and Control, San Francisco: Holden-Day.

Bricaud, A., Morel, A., Babin, M., Allali, K., Claustre, H., 1998. Variations of light absorption by suspended particles with chlorophyll-*a* concentration in oceanic (case 1) waters. Analysis and implications for bio-optical models. J. Geophys. Res. 103, 31033–31044.

Brock, J.C., McClain, C.R., Luther, M.E., Hay, W.W., 1991. The phytoplankton bloom in the northwestern Arabian Sea during the southwest monsoon of 1979. Journal of Geophysical Research 96, 20613-20622.

Broomhead, D.S., King, G.P., 1986. Extracting qualitative dynamics from experimental data. Physica 20D, 217-236.

Charles Troupin, 2011. Comparison between satellite and in situ sea surface temperature data in the Western Mediterranean Sea. Ocean Dynamics. Doi: 10.1007/s10236-011-0403-x.

Chauhan, P., Mohan, M., Sarangi, R.K., Kumari, B. and Nayak, S., 2002. Surface chlorophyll-*a* estimation in the Arabian Sea using IRS P4 Ocean Colour Monitor (OCM) satellite data, Int. J. Remote Sensing, 23 (8), 1663-1676.

Chauhan, P., Nagur C. R. C., Mohan, M., Nayak, S., and Navalgund, R. R., 2001. Surface chlorophyll-*a* distribution in Arabian Sea and Bay of Bengal using IRS P4 OCM satellite data, Curr. Sci., 80 (2), 127-129.

Chauhan, P., Sahay, A., Rajawat, A.S., Nayak, S., 2003. Remote sensing of diffuse attenuation coefficient (K490) using IRS P4 Ocean Colour Monitor (OCM) sensor, Ind. J. Marine Sciences 32(4), 279-284.

Conkright, M.E., Levitus, S., Boyer, T.P., 1994a. World Ocean Atlas 1994. Vol. 1 of NOAA Atlas NESDIS. NODC.

Conkright, M.E., Levitus, S., Boyer, T. P., 1994b. NOAA Atlas NESDIS 1: World Ocean Atlas 1994, vol.1, Nutrients. Tech. Rep., NODC.

Conkright, M.E., O'Brien, T. D., Levitus, S., Boyer, T. P., Stephens, C., Antonov, J.I., 1998. World Ocean Atlas 1998. Vol. 12 of NOAA Atlas NESDIS. NODC.

Cai, W., Pan, A., Roemmich, D., Cowan, T., Guo, X., 2009. Argo profiles a rare occurrence of three consecutive positive Indian Ocean Dipole events, 2006-2008. Geophysical Research Letters 36, L08701.

Christian, J.R., Murtugudde, R., 2003. Tropical Atlantic variability in a coupled physical-Biogeochemical ocean model, Deep-Sea Research II 50, 2947-2969.

Clarke, A. J., Liu, X., 1993. Observations and dynamics of semiannual and annual sea levels near the eastern equatorial Indian Ocean boundary. Journal of Physical Oceanography 23, 386-399.

Climate Institute (2010). Oceans and Sea Level Rise: Consequences of Climate Change on the Oceans. http://www. Climate.org/topics/sea-level/index.html (Accessed on 22 November 2010).

Currie, J.C., Lengaigne, M., Vialard, J., Kalpana, D.M., Aumont, O., Naqvi, S.W.A., Maury, O., 2013. Indian Ocean Dipole and El Nino/Southern Oscillation impacts on regional chlorophyll anomalies in the Indian Ocean. Biogeosciences 10, 6677-6698.

Currie, J.C., Lengaigne, M., Vialard, J., Kalpana, D.M., Aumont, O., Naqvi, S.W.A., Maury, O., 2013. Indian Ocean Dipole and El Nino/Southern Oscillation impacts on regional Chlorophyll anomalies in the Indian Ocean. Biogeosciences 10, 6677-6698.

Daubechies, I., 1992. Ten lectures on wavelet. CBMS-NSF regional conf. series in appl. Math. 61, society for industrial and applied mathematics, 357 pp.

Dueing, W., Schott, F., 1978. Measurements in the source region of Somali current during the monsoon reversal. Jour. of Phys. Oceanography 8, 278-289.

Emery, W.J., Thomson, R.E., 2001. Data analysis methods in Physical Oceanography. Elsevier Science, Amsterdam.

Falkowski, P.G., Barber, R.T., Smetacek, V., 1998. Biogeochemical controls and feedbacks on ocean primary production, Science 281, 200-206.

Falkowski, P. G., Ziemann, D., Kolber, Z., Bienfang, P. K., 1991. Role of eddy pumping in enhancing primary production in the ocean. Nature 352: 55–58.

Farge, M., 1992. Wavelet transforms and their applications to turbulence. Annual Review of Fluid Mechanics 24, 395-457.

Feng, J.F., Zhu, L., 2012. Changing trends and relationship between global ocean Chlorophyll and sea surface temperature. Procedia Environmental Sciences 13, 626-631.

Foufoula-Georgiou E., Kumar, P., 1995. Wavelets in Geophysics, Academic Press 373pp.

Gamage, N., Blumen, W., 1993. Comparative analysis of low-level cold fronts: Wavelet, Fourier, and empirical orthogonal function decompositions. Monthly Weather Review 121, 2867-2878.

Gandhi, N., Kumar, S., Prakash, S., Ramesh, R., Sheshshayee, M. S., 2011a. Measurement of marine productivity using ^{15}N and ^{13}C tracers: some methodological aspects. J. Earth System Sci. 120: 1–13.

Gandhi, N., Prakash, S., Ramesh, R., and Kumar, S., 2010. Nitrogen uptake rates and new production in the Indian Ocean. Indian J. Mar. Sci. 39: 362–368.

Gandhi, N., Ramesh, R., Prakash, S., Kumar, S., 2011b. Nitrogen sources for new production in the NE Arabian Sea. J. Sea Res. 65: 265–274.

Gauns, M., Madhupratap, M.., Ramaiah, N., Jyothibabu, R., Fernandes, V., Paul, J.T., Prasanna Kumar, S., 2005. Comparative accounts of biological productivity characteristics an estimates of carbon fluxes in the Arabian Sea and the Bay of Bengal, Deep-Sea Research II, 52, 2003- 2017.

Gent, P.R., O'Neill, K., Cane, M.A., 1983. A model of the semiannual oscillation in the Equatorial Indian Ocean. J. Phys. Oceanogr. 13, 2148-2160.

Goes, J.I., Thoppil, P.G., Gomes, H.R., Fasullo, J.T., 2005. Warming of the Eurasian landmass is making the Arabian Sea more productive. Science 308: 545–547, doi:10.1126/science.110661

Gomes, H.R., Goes, J. I., Saino, T., 2000. Influence of physical processes and fresh water discharge on seasonality of phytoplankton regime in the Bay of Bengal, Cont. Shelf Res., 20, 313-330.

Gopalan, A.K.S., Gopala Krishna, V.V., Ali, M.M., Sharma, R., 2000. Detection of Bay of Bengal eddies from TOPEX and in situ observations. J. Mar. Res. 58: 721-734.

Grinsted A., Moore, J.C., Jevrejeva, S., 2004. Application of the cross wavelet transform and wavelet coherence to geophysical time series. Nonlinear Processes Geophys. 11, 561–566, doi: 10.5194/npg-11-561-2004.

Gu, D., Philander, S.G.H., 1995. Secular changes of annual and interannual variability in the Tropics during the past century. J. Climate, 8, 864-876

Han, J.P., McCreary, J.D., Anderson, L.T., 1999: On the dynamics of the eastward surface jets in the equatorial Indian Ocean. Journal of phys. Oceanogr. 29, 2191-2209.

Han, W., Meehl, G., Rajagopalan, B., Fasullo, J., Hu, A., Lin, J,. Large, W., Wang, J-W., Quan, X.W., Trenary, L., Wallcraft, A., Shinoda, T., Yeager, S., 2010. Patterns of Indian Ocean sea- level change in a warming climate. Nature Geoscience 3, 546-550.

Hastenrath, S., 2002. Dipoles, temperature gradients, and tropical climate anomalies. Bulletin American Meteor.Soc. 83, 735-740.

Hawaiiedu.2015. Hawaiiedu.Retrieved 24 March, 2015, from http://apdrc.soest.hawaii.edu. Hendon, H.H., Salby, M., 1994. The life cycle of the Madden-Julian Oscillation. Journal of Atmospheric Sciences 15, 2225-2237.

Holschneider, M., 1995. Wavelet analysis over abelian groups. Applied and Computational Harmonic Analysis 2: 52-60.

Howell, E. A., Doney, S. C., Fine, R. A., Olson, D. B., 1997. Geochemical estimates of denitrification in the Arabian Sea and the Bay of Bengal during WOCE. Geophys. Res. Lett. 24: 2549–2552, doi:10.1029/97GL01538.

Iskandar, I., Mardiansyah, W., Masumoto, Y., Yamagata, T., 2005. Intraseasonal kelvin waves along the southern coast of Sumatra and Java. J. Geophys. Res. 110, C04013, doi:10.1029/2004JC002508.

Jamstecgojp. 2009. Jamstecgojp. Retrieved 2009, from http://www.jamstec.go.jp/frcgc/research/d1/iod/iod_home_s.html.en

Jensen, V.E., Samuel, P., Johnannessen, O.M., 2014. Studying the monsoon circulation in the Indian Ocean using altimeter data. Geoscience and Remote Sensing, 1997. IGARSS'97. Remote Sensing – A Scientific Vision for Sustainable Development 4, doi: 10.1109/IGARSS.1997.609030.

Jochum, M., Murtugudde, R., 2005. Interannual variability of Indian Ocean SST. Journal of Climate 18, 3726-3738.

Joseph, S., Wallcraft, A.J., Jensen, T.G., Ravichandran, M., Shenoi, S.S.C., Nayak, S., 2012. Weakening of spring Wyrtki jets in the Indian Ocean during 2006- 2011. Journal of Geophysical Research 117, doi: 10.1029/2011JC007581.

Jyothibabu, R., Madhu, N.V., Habeebrehman, H., Jayalakshmy, K.V., Nair, K.K.C., Achuthankutty, C.T., 2010. Re-evaluation of 'paradox of mezozooplankton' in the eastern Arabian Sea based on ship and satellite observations. Journal of Marine Systems 81, 235-251.

Jyothibabu, R., Maheswaran, P.A., Madhu, N.V., Ashraf, T.T.M., Gerson, V.J., Haridas, P.C., Venugopal, P., Revichandran, C., Nair, K.K.C., Gopalakrishnan, T.C., 2004. Differential response of winter cooling on biological production in the northeastern Arabian Sea and northwestern Bay of Bengal, Current Science, 87(6), 783-791.

Kahru, M., Gille, S.T., Murtugudde, R., Strutton, P., Manzano-Sarabia, M., Wang, H., Mitchell, B.G., 2010. Global correlations between winds and ocean chlorophyll. Journal of Geophysical Research 115, C12040, doi: 10.29/2010jC006500.

Kara, B.A., Hurlburt, H.E., Wallcraft, A.J., Bourassa, M.A., 2005. Black Sea Mixed Layer Sensitivity to Various Wind and Thermal Forcing Products on Climatological Time Scales, Journal of Climate, 18(51), 5266-5293.

Kettle, H., Merchant, C.J., 2008. Modeling ocean primary production: sensitivity to spectral resolution of attenuation and absorption of light. Progress in Oceanography, doi:10.1016/j.pocean.2008.04.002.

Krishnamurthy, V., Kirtman B.P., 2003. Variability of the Indian Ocean: Relation to monsoon and ENSO. Quart. J. Roy. Met. Soc. 129, 1623-1646.

Kumar, S., Ramesh, R., 2005. Productivity measurements in the Bay of Bengal using the ^{15}N tracer: implications to the global carbon cycle, Ind. J. Mar. Sci. 34(2), 153-162.

Kumar, S., Ramesh, R., Bhosle, N.B., Sardesai, S., and Sheshshayee, M.S., 2004b, Natural isotopic composition of nitrogen in suspended particulate matter in the Bay of Bengal. Biogeosciences 1, 63-70.

Kumar, S., Ramesh, R., Sardesai S., Sheshshayee, M.S., 2004a, High new production in the Bay of Bengal: possible causes and implications. Geophys. Res. Lett. 31, L18304, doi: 10. 1029/2004GL021005.

Kummerow, C., Barnes, W., Kozu, T., Shiue, J., Simpson, J.,1998. The tropical rainfall measuring mission (TRMM) sensor package. J. Atmos. Oceanic Technol., 15, 809-817.

Lehodey, P., Bertignac, M., Hampton, J., Lewis, A., Picaut, J., 1997. El Nino-Southern oscillation and tuna in the western pacific. Nature 389: 715-718.

Levy, R.C., Remer, L.A., Mattoo, S., Vermote, E.F., Kaufman, Y.J., 2007. Second-generation operational algorithm: Retrieval of aerosol properties over land from inversion of Moderate Resolution Imaging Spectroradiometer spectral reflectance, J. Geophys. Res. 112, D13211. doi 10.1029/2006JD007811.

Longhurst, A.L., 1993. Seasonal cooling and blooming in tropical oceans. Deep-Sea Research 40, 2145-2165.

Lin, P., Liu, H., Zhang, X., 2007. Sensitivity of the upper ocean Temperature and circulation in the equatorial Pacific to solar radiation penetration due to phytoplankton. Advances in atmospheric sciences 24, 765-780.

Lin, P., Liu, H., Zhang, X., 2008. Effect of chlorophyll-*a* spatial distribution on upper ocean temperature in the central and eastern equatorial Pacific. Advances in atmospheric sciences 25, 585-596.

Liu L., Feng, L., Weidong, Y.U., Wang, H., Liu, Y., Sun, S., 2013. The distribution and variability of simulated Chlorophyll concentration over the Tropical Indian Ocean from five CMIP5 Models. Journal Ocean University China (Oceanic and Coastal Sea Research) 12(2), 239-259.

Liu, W., Shang-Ping, X., Lu, J., 2016. Tracking ocean heat uptake during the surface warming hiatus. Nature communications. Doi: 10.1038/ncomms10926.

Madden, R., Julian, P., 1971. Detection of a 40-50 day oscillation in the zonal wind in the tropical Pacific, Journal of Atmospheric Science 29, 702-708.

Madhu, N. V., Maheswaran, P.A., Jyothibabu, R., Sunil, V., Revichandran, C., Gopalakrishnan, T.C., and Nair, K.K.C., 2002. Enhanced biological production off Chennai triggered by October 1999 super cyclone, Current Science 82(12), 1472-1479.

Madhupratap, M., Gauns, M., Ramaiah, N., Prasanna kumar S., Muraleedharan P.M., Desouza S.N., Sardessai S., Muraleedharan U., 2003. Biogeochemistry of the Bay of Bengal: physical, chemical and primary productivity characteristics of the central and western Bay of Bengal during summer monsoon 2001. Deep-Sea Res. II, 50, 881-896.

Madhupratap, M., Prasanna Kumar, S., Bhattathiri, M. A., Dileep Kumar, M., Raghukumar, S., Nair, K. K. C., Ramaiah, N., 1996. Mechanism of the biological response to winter cooling in the northeastern Arabian Sea. Nature 384**,** 549–552.

Ma, J., Liu, H., Lin, P., Zhan, H., 2015. Effects of the interannual variability in chlorophyll concentrations on sea surface temperatures in the east tropical Indian Ocean. Journal of Geophys. Res. oceans 120, 7015-7027.

Masumoto, Y., Hase, H., Kuroda, Y., Matsuura, H., Takeuchi, K., 2005. Intraseasonal variability in the upper layer currents observed in the eastern equatorial Indian Ocean. Geophys. Res. Lett. 32, doi: 10.1029/2004GL021896.

McCreary, J.P., Murtugudde, R., Vialard, J., Vinayachandran, P.N., Wiggert, J.D., Hood, R.R., Shankar, D., Shetye, S., 2009. Biophysical processes in the Indian Ocean. Geophys. Monogr.Ser. doi:10.1029/2008GM000768.

McCreary, J.P., Kundu, P.K., Molinari, R.L., 1993. A numerical investigation of dynamics, thermodynamics and midex-layer processes in the Indian Ocean. Prog. Oceanogr. 31, 181-244.

McPhaden, M.J., Zebiak, S.E., Glantz, M. H., 2006. ENSO as an Integrating concept in Earth Science 314, 1740-1745.

Meehl, G. A., Arablaster, J.M., 2001. The Tropospheric Biennial Oscillation and Asian – Australian Monsoon Rainfall. Journal of Climate 15, 722-744.

Meyers, S.D., Kelly, B.G., O'Brien, J.J., 1993. An introduction to wavelet analysis in oceanography and meteorology: With application to the dispersion of Yanai waves. Monthly weather review 121, 2858-2866.

Milliff, R.F., Large, W.G., Morzel, J., Danabasoglu G,. Chin, T.,1999. Ocean General circulation model sensitivity to forcing from scatterometer winds. J. Geophys. Res., 11337- 11358.

Mitchell, P., Ellie, E.P., 1990. Atlas and lakes: University of Alberta, Canada.

Mohanty, P.C., 2008. Study of Intra and Inter annual variability of air sea interaction process over North Indian Ocean. M.Tech thesis, Indian institute of remote Sensing.

Mohanty, U.C., 2014. Monitoring and prediction of Tropical Cyclones in the Indian Ocean and climate change. Springers, pp-94.

Morrison, J.M., 1997. Inter-monsoonal changes in the T-S properties of the near-surface waters of the northern Arabian Sea. J. Geophys. Res. Lett. 2553-2556.

Muraleedharan, K.R., Jasmine, P., Achuthankutty, C. T., Revichandran, C., Dinesh Kumar, P. K., Anand, P., Rejomon, G., 2007. Influence of basin–scale and mesoscale physical processes on biological productivity in the Bay of Bengal during the summer monsoon. Prog. Oceanogr. 72: 364–383.

Murtugudde, R.G., Signorini, S.R., Christian, J.R., Busalacchi, A., McClain, C.R., Picaut, J., 1999. Ocean color variability of the tropical Indo-Pacific basin observed by SeaWIFS during 1997-1998. Journal of Geophysical Research 104(C8): 18,351- 18,366 doi: 10.1029/1999JC900135.

Murakami, H., Ishizaka, J., Kawamura, H., 2000. ADEOS observations of chlorophyll-*a* concentration, sea surface temperature, and wind stress change in the equatorial Pacific during the 1997 El Nino onset. Journal of Geophysical Research 15, 19,551-19,559.

Murtugudde, R., Busalachi, A. J., 1999. Interannual variability of the dynamics and thermodynamics of the tropical Indian Ocean. Journal of Climate 12, 2300-2326.

Murtugudde, R., McCreary, J.P., Busalacchi, A.J., 2000. Oceanic processes associated with anomalous events in the Indian Ocean with relevance to 1997-1998. Journal of Geophysical Research 105: 3295-3306.

Murty, V. S. N., Sarma, M.S.S., Lambata, B.P., Gopalakrishna, V.V., Pednekar, S.M., Rao, A.S., A.J., Luis, A. R., Kaka, Rao, L.V.G., 2000. Seasonal variability of upper-layer geostropic transport in the tropical Indian Ocean during 1992-1996 along TOGA-1 XBT tracklines. Deep-Sea Research 47, 1569-1582 (14)

Nakamoto, S., Kumar, S.P., Oberhuber, J.M., Ishizaka, J., Muneyama, K., Frouin, R., 2001. Response of the equatorial pacific to chlorophyll pigment in a mixed layer isopycnal ocean general circulation model. Geophysical Research Letters 28, 2021-2024.

Nair, P.V.R., Samuel, S., Joseph, K.J., Balachandran, V.K.., 1973. Primary production and potential fishery resources in the seas around India, In: Proceedings of the symposium on Living Resources of the Seas Around India, 1968, special publication, Central Marine Fisheries Research Institute, Cochin, 184-198.

Narvekar, J., Prasanna Kumar, S., 2010. Upper ocean variability of the equatorial Indian Ocean Ocean and its relation to Chlorophyll pigment concentration. Proceedings of ocean observations and information for Society 4pp.

Naqvi, S.W.A., Naik, H., Narvekar, P.V., 2003. The Arabian Sea, in Biogeochemistry of Marine systems. Sheffield Academic press, Sheffield, 156-206.

Nasagov.2015. Nasagov.retrieved 21 March, 2015 from http://oceancolor.gsfc.nasa.gov/cms.

Niiler, P.P., Maximenko, N.A., McWilliams, J. C., 2003. Dynamically balanced absolute sea level of the global ocean derived from near-surface velocity observations. Geophysical Research Letters 30, No. 22, 2164, doi: 10.1029/2003GL018628.

Niiler, P.P., Sybrandy, A.S., Bi, K. N., Poulain P.M., Bitterman, D,. 1994. Measurements of the water- following capability of holey-sock and TRISTAR drifters. Deep-Sea Res. 42, 1951.

Noaagov.2015. Noaagov. Retrieved 26 March, 2015 from ftp://ftp.cdc.noaa.gov.

Noaagov.2015. Noaagov. Retrieved 28 March, 2015 from http://oceanwatch.pifsc.noaa.gov/las/servlets/dataset?var=15

Nuncio, M., Prasanna Kumar, S., 2012. Life cycle of eddies along the western boundary of the Bay of Bengal and their implications. J. Mar. Syst. 94: 9–17.

O'Reilly, J.E., 1998. Ocean colour chlorophyll algorithms for SeaWiFS. J. Geophys. Res. 103, 24,937- 24,953.

Park, J.Y., Kug, J.S., Park, J., Yeh, S.W., Jang, C.J., 2011. Variability of Chlorophyll associated with El Nino- Southern Oscillation and its possible biological feedback in the equatorial Pacific. Journal of Geophysical Research 116: C10001.

Platt, T., Sathyendranath, S., 1993.Estimators of primary production for interpretation of remotely sensed data on ocean color, J. Geophys. Res., 98, 14561-14576.

Polovina, J.J., Kleiber, P. Kabayashi, D.R., 1999. Application of Topex/Poseidon satellite altimetry to simulate transport dynamics of larvae of the spiny lobster (Panulirus marginatus) in the northwestern Hawaiian Islands 1993-96. Fishery Bulletin 97, 132-43.

Prakash, P., Prakash, S., Rahaman, H., Ravichandran, M., Nayak, S., 2012. Is the trend in chlorophyll-*a* in the Arabian Sea decreasing? Geophysical Research Letters 39, L23605, doi: 10.1029/2012GL054187.

Prakash, S., Ramesh, R., 2007. Is the Arabian Sea getting more productive?, Current Science 92, 667-671.

Prakash, S., Ramesh, R., Sheshshayee, M.S., Mohan, R., Sudhakar, M., 2015. Nitrogen Uptake rates and *f*-ratios in the equatorial and Southern Indian Ocean. Current science 108, 2.

Prasanna Kumar, S., Madhupratap, M., Dileep Kumar, M., Muraleedharan, P.M., De Suza, S.N., Surekha Sawat, Mangesh Gauns Sarma, V.V.S.S., 2001. High biological productivity in the interior Arabian Sea during summer monsoon driven by Ekman Pumping and lateral advection. Current Science 891: 1633-1638.

Prasanna Kumar, S., Muraleedharan, P.M., Prasad, T.G., Gauns, M., Ramaiah, N., de Souza, S.N., Sardesai, S., Madhupratap, M., 2002. Why is the Bay of Bengal less productive during summer monsoon compared to the Arabian Sea? Geophysical Research Letters 29, NO. 24, 2235, doi: 10.1029/2002GL016013.

Prasanna Kumar, S., Narvekar, J., Nuncio, M., Gauns, M., Sardesai, S., 2010. What Drives the Biological Productivity of the Northern Indian Ocean? In Indian Ocean Biogeochemical Processes and Ecological Variability, Geophysical Monograph Series 185**:** doi: 10.1029/2008GM000757.

Prasanna Kumar, S., Nuncio, M., Narvekar, J., Kumar, A., Sardesai, S., de Souza, S. N., Gauns, M., Ramaiah, N., Madhupratap, M., 2004. Are eddies nature's trigger to enhance biological productivity in the Bay of Bengal? Geophys. Res. Lett. 31: L07309, doi:10.1029/2003GL019274.

Prasanna Kumar, S., Nuncio, M., Ramaiah, N., Sardesai, S., Narvekar, J., Fernandes, V., Paul, J.T., 2007. Eddy−mediated biological productivity in the Bay of Bengal during fall and spring inter-monsoons. Deep Sea Res. Part I 54: 1619–1640.

Prasanna Kumar, S., Sardesai, S., Ramaiah, N., 2009. A decade of physical and Biogeochemical measurements in the northern Indian Ocean. Proceedings of Ocean Obs'09: Sustained ocean observations and information for society, 21-25 September 2009).

Qasim S.Z., 1977, Biological productivity of the Indian Ocean, Ind. J. Mar. Sci., 6, 122-137.

Radhakrishna K., 1978, Primary productivity of the Bay of Bengal during March-April, 1975, *I*nd. J. Mar. Sci., 7, 58-60.

Rahul, C. R., Salvekar, P.S., 2008. Phytoplankton blooms induced/sustained by cyclonic eddies during the Indian Ocean Dipole event of 1997 along the southern coasts of Java and Sumatra. Biogeosciences Discussions 5: 3905-3918.

Ramasastry, A. A., Balaramamurty, C., 1957. Thermal fields and oceanic circulation along the east coast of India. Proc. Ind. Acad. Sci. 46: 293–323.

Rao, A.S., Yamagata, T., 2004. Abrupt termination of Indian Ocean Dipole events in response to intraseasonal disturbances. Geophysical Research Letters 31, L19306, doi: 10.1029/2004GL020842.

Rao, K.H., Smitha, A., and Ali, M.M., 2006, A study on cyclone induced productivity in south-western Bay of Bengal during November- December 2000 using MODIS (SST and Chlorophyll-a) and altimeter Sea surface height observations, Ind. J. Mar. Sci., 35(2), 153-160.

Ravichandran, M., Girishkumar, M.S., Stephen, R., 2012. Observed variability of Chlorophyll-*a* using Argo profiling floats in the southeastern Arabian Sea. Deep-Sea Research I 65, 15-25.

Reiniger, R.F., Ross, C.K., 1968. A method of interpolation with application to oceanographic data Deep Sea Research 15, 185-193.

Resplandy, L., Levy, M., Madec, G., Pous, S., Aumont, O., Kumar, D., 2011. Contribution of mesoscale processes to nutrient budgets in the Arabian Sea. Journal of Geophysical Research 116, C11007, doi:10.1029/2011JC007006.

Reverdin, G., Cadet, D.L., Gutzler, D.,1986. Interannual displacements of convection and surface circulation over the equatorial Indian Ocean.Quart. J. Roy. Meteor. Soc. 112, 43-67.

Risien, C.M., Chelton, D.B., 2008. A global climatology of surface wind and wind stress fields from 8 years of QuickSCAT scatterometer data. Journal of Physical Oceanography 38, 2379-2413.

Roxy, M., 2014. Sensitivity of precipitation to sea surface temperature over the tropical summer monsoon quantification. Climate Dynamics 43, pp- 1159-1169.

Roxy, M.K., Aditi, M., Raghu, M., Vinu, V., Swapna, P., Prasannakumar, S., Ravichandran, M., Vichi, M., Levy, M., 2016. A reduction in primary productivity driven by rapid warming over the tropical Indian Ocean. Geophys. Res. Lett. 43(2), 826-833.

Saji, N.H., Goswami, B.N., Vinayachandran, P.N., Yamagata, T., 1999. A dipole mode in the tropical Indian Ocean. Nature, 401, 360-363.

Saji, N. H., Yamagata, T., 2003a. Possible impacts of Indian Ocean dipole mode events on global climate. Climate Research 25, 151-169.

Saji, N.H., Yamagata, T., 2003b. Structure of SST and Surface Wind Variability during Indian Ocean Dipole Mode Events: COADS Observations. Journal of Climate 16 (16), 2735- 2751.

Sakova, I.V., Meyers, G., Colemen, R., 2006. Interannual variability in the Indian Ocean using altimeter and 1X1 –expendable bathy-thermograph (XBT) data: Does the 18-month signal exist?. Gephys. Res. Lett. 33, L20603. doi:10.1029/2006GL027117.

Sarangi, R.K., Chauhan, P., Mohan, M., Nayak, S.R., 2004, Time series analysis of chlorophyll-*a* distribution in the northern Arabian sea using IRS-P4 OCM Satellite data, Asian Journal of Geoinformatics, 5(1), 55-60.

Sarangi, R.K., Chauhan, P., Mohan, M., Nayak, S.R., Navalgund, S.R., 2001, Phytoplankton distribution in the Arabian Sea using IRS-P4 OCM satellite data, Int. J. Remote Sensing, 22(15), 2863-2866.

Sardessai, S., Shetye, S., Maya, M.V., Mangala, K.R., PrasannaKumar, S., 2010. Nutrient characteristics of the water masses and their seasonal variability in the eastern equatorial Indian Ocean. Mar. Environ. Res. 70(3-4), 272-282.

Sarma, V.V.S.S., 2006. The influence of Indian Ocean Dipole (IOD) on biogeochemistry of carbon in the Arabian Sea during 1997-98. Journal of Earth System Science 115, 433-450.

Sasamal, S. K., 2007. Island wake circulation off Maldives during boreal winter, as visualized with MODIS derived Chlorophyll-*a* data and other satellite measurements. International Journal of Remote Sensing 28(5), 891-903.

Schiller, A., McIntosh, P.C., Meyers, G., Fiedler, R., 2000. Interannual dynamics and thermodynamics of the Indo-Pacific Oceans. J. Phys. Oceanogr. 30, 987-1012.

Schott, F., Fischer, J., 2000. The winter monsoon circulation of the northern Arabian Sea and Somali Current. J. Geophys. Res. 105(C3): 6 359–6 376.

Schott, F.A., McCreary, J.P., 2001. The monsoon circulation of the Indian Ocean. Progress in Oceanography 51**,** 1-123

Schott, F., Swallow, J.C., Fieux, M., 1990. The Somali Current at the equator: annual cycle of currents and transports in the upper 1000 m and connection to neighboring latitudes. Deep-Sea Research 37, 1825–1848.

Shetye, S.R., Gouveia, A.D., Shenoi, S.S.C., Sundar, D., Michael, G.S., Nampoothiri, G., 1993. The western boundary current of the seasonal subtropical gyre in the Bay of Bengal. J. Geophys. Res. 98: 945–954.

Shetye S.R., Shenoi S.S.C., Gouveia A.D., Michael G. S., Sundar D. Nampoothiri G., 1991, Wind-driven coastal upwelling along the western boundary of the Bay of Bengal during the southwest monsoon, Cont. Shelf Res., 11, 1397-1408.

Shi, W., Morrison, J.M., Bohm, E., Manghnani, V., 2000. The Oman upwelling zone during 1993, 1994 and 1995. Deep-Sea Research II 47, 1227–1247.

Signorini, S. R., Murtugudde, R.G., McClain, C.R., Christian, J.R., Picaut, J., Busalacchi, A.J., 1999. Biological and physical signatures in the tropical and Subtropical Atlantic. Journal of Geophysical Research 18, 367–18, 382. doi:10.1029/1999JC900134.

Singh, A., Ramesh, R., 2011.Contribution of riverine dissolved Inorganic Nitrogen Flux to new production in the coastal northern Indian Ocean: An assessment. International Journal of Oceanography vol. 2011.doi:10.1155/2011/983561.

Smith, R.L., Bottero, J,S., 1977. On upwelling in the Arabian Sea. In a voyage of discovery. Ed. M. Angel, Pergamon Press: New York, pp. 291-304.

Smith, S.L., 2001. Understanding the Arabian Sea: Reflections on the 1994–1996 Arabian Sea Expedition. Deep-Sea Research II 48, 1385-1402.

Sorokin, Yu. I., Kopylov, A.I., Mamaeva, N.V., 1985. Abundance and dynamics of Microplankton in the central tropical Indian ocean. Marine Ecology – Progress Series 24, 27-41.

Spintall, J., Gordon, A.L., Murtugudde, R., Susanto, R.D., 2000. A semiannual Indian Ocean forced kelvin wave observed in the Indonesian seas in May 1997. Journal of Geophysical Research 105: 17, 217-17, 230.

Strutton, P.G., Coles, V.J., Hood, R.R., Matear, R.J., McPhaden, M.J., Philips, H.E., 2014. Biogeochemical variability in the equatorial Indian Ocean during the monsoon transition. Biogeosciences 11: 6185-6219.

Sukresno, B., 2010. Empirical Orthogonal functions (EOF) analysis of SST variability in Indonesian water concerning with ENSO and IOD. Intl. Archives of the Photogrammetry, Remote Sensing and Spatial Information Science. Vol. 38, 1-6.

Susanto, R.D., Marra, J., 2005. Effects of the 1997/98 El Nino on Chlorophyll-*a* variability along the southern coasts of Java and Sumatra. Oceanography 18, 124-127.

Strutton, P.G., Coles, V.J., Hood, R.R., Matear, R.J., McPhaden, M.J., Philips, H.E., 2015. Biogeochemical variability in the central equatorial Indian ocean during the monsoon transition. Biogeiosciences 12, 2367-2382.

Swallow, J.C., Schott, F., Fieux, M., 1991. Structure and transport of the East African Coastal Current. J. Geophys. Res., 96, 22254-22267.

Thadathil, P., Muraleedharan, P.M., Rao, R.R., Somayajulu, Y.K., Reddy, G.V., Revichandran, C., 2007. Observed seasonal variability of barrier layer in the Bay of Bengal. Journal of Geophysical Research 112, C02009, doi:10.1029/2006JC 003651.

Torrence, C., Compo, G., 1998. A practical guide to wavelet analysis. Bull. Amer. Meteor.Soc 79: 61-78.

Tozuka, T. J., Luo, J., Masson, S., Yamagata, T., 2008. Tropical Indian Ocean variability revealed by self-organizing maps. Climate Dynamics 31, 333-343.

UNEP/WTO (2010). Sea-level Rise in the Indian Ocean Differs by Region and Low-lying Pacific.

Veldhuis, M.J.W., Kraay, G.W., van Bleijswijk, J.D.L., Baars, M.A., 1997. Seasonal and spatial variability in phytoplankton biomass, productivity and growth in the Indian Ocean: The southwest and northeast monsoon, 1992–1993; Deep-Sea Res. I 44, 425–449.

Vidya, P.J., Prasanna Kumar, S., Gauns, M., Verenkar, A., Unger, D., Ramaswamy, V., 2013. Influence of physical and biological process on the seasonal cycle of biogenic flux in the equatorial Indian Ocean. Biogeosciences 10, 7493-7507.

Velleman, P.F., Hoaglin, D.C., 1981. Applications, Basics, and computing of exploratory data analysis. Bostan, Massachusetts: Dxubury Press.

Vinayachandran, P.N., Francis, P.A., Rao, S.A., 2009. Indian Ocean Dipole: Processes and Impacts. Current Trends in Science: 569-589.

Vinaychandran P.N., Mathew S., 2003. Phytoplankton bloom in the Bay of Bengal during the northeast monsoon and its intensification by cyclones, Geophys. Res. Lett., 30 (11), 1572, doi: 10.1029/2002GL016717.

Vinayachandran, P. N., Saji, N.H., 2008. Mechanisms of south Indian Ocean Intra-seasonal cooling. Geophysical Research Letters 35, L23607.

Vinayachandran, P. N., Saji, N.H., Yamagata, T., 1999. Response of the equatorial Indian Ocean to an anomalous wind event during 1994. Geophysical Research Letters 26,1613-1615.

Webster, P.J., Moore, A.M., Loschnigg, J.P., Leben, R.R., 1999. Coupled ocean-atmosphere dynamics in the Indian Ocean during 1997-98. Nature 401, 356-360.

Weng, H., Lau, K.M., 1994. Wavelets, period doubling, and time-frequency localization with application to organization of convection over the tropical western Pacific. J. Atmos. Sci. 51, 2523- 2541.

Wiggert, J.D., Hood, R.R., Banse, K., Kindle, J., 2005. Monsoon-driven biogeochemical Processes in the Arabian Sea. Progress in Oceanography 65(2-4), 176-213, doi: 10.1016/j.pocean. 2005.03008.

Wiggert, J.D., Hood, R.R., Naqvi, S.W.A., Brink, K.H., Smith, S.L., 2009. Introduction to Indian Ocean biogeochemical processes and ecological variability: Current understanding and emerging perspectives. American Geophysical Union, Washington D.C 185, 9-7. doi:10.1029/2009GM000906.

Wyrtki, K., 1973. Physical Oceanography of the Indian Ocean. In: Zeitzschel B (Ed.). Ecological studies: Analysis and synthesis. Springer 3, 18-36.

Xie, S.P., Annamalai, H., Schott, F.A., McCreary J.P., 2002. Structure and mechanisms of south Indian Ocean climate variability. Journal of Climate 15, 867-878.

Xiu, P., Liu, Y., 2006. Study on the correlation between Chlorophyll maximum and Remote Sensing data. Journal of Ocean University of China vol.5, pp.213-218.

List of Publications

Research Papers

1. Shiva Kumar, G., Prakash, S., Ravichandran, Narayana, A.C., 2016. Trends and Relationship between Chlorophyll-a and Sea Surface Temperature in the Central Equatorial Indian Ocean. *Remotes Sensing Letters* (accepted).

2. Shiva Kumar, G., Srilakshmi, S., Narayana, A.C., 2016. Inter-annual variability of SST and Chlorophyll-*a* in the Western Equatorial Indian Ocean: Possible linkages with the Indian Ocean Dipole. *Journal of Marine System* (in press).

Papers presented in conferences

1. Shiva Kumar, G., Srilakshmi, S., Narayana, A.C., Understanding the Relevance of Ocean dynamics in the productivity of the Western Equatorial Indian Ocean. *National Climate Science Conference*, Indian Institute of Science, Bangalore, 2-3 July, 2015.

2. Shiva Kumar, G., Narayana, A.C., Variability of Chlorophyll-a and Sea Surface Temperature over the Equatorial Indian Ocean. *Dynamics of the Indian Ocean: Perspective and Retrospective*, Goa, India, 30th November – 4th December 2015.